

Physical Properties of Bitumen Distillation Fractions
and Solvent Effect on Free Radical Content

by

Diana Tulegenova

A thesis submitted in partial fulfillment of the requirements for the degree of

Master of Science

in

Chemical Engineering

Department of Chemical and Materials Engineering
University of Alberta

© Diana Tulegenova, 2022

Abstract

The main target of bitumen upgrading is to reduce its viscosity. One of the pathways to achieve it is visbreaking. It takes place through thermal cracking by a free radical mechanism. The impact of the bulk liquid (solvent) environment on persistent free radical content was evaluated.

Electron Spin Resonance (ESR) spectroscopy was used to generate data on how different solvents affected the free radical content in bitumen by changing the dissociation equilibrium of radical pairs. The solubility of bitumen was checked in 54 different solvents, and only the soluble solvents were evaluated in the study. Depending on the solvent, it was found that the free radical content of the bitumen could be varied over the range 6×10^{17} to 1.5×10^{18} spins/g.

The g-factor and analyte spin content generated from the quantitative analysis of the ESR spectra were correlated with the solvents' properties such as the dipole moment, dielectric constant, ionization potential, molecular weight, density, dynamic and kinematic viscosities. The g-factor of dissociated radical pairs was shifted depending on the dipole moment of the solvent. The higher the dipole moment, the more shifted the g-factor is. Surprisingly, the ionization potential of sulfur-containing, monoaromatic and diaromatic solvents was linearly proportional to the free radical concentration observed in bitumen. Free radical concentration was poorly correlated with the other solvent properties.

Another approach was to interrogate the change of viscosity with respect to distillation temperature, and for this purpose hands-on fractional distillation was applied to obtain liquid oil products from bitumen. While atmospheric distillation did not yield any liquid, vacuum distillation of bitumen was performed five times with an average liquid yield of 25 wt.%. It resulted in about

15 fractions for each of the five distillations with a temperature range of 20°C for each cut. This material was used for further study.

The 15 distillation fractions were characterized by physical properties such as viscosity, density and refractive index. Next, 14 blends were created to compare different bitumen distillation fractions by forming a blend with known ratios. Refractive index and density data demonstrated that properties between the blends are related to weight composition, i.e. knowing the density of two pure distillation fractions, refractive index and density of the blended material can be accurately estimated by only knowing wt.% of each. However, one blend consisting of 70 wt.% of bitumen distillation fraction with a boiling range of 310-330°C and 30 wt.% of 410-430°C repeatedly deviated from that relationship for a reason that could not be determined.

Overall, it was found that the relationship between density and measurement temperature in a blend is linear over the range of 20-60°C, with density decreasing with an increase in temperature at the rate of $-0.0007 \text{ g/cm}^3/\text{°C}$. The Refractive index values also decreased with a temperature increase with a slope of the line equal to -0.0004 nD/°C .

The viscosity of the blends was measured, but not evaluated against binary mixing rules. This is recommended as a good starting point for a follow-up study.

Keywords: bitumen upgrading, free radicals, Electron Spin Resonance, ESR, EPR, fractional distillation, viscosity, density, refractive index, blending, mixing.

Preface

(Mandatory due to collaborative work)

Chapter 3 of this thesis will be submitted for publication as “Tannous, J. H.; Tulegenova, D.; De Klerk, A. “Effect of solvent on the free radical content in the absence of reaction.” It was also presented as part of ACS Spring 2021. I was responsible for conducting the experiments, determining bitumen solubility in 54 solvents, running Electron Spin Resonance spectrometer, checking the bitumen solubility under a stereomicroscope and documenting the results. Dr. Joy H. Tannous developed a background for the project, trained me on the equipment, analyzed the results, discussed the findings and organized the writings in the paper. Dr. Arno de Klerk proposed edits, supported by the writing and data organization. Dr. Lusine Tonoyan and Dr. Arno Siraki assisted with the data reproducibility study.

During the work described in Chapter 4, Dr. Cibele Melo Halmenschlager trained me and assisted me with work on the distillation system. She ran the system and collected the fractions on day 3 of Distillation 2.

Dr. Arno de Klerk supported proposed corrections and explanations throughout all the work described in this thesis.

Dedication

*I dedicate this thesis to Alberta's Oil Sands Industry
since I passionately believe in the future it holds.*

Acknowledgments

First of all, I want to express my greatest appreciation to my supervisor Dr. Arno de Klerk. Because of him, I grew so much as an engineer. Working together, he always listened to what I had to say and considered what I wanted to do during the work. His belief in the integrity of everyone gave me a lot of strength and inspiration to work towards my thesis.

I'm grateful to all the friends I made while at the University of Alberta. I'm always smiling when I think about how supportive and close people in our research group are. Every single one of you left a positive impact on my life. Great friends that I made when taking my courses, I value our friendship very highly.

My gratitude goes to my mom and family, for listening and helping with achieving my goals. For my friends from Kazakhstan, who wait for me there and who I made while here, I'm really grateful.

Also, I want to express my thanks to the student services that the University of Alberta provides, I had support during every moment of my degree.

Lastly, I want to thank my future employer. I'm so excited to be starting a job that employs so many of my skills and interests.

TABLE OF CONTENTS

CHAPTER 1 – INTRODUCTION	1
1.1 Background	1
1.2 Objectives	3
1.3 Scope of work	3
REFERENCES	4
CHAPTER 2 – LITERATURE REVIEW	6
SECTION A	7
2.1 Oil sands bitumen	7
2.2 Upgrading of oil sands bitumen	7
2.2.1 Visbreaking	8
SECTION B	10
2.3 Free radicals in bitumen	10
2.4 Chemistry of thermal cracking	10
2.5 Basic principles of electron spin resonance (ESR) spectroscopy	11
2.5.1 ESR Quantification	13
2.6 Stereomicroscopy	13
2.7 Distillation of bitumen	15
2.7.1 Industrial distillation of bitumen	16
2.7.2 Simulated distillation of bitumen	18
2.7.3 Vacuum distillation of bitumen	18
2.8 Viscosity of bitumen	19
2.8.1 Practical Relationships in Viscosity of Bitumen	20
2.8.2 Density	22

2.8.3 Refractive Index.....	23
REFERENCES	24
CHAPTER 3 – SOLVENT EFFECT ON THE FREE RADICAL CONTENT IN BITUMEN IN THE ABSENCE OF REACTION	27
Abstract.....	27
3.1. Introduction.....	28
3.2. Experimental	30
3.2.1 Materials	30
3.2.2 Equipment and procedures.....	34
3.2.3 Analyses.....	37
3.3 Results.....	39
3.3.1 Solubility of bitumen in different solvents	39
3.3.2 Effect of solvent properties on the g-factor	44
3.3.3 Effect of solvent properties on the free radical content.....	46
3.4. Discussion.....	50
3.4.1 Effect of the feed bulk liquid properties	50
3.4.2 Effect of the feed bulk liquid properties on the free radical content	51
3.5 Conclusions.....	57
CHAPTER 4 – BITUMEN VACUUM DISTILLATION AND REFRACTIVE INDEX MEASUREMENTS OF THE FRACTIONS.....	65
Abstract.....	65
4.1 Introduction.....	66
4.2 Experimental.....	67
4.2.1 Prevention and Safety Measures during the work	67
4.2.2 Materials	67
4.2.3 Equipment and Procedure	68

4.2.3.1 Crude Oil Distillation System.....	68
4.2.4 Analyses.....	72
4.2.4.1 Refractive Index.....	72
4.2.4.2 Penetration Index.....	72
4.2.4.3 Estimated Level of Uncertainty.....	72
4.3 Results.....	74
4.3.1 Distillation.....	74
4.3.2 Penetration Index.....	82
4.4 Discussion.....	83
4.4.1 Analysis of the fractions mixing.....	83
4.4.2 Penetration Index.....	84
4.5 Conclusion.....	85
REFERENCES.....	86
CHAPTER 5 – RELATIONSHIPS IN PHYSICAL PROPERTIES OF BITUMEN FRACTIONS	
.....	87
Abstract.....	87
5.1 Introduction.....	89
5.2 Experimental.....	90
5.2.1 Materials.....	90
5.2.2 Analyses.....	91
5.2.2.1 Refractive Index.....	91
5.2.2.2 Viscosity.....	91
5.2.2.2.1 Anton Paar Cold Properties Kinematic Viscometer.....	91
5.2.2.2.2 RheolabQC rotational rheometer.....	92
5.2.2.3 Density.....	92

5.2.2.4 Elemental Analysis	93
5.2.2.5 Electron Spin Resonance (ESR) Spectroscopy	93
5.2.3 Blending procedure	93
5.2.4 Coefficient of Determination (R^2)	94
5.3 Results.....	95
5.3.1 Physical properties of the 15 fractions.....	95
5.3.1.1 Electron Spin Resonance (ESR) Spectroscopy.....	98
5.3.2 Blending results	102
5.3.3 Analyses of the blends	102
5.4 Discussion.....	106
5.4.1 Processing of the experimental results from the 15 fractions	106
5.4.2 ASTM D341 – 20 ^{e1} evaluation	107
5.4.3 Evaluating Hildebrand Molar Volume Postulate.....	109
5.4.4 Evaluating Refractive Index of Bitumen Distillation Blends	112
5.4.5 Evaluating Density of Bitumen Distillation Blends.....	114
5.4.6 Evaluating Viscosity of Bitumen Distillation Blends.....	116
5.5 Conclusion	118
REFERENCES	119
CHAPTER 6 – CONCLUSION	120
6.1 Introduction.....	120
6.2 Solvent Effect on Bitumen Free Radical Content.....	120
6.2.1 Major conclusions.....	120
6.3 Bitumen Vacuum Distillation and Refractive Index Measurements	120
6.3.1 Major achievements.....	121
6.4 Relationships in Physical Properties of Bitumen Fractions.....	121

6.4.1 Major conclusions	121
BIBLIOGRAPHY	123
APPENDIX A	133
APPENDIX B	142
APPENDIX C	149

LIST OF TABLES

Table 2.1 Boiling ranges in refining and bitumen upgrading	15
Table 2.2 API gravity distribution.	23
Table 3.1 Solvents used to dissolve the bitumen along with their purities and suppliers.....	30
Table 3.2 The concentration of the bitumen samples tested for solubility in different solvents. .	34
Table 3.3 Solubility of bitumen in different solvents at a concentration of 50-60 mg bitumen/ml solvent.	39
Table 3.4 Solvents' characteristics and free radical content in bitumen sample dissolved in various solvents at the concentration of 50-60 mg bitumen/ml solvent.	47
Table 4.1 Characterization of the feed: Athabasca oil sands bitumen from Suncor.	67
Table 4.2 Assigned number (Fraction Identification Number (FIN)) and the temperature range of the mixed fractions.....	71
Table 4.3 Collected fractions for the Distillation 1.....	75
Table 4.4 Material balance of the Distillation 1.	76
Table 4.5 Collected fractions for the Distillation 2.....	76
Table 4.6 Material balance of the Distillation 2.	77
Table 4.7 Collected fractions for the Distillation 3.....	77
Table 4.8 Material balance of the Distillation 3.	78
Table 4.9 Collected fractions for the Distillation 4.....	78
Table 4.10 Material balance of the Distillation 4.	79
Table 4.11 Collected fractions for the Distillation 5.....	79
Table 4.12 Material balance of the Distillation 5.	80
Table 4.13 Summarized Refractive Index data from every fraction from 5 distillations.	81
Table 4.14 Penetration Index values for the feed bitumen and vacuum residue.	82
Table 5.1 Assigned number (Fraction Identification Number (FIN)) and the temperature range of the mixed fractions.....	90
Table 5.2 Density of the 15 fractions with R^2 and slope of the line value.....	95
Table 5.3 Viscosity of the 15 fractions in mPa·s.....	96
Table 5.4 Refractive Index values for the 15 fractions with R^2 and slope of the line.	97
Table 5.5 Elemental Analysis of the 15 fractions.	98

Table 5.6 Blended fractions with assigned Blend Identification Number (BIN) expressed by wt.% of the two blended FIN.	102
Table 5.7 Refractive Index of the Blends designated by BIN with R ² and slope of the line value.	103
Table 5.8 Density of the Blends.....	104
Table 5.9 Viscosity of the Blends designated by BIN.....	105
Table 5.10 Values calculated from ASTM D341 – 20 ^{e1}	108
Table 5.11 Molecular Weight calculated from the Riazi extended formula for heavy hydrocarbons.	110
Table B.1 Refractive Index values of liquid products from Distillation 1.....	142
Table B.2 Refractive Index values of liquid products from Distillation 2.....	143
Table B.3 Refractive Index values of liquid products from Distillation 3.....	144
Table B.4 Refractive Index values of liquid products from Distillation 4.....	145
Table B.5 Refractive Index values of liquid products from Distillation 5.....	146
Table B.6 Complete Refractive Index data set for the 15 fractions.....	147
Table B.7 Complete data set of refractive index for the 14 blends by BIN.....	148

LIST OF FIGURES

Figure 2.1 A soaker visbreaking unit.....	9
Figure 2.2 Divergence of energies of the two spin states of an unpaired electron.	12
Figure 2.3 Stereomicroscope design and ray paths.....	14
Figure 2.4 Distillation profiles of oilsands bitumen and other oil samples.	16
Figure 2.5 Outline of feed processing in a petroleum refinery.	17
Figure 2.6 Bitumen distillation profile under conceptual different operating pressures.	19
Figure 3.1 Snapshot from the stereomicroscope for a mixture of bitumen with (a) hexadecane and (b) 1-undecene showing insoluble matter.	42
Figure 3.2 Snapshot from the stereomicroscope for a mixture of bitumen with (a) o-xylene, (b) indane, (c) benzenethiol, (d) tetrahydrofuran and (e) chloroform showing total solubility.	42
Figure 3.3 Snapshot from the stereomicroscope for a mixture of bitumen with (a) 1-decyne, (b) 1-tetradecyne, and (c)1-hexadecyne showing negligible amounts of insoluble matters.....	43
Figure 3.4 Electron spin resonance spectra of bitumen dissolved in three different solvents: styrene, THF (tetrahydrofuran) and methylene chloride.....	44
Figure 3.5 Correlation of the g-factor of the bitumen sample dissolved in various solvents with the dipole moment of the solvent.....	46
Figure 3.6 Correlation of the free radical content of the bitumen sample dissolved in various solvents with the molecular weight of the solvent.....	51
Figure 3.7 Correlation of the free radical content of the bitumen sample dissolved in various solvents with the dipole moment of the solvent.....	52
Figure 3.8 Correlation of the free radical content of the bitumen sample dissolved in various solvents with the dielectric constant of the solvent.	52
Figure 3.9 Correlation of the free radical content of the bitumen sample dissolved in various solvents with the density of the solvent.	53
Figure 3.10 Correlation of the free radical content of the bitumen sample dissolved in various solvents with the dynamic viscosity of the solvent.....	53
Figure 3.11 Correlation of the free radical content of the bitumen sample dissolved in various solvents with the kinematic viscosity of the solvent.....	54

Figure 3.12 Correlation of the free radical content of the bitumen sample dissolved in various solvents with the refractive index of the solvent.	54
Figure 3.13 Correlation of the free radical content of the bitumen versus the ionization potential of (a) all the solvents; (b) sulfur containing solvents. (c) diaromatic hydrocarbon solvents.	55
Figure 4.1 Mini Fractional Crude Oil Distillation System by B/R Instrument (edited)	69
Figure 4.2 Distillation curve.	81
Figure 4.3 Refractive Index values with the average difference expressed by error bars.	83
Figure 5.1 ESR spectrum of FIN 4.	99
Figure 5.2 ESR spectra of the 15 fractions.	101
Figure 5.3 Temperature-Viscosity chart for the first 7 fractions.	106
Figure 5.4 Temperature-Viscosity chart for FIN 1.	107
Figure 5.5 Linearization from ASTM D341 – 20 ^{e1} for FIN 4 as an example.	108
Figure 5.6 Fluidity dependence on molar volume.	111
Figure 5.7 Molar Volume Fluidity relationship for FIN 3 and FIN 15.	112
Figure 5.8 Refractive Index distribution for the FIN 8/FIN 15 blends.	112
Figure 5.9 Refractive Index distribution for the FIN 5/FIN 15 blends.	113
Figure 5.10 Refractive Index distribution for the FIN 10/FIN 15 blends.	114
Figure 5.11 Density distribution for the FIN 8/FIN 15 blends.	115
Figure 5.12 Density distribution for the FIN 5/FIN 15 blends.	115
Figure 5.13 Viscosity distribution for the blends FIN 5/FIN 15 (a) with pure FIN 15 (blue line), (b) without pure FIN 15	116
Figure 5.14 Viscosity distribution for the blends FIN 8/FIN 15.	117
Figure A.1 Distillation data of the 1 st day of Distillation 1 (Jul 14, 2020).	133
Figure A.2 Distillation data of the 2 nd day of Distillation 1 (Jul 15, 2020).	134
Figure A.3 Distillation data of the 3 rd day of Distillation 1 (Jul 16, 2020).	134
Figure A.4 Distillation data of the 1 st day of Distillation 2 (Jul 21, 2020).	135
Figure A.5 Distillation data of the 2 nd day of Distillation 2 (Jul 22, 2020).	135
Figure A.6 Distillation data of the 3 rd day of Distillation 2 (Jul 23, 2020).	136
Figure A.7 Distillation data of the 1 st day of Distillation 3 (Aug 11, 2020).	136
Figure A.8 Distillation data of the 2 nd day of Distillation 3 (Aug 12, 2020).	137
Figure A.9 Distillation data of the 3 rd day of Distillation 3 (Aug 13, 2020).	137

Figure A.10 Distillation data of the 1 st day of Distillation 4 (Aug 17, 2020).....	138
Figure A.11 Distillation data of the 2 nd day of Distillation 4 (Aug 18, 2020).....	138
Figure A.12 Distillation data of the 3 rd day of Distillation 4 (Aug 19, 2020).	139
Figure A.13 Distillation data of the 1 st day of Distillation 5 (Aug 20, 2020).....	139
Figure A.14 Distillation data of the 2 nd day of Distillation 5 (Aug 21, 2020).....	140
Figure A.15 Distillation data of the 3 rd day of Distillation 5 (Aug 22, 2020).	140
Figure A.16 Atmospheric distillation (Jul 20, 2020).	141

CHAPTER 1 – INTRODUCTION

1.1 Background

In Alberta, Canada oil sands bitumen has been the subject of much development. This heavy feedstock has also been available at lower prices because of its properties relative to conventional oil. Notably, the bitumen is too viscous to be transported by pipeline. Nevertheless, bitumen after refining is a source of liquid fuels and other products that are used in large quantities.¹ Considering Alberta's oil sands' proven reserves are equal to about 165.4 billion barrels (bbl),² or $2.6 \times 10^{10} \text{ m}^3$, the development is justified with a promising future.

One of the main aims of post-recovery processing bitumen is to reduce its viscosity. Viscosity reduction of bitumen takes place to enable pipeline transport. It can be implemented via dilution with a solvent or upgrading of the bitumen. In the case of dilution, the diluent must then be removed and either returned to the point of production for reuse in the pipeline or it must be used in the receiving refinery to make fuels. When it comes to upgrading, the main input is bitumen, whereas the output is a lighter crude oil with a potentially higher value.³

The work in this study is tied together by viscosity reduction of bitumen as a theme by investigating two different topics under it.

The first topic of study was an investigation dealing with a way to manipulate thermal conversion in visbreaking by changing the concentration of free radicals. Visbreaking (viscosity breaking) is a process of viscosity reduction that can be characterised as a mild form of thermal cracking. It was developed to reduce the viscosity of residua or bitumen to produce fuel oil that potentially meets pipeline specifications.⁴

Generally, free radical reactions that occur in thermal non-catalytic processes such as visbreaking lack the control that is evident (from product distribution) in catalytic processes. The efficiency and economics of thermal cracking reactions are based mainly on the achievement of maximum conversion while controlling the undesirable free radical reactions (such as free radicals addition reaction that results in the formation of a heavier product).⁵

Bitumen is known to initially contain free radicals. Because of that, during thermal conversion, homolytic bond dissociation is not the only factor in forming free radicals and initiating the

reaction.⁶ This indicates how important free radical chemistry is for thermal cracking. But still, little is known about the essence of the persistent free radicals species in oil sands bitumen. The structure in multinuclear aromatics could be one of the reasons behind bitumen containing persistent free radicals.⁷ Another reason may be a dynamic equilibrium between free radical pairs.⁸

As it is often with bitumen, empirical evidence shows that at room temperature persistent free radicals in bitumen affect thermally processed bitumen storage stability.⁹ The kinetics of bitumen visbreaking is also affected by the persistent free radicals when the temperature is lower than 400°C. In this case, persistent free radicals become the major contributors to the concentration of the free radicals present in that bitumen.¹⁰ Thus, radical pairs dissociation equilibrium could be potentially altered by dissociation promotion or inhibition with organic solvents. If the understanding behind mechanisms of the solvent effect on dissociation can be further advanced, it could be used to directly control the free radical content, for example, during visbreaking.

Recent research uncovered that solvent dilution has an effect on free radical content in materials obtained from bitumen.⁶ In the cited work,⁶ the free radical content was measured by electron spin resonance (ESR) spectroscopy. In this thesis, quantitative ESR spectroscopy will be used to study the effect of different solvents on the persistent free radical content specifically in bitumen at ambient temperature. Overall, this work on the impact of the bulk liquid medium on the free radical content is largely based on the learning from persistent free radicals findings.

The second topic of study was an investigation to deepen the understanding of viscosity reduction during visbreaking. The viscosity reduction is generally attributed to thermal cracking leading to a lighter product, and there are several empirical and semi-empirical descriptions for the viscosity of bitumen that relate viscosity to properties such as average boiling point or density.³ It appears that the viscosity descriptions of bitumen and that of the product from visbreaking bitumen are different.

A few studies investigated the description of viscosity after the thermal conversion of bitumen.^{11,12,13} They have been involved with developing semi-empirical relations and experimental models to predict the viscosity of heavy fractions. This study aims to look deeper into the physically meaningful correlations behind viscosity reduction.

Finally, correlations for viscosity and temperature dependence¹⁴ along with being robust often lack a comprehensive physical meaning behind it. Fractionation of bitumen will be employed with further fractions characterization to build a bigger picture of viscosity origins. This can help achieve multiple goals of improving the partial upgrading process by uncovering the physical meaning behind viscosity distribution based on boiling point and how properties such as molar volume are related to viscosity change.

1.2 Objectives

The objective of this thesis is to study the effect of solvents on free radical content in bitumen, perform fractional distillation of bitumen and analyse the physical properties of the obtained fractions.

1.3 Scope of work

This thesis takes three main approaches. The first approach (Chapter 3) is concerned with the effect of different solvents on free radical content in bitumen. The second (Chapter 4) gives practical information on Athabasca bitumen physical distillation in a laboratory setting. Third (Chapter 5), studies viscosity relations in the bitumen fractions and their blends. Chapter 2 demonstrates the necessary background for understanding the completed work. And Chapter 6 summarises the findings and proposes leads for future research in this area.

REFERENCES

- (1) Speight, J. G. *Heavy Oil Recovery and Upgrading*; Elsevier Science, 2019.
- (2) Alberta Energy. Oil sands facts and statistics <https://www.alberta.ca/oil-sands-facts-and-statistics.aspx>.
- (3) Gray, M. *Upgrading Oilsands Bitumen and Heavy Oil*; University of Alberta Press: Edmonton, 2015.
- (4) Speight, J. G. Visbreaking: A Technology of the Past and the Future. *Scientia Iranica* **2012**, *19* (3), 569–573. <https://doi.org/10.1016/j.scient.2011.12.014>.
- (5) Speight, J. G. Chapter 10 - Fouling During Thermal Processes; Gulf Professional Publishing: Boston, 2015; pp 237–269. <https://doi.org/10.1016/B978-0-12-800777-8.00010-3>.
- (6) Tannous, J. H.; de Klerk, A. Quantification of the Free Radical Content of Oilsands Bitumen Fractions. *Energy & Fuels* **2019**, *33* (8), 7083–7093. <https://doi.org/10.1021/acs.energyfuels.9b01115>.
- (7) Zhang, Y.; Siskin, M.; Gray, M. R.; Walters, C. C.; Rodgers, R. P. Mechanisms of Asphaltene Aggregation: Puzzles and a New Hypothesis. *Energy & Fuels* **2020**, *34* (8), 9094–9107. <https://doi.org/10.1021/acs.energyfuels.0c01564>.
- (8) Alili, A. S.; Siddiquee, M. N.; de Klerk, A. Origin of Free Radical Persistence in Asphaltenes: Cage Effect and Steric Protection. *Energy & Fuels* **2020**, *34* (1), 348–359. <https://doi.org/10.1021/acs.energyfuels.9b03836>.
- (9) Yan, Y.; C. Prado, G. H.; de Klerk, A. Storage Stability of Products from Visbreaking of Oilsands Bitumen. *Energy & Fuels* **2020**, *34* (8), 9585–9598. <https://doi.org/10.1021/acs.energyfuels.0c01899>.
- (10) de Klerk, A. Thermal Conversion Modeling of Visbreaking at Temperatures below 400 °C. *Energy & Fuels* **2020**, *34* (12), 15285–15298. <https://doi.org/10.1021/acs.energyfuels.0c02336>.
- (11) Dente, M.; Bozzano, G.; Bussani, G. A Comprehensive Program for Visbreaking Simulation: Product Amounts and Their Properties Prediction. *Computers & Chemical Engineering* **1997**, *21* (10), 1125–1134. [https://doi.org/10.1016/S0098-1354\(96\)00323-7](https://doi.org/10.1016/S0098-1354(96)00323-7).

- (12) Rueda-Velásquez, R. I.; Gray, M. R. A Viscosity-Conversion Model for Thermal Cracking of Heavy Oils. *Fuel* **2017**, *197*, 82–90. <https://doi.org/10.1016/j.fuel.2017.02.020>.
- (13) Marquez, A.; Schoeggl, F. F.; Taylor, S. D.; Hay, G.; Yarranton, H. W. Viscosity of Characterized Visbroken Heavy Oils. *Fuel* **2020**, *271*. <https://doi.org/10.1016/j.fuel.2020.117606>.
- (14) ASTM D341. Standard Practice for Viscosity-Temperature Equations and Charts for Liquid Petroleum or Hydrocarbon Products. 2020, pp 1–6.

CHAPTER 2 – LITERATURE REVIEW

The following literature review provides the necessary background to the work performed in this thesis. The covered topics are organized in a way of following the plan for the experimental parts of the two main topics.

Section A: General background on oilsands bitumen and thermal upgrading. (2.1, 2.2, 2.3).

Section B: Free radicals in thermal upgrading relevant to the study in Chapter 3. (2.3, 2.4, 2.5, 2.6). It starts with the discussion of the free radicals already present in bitumen, then free radicals formed by thermal conversion and then the use of ESR as a tool for the analysis of free radicals.

Section C: Viscosity of distillation fractions relevant to the study in Chapters 4 and 5 (2.7, 2.8). The description is given to bitumen and its distillation fractions and relations between their physical properties. Lastly, an introduction is given to the techniques used for analysis.

SECTION A

2.1 Oil sands bitumen

Bitumen is a heavy, viscous black crude obtained from oil sands in Canada. A major part of the oil sands deposits is located in north and eastern Alberta in an area of 50,000 square kilometers. There are four main deposits in Alberta, the largest ones being Athabasca and Cold Lake.¹ In October 2021, oil production in Alberta was 19 million cubic metres, of which, oil sands production composed 86%.²

One of the biggest challenges in bitumen recovery is separating oil, water and sand mixture. Methods such as mining and steam-assisted gravity drainage (SAGD) are implemented to extract bitumen from oil sands.¹ In the hot water separation process that is used for recovering bitumen from mined oilsands bitumen and water have almost the same density. Air is used for the flotation and then the froth (60% bitumen, 30% water, 10% minerals) is further separated.

2.2 Upgrading of oil sands bitumen

After bitumen is separated from oil sands it can be diluted with a solvent or its viscosity can be reduced through visbreaking to enable transportation and achieve further quality improvement. There are several requirements for bitumen physical and chemical characteristics to be eligible to be transported by a pipeline. Those requirements are met through a process called upgrading.³

Upgrading processes generally have a common goal of increasing the hydrogen-to-carbon ratio (H/C). This goal can be reached by rejecting carbon or adding hydrogen. This is a complex engineering decision and in a very broad sense, it involves deciding if additional investments are necessary to add hydrogen or are better to reject (for example produce coke during a high-temperature process) otherwise valuable carbon.⁴

Upgrading of bitumen by thermal cracking has the advantage of not requiring high pressure or expensive catalysts because the main principle of the process is in operation at high temperatures. Nowadays, processes of conversion by visbreaking or delayed coking are the most popular for bitumen and heavy oils. Considering economic attractiveness and innovations made in this field, these processes are predicted to stay relevant for a long time.⁵

2.2.1 Visbreaking

The main target of visbreaking is to reduce the viscosity of the bitumen. This gives it an advantage by only requiring mild conditions compared to other residue upgrading processes which are cheaper to establish since it does not necessarily require a large amount of chemical conversion to low boiling liquid products. There are some distillates produced during the process. Application for the distillates can be as a solvent for dilution of bitumen or in place of fuel if it did not reach a point of coking.⁵

Soaker visbreaking and coil visbreaking are the types of the process most widely used. They mainly differentiate by soaker type requiring longer residence time, provided in the soaker's vessel, but less heating at the coil outlet. While coil type, otherwise, requires a shorter residence type but a higher temperature at the coil outlet. Conditions for coil visbreaking are in the range of 455-510°C for temperature with 350-2050 kPa pressure and a short residence time.⁶

Figure 2.1 represents a flow diagram of a soaker visbreaking with residue as a feed. It should be noted that vapor and liquid phase products are produced as two different streams. The feed goes to a furnace where the feed temperature is increased and reaches a plateau with the coil outlet representing the highest temperature. Consequently, most of the conversion takes place in the soaker with some conversion inside the heater. The process is designed and manipulated in a way to achieve the desired viscosity reduction.⁵

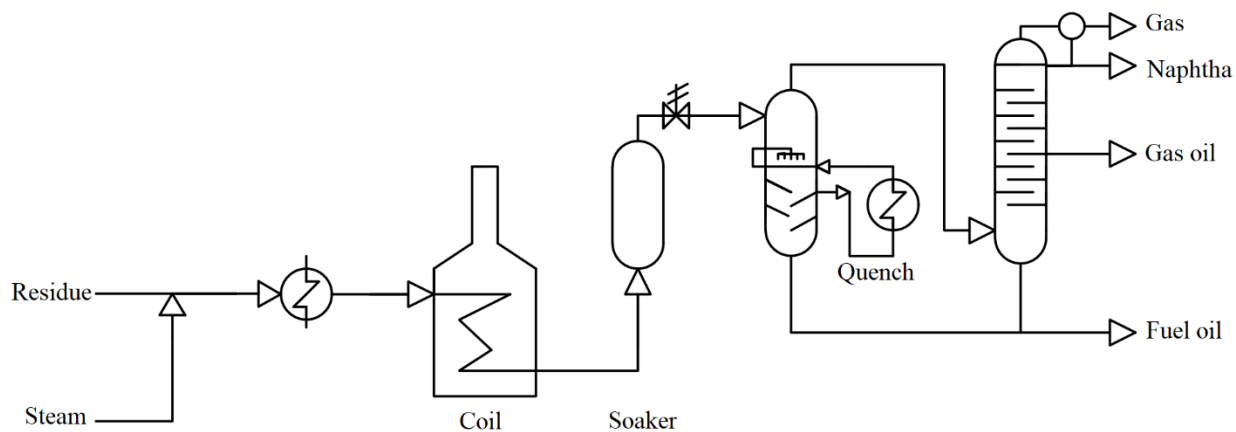


Figure 2.1 A soaker visbreaking unit.⁷

(Reprinted from de Klerk, A. Thermal Conversion in Upgrading Part II: Visbreaking. University of Alberta: Edmonton 2020, p 29., with permission from Elsevier).

SECTION B

2.3 Free radicals in bitumen

Oil sands bitumen is paramagnetic, which means that the bitumen has stable free radicals. The main method to investigate these free radicals is electron spin resonance (ESR).⁸ In the past studies on asphaltenes (they can be broadly described as a solubility class in bitumen) two types of free radicals were identified: the vanadium radical ion in the vanadyl porphyrin (VO^{2+} porphyrin) and ESR spectroscopically indistinguishable carbon free radicals. The structure of the free radicals is directly connected to the molecules they originated from. The free radical content in bitumen can be quantified and the free radicals were shown to be reactive despite their apparent persistence in bitumen.⁹⁻¹¹

A study, preceding this thesis, found that free radical content in Athabasca bitumen is 1.1×10^{18} spins/g.¹¹ One aspect in that work that required explanation was the observation that the measured free radical content of the bitumen-derived materials changed with solvent dilution. The origin of the observations did not appear to be related to the analytic procedure. Although a change in sample concentration affected liquid properties and thereby the ESR quality factor, an explanation based on a change in liquid properties was inconsistent with the observed reduction of the measured spin concentration.¹¹

Another observation from that study was that free radical content differed when different solvents were added even to the same material. It appeared to be related to the solvent's dipole moment in a way that the higher the dipole moment of the solvent the lower the free radical content of the sample is (for dilute solutions of asphaltenes ~0.4 wt.% and dilute solutions of bitumen 7-9 wt.%). For example, in one of the experiments, the free radical content of asphaltenes in toluene was about 4 times larger compared to the free radical content measured in dichloromethane, which has a larger dipole moment.¹¹ The change in free radical concentration could also be explained in terms of the impact of the solvent on the dissociation constant of radical pairs. These are observations that will be further explored in Chapter 3.¹⁰

2.4 Chemistry of thermal cracking

As was mentioned in the previous part, radical pairs dissociation equilibrium could be potentially altered by dissociation promotion or inhibition with organic solvents. If the understanding behind

mechanisms of the solvent's effect on dissociation can be further advanced, it could be used to directly control the free radical content, for example, during visbreaking. There are very promising potential applications in the chemical engineering process for the manipulation of cracking initiation.¹¹ Along with higher temperatures cracking, the notion of regulating free radical concentration through the bulk medium draws on the association-dissociation constant for radical pairs.

The theoretical basis behind the thermal conversion is that it takes place by a free radical mechanism. It can be illustrated by chain reactions with free radicals that act through basic three stages:¹²

1. Initiation: Breakage of a chemical bond in a molecule to form free radicals. It was also addressed that because of naturally occurring persistent free radicals in bitumen, sometimes initiation step is not necessary for cracking to take place due to the presence of persistent free radicals.¹²
2. Propagation: Once free radicals are formed, they react with other free radicals or molecules which results in even more free radicals. Propagation reactions repetitively take place.
3. Termination: During the end of a reaction free radicals react with each other to form a stable product.

In the chain process, propagation occurs many times for each bond broken. The formation of free radicals is energy-intensive and these active species are never present in high concentrations. However, the propagation reactions have much lower energy barriers than that of bond dissociation. The overall energy of the cracking reaction, therefore, is a composite of the initiation, propagation and termination reactions.³

2.5 Basic principles of electron spin resonance (ESR) spectroscopy

Giving a more in-depth summary of the ESR: “Electron spin resonance (ESR) or electron paramagnetic resonance (EPR) spectroscopy is a magnetic resonance technique commonly used in the detection of paramagnetic species” as defined by Villamena (2017).¹³ Here, an unpaired electron transitions between two spin states by absorbing radiation under an applied magnetic field.¹³ Due to an unpaired electron possessing a spin and a magnetic moment, two orientations are possible with magnetic quantum numbers $M_s+1/2$ and $M_s-1/2$. They define two energy states.¹⁴

A paramagnetic substance can be defined as a substance that has no magnetic moment if a magnetic field is not applied but gains the magnetic moment by being under an external magnetic field in the direction towards that field with the size defined as a function of the applied magnetic field.¹⁵ The principle of ESR spectroscopy lays in the Zeeman effect. It's an interaction between the magnetic moment of an unpaired electron and an external magnetic field which results in the splitting of the unpaired electron's energy levels.¹⁶

To measure ESR chemical shifts a concept of the g factor is used, which will be explained later on. Its behaviour is independent of the field. In the ESR spectrum, large spin-spin splitting occurs which is designated as hyperfine interactions and measured in gauss.¹⁴

Since a single unpaired electron has only two energy states, a lower energy state is defined as when the moment of the electron (μ) is aligned towards the magnetic field and higher energy when μ is aligned against the magnetic field. During the scanning of the magnetic field, divergence occurs between the energies of the two spin states. Consequently, resonance is when the absorption of energy by the spins takes place and the magnetic field with the energy difference between the two electron spins equals $h\nu$ (Figure 2.2).¹⁷

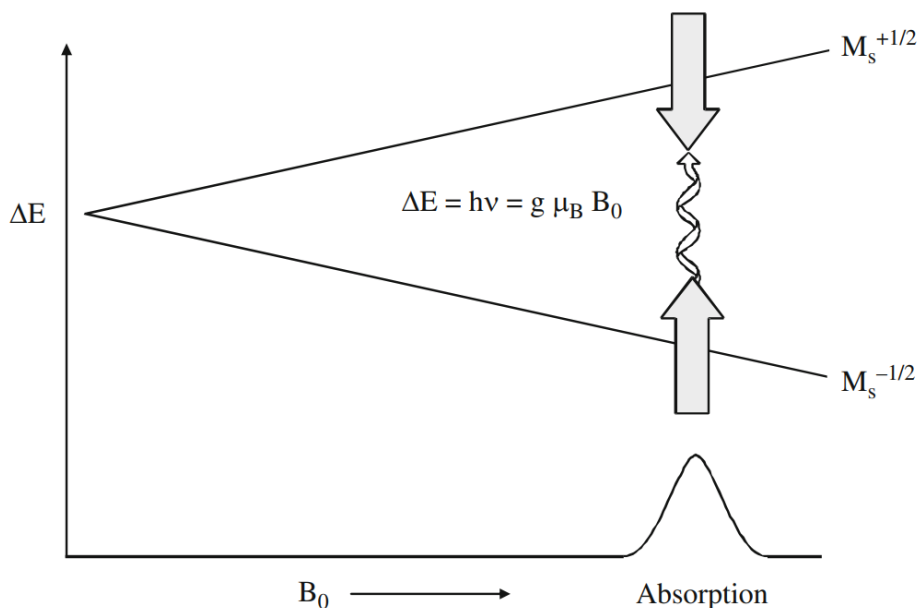


Figure 2.2 Divergence of energies of the two spin states of an unpaired electron.¹⁷

(Reprinted by permission from Springer Nature: Eaton, G. R.; Eaton, S. S.; Barr, D. P.; Weber, R. T. Quantitative EPR; Springer Vienna: Vienna, 2010).

2.5.1 ESR Quantification

Since the scanning of microwave frequency is not as straightforward, most ESR spectrometers perform scanning for the magnetic field keeping the microwave frequency constant. The microwave frequency of Active Spectrum micro-ESR is 9.68×10^9 Hz. The Landé g -factor, which is independent of the microwave frequency, and hence independent of the spectrometer used, is a good tool for comparison amongst several samples. Most commonly, g -factor is calculated using Equation 1.1:¹⁸

$$g = \frac{h \times \nu}{\mu_B \times B_0} \quad (\text{Equation 2.1})$$

g is the g -factor, h is the Planck's constant = 6.626×10^{-34} J/s, ν is the microwave frequency of the ESR = 9.68×10^9 Hz, μ_B is the Bohr magneton = 9.273×10^{-28} J/Gauss and B_0 is the magnetic field in Gauss.

The intersection of the hyperfine line with the x-axis gives the value of the magnetic field that is to be plugged into the equation to calculate the g -factor. Then g -factor can be normalized using the g -factor value of a standard run (for example, DPPH in Arabinose).

2.6 Stereomicroscopy

Because this part of the work is focused on the impact of bulk liquid medium (organic solvent) on the free radical content in bitumen, a practical challenge occurred is the insufficient data in the literature about what solvents are able to dissolve oil sands bitumen. While generating the data during experimental work it was decided to simultaneously check the prepared samples under a stereomicroscope. The findings are summarized in the Results and Discussion sections of Chapter 3. Here, the theoretical background of the technique is provided.

Generally, stereomicroscopes use reflected light for the sample examination. Their application is most useful when three-dimensional observation is necessary while also keeping the perception of depth and contrast to characterize the sample's structure. In essence, stereomicroscope has two microscopes, with directions offset by about $8-10^\circ$ to produce an image that's laterally correct with a good depth perception.¹⁹

The most widely used design for a stereomicroscope nowadays is the common main objective design. It produces the light as a parallel bundle by the optical path between the body and

microscope and has sufficient light-gathering power. The stereo effect arises from the tilted beam path of the two telescope ray paths after leaving the objective (Figure 2.3).¹⁹

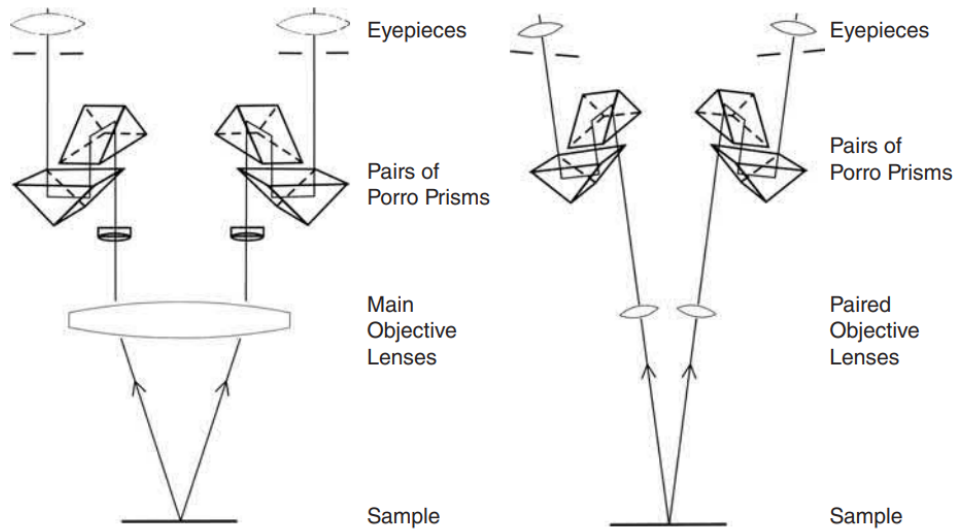


Figure 2.3 Stereomicroscope design and ray paths.¹⁹

(Reprinted from Sanderson, J. Understanding Light Microscopy; RMS - Royal Microscopical Society; Wiley, 2019, with permission from John Wiley and Sons).

In this thesis, stereo microscopy was employed to detect insolubility in bitumen-solvent mixtures that appeared homogeneous.

2.7 Distillation of bitumen

The distillation curve for bitumen is illustrated as a function of temperature during a distillation process (Figure 2.4). It is important because it represents the fraction of the substance that can be distilled. The fraction itself is designated by weight or volume. The starting point of the distillation curve is the initial boiling point (IBP) and the end is the final boiling point (IBP). For bitumen, the final boiling point is sometimes also called the limiting temperature. In the literature, the limits are set to be about 524°C for vacuum distillation and 750°C for simulated distillation. ³ In practice, however, vacuum distillation limit is very difficult to achieve and requires specialized equipment and conditions.

ASTM International provides standard practices for conducting testing and distillation of oil samples. But because of how complex the bitumen samples are there is always variation. After the distillation curve, there is always a tail that indicates a range of compounds that do not fall under the nominal range. Boiling ranges and applications in refining and bitumen upgrading are shown in Table 2.1.³

Table 2.1 Boiling ranges in refining and bitumen upgrading.³

Name	Boiling range, °C	Uses
Naphtha	26-193	Reformed for gasoline or bitumen diluent
Kerosene	165-271	Jet fuel
Light gas oil (LGO)	215-321	Diesel fuel
Heavy gas oil (HGO)	321-426	Feedstock for catalytic cracker or hydrocracker
Vacuum gas oil (VGO)	426-565	Feedstock for catalytic cracker or hydrocracker
Vacuum residue	>524-565	Asphalt or feedstock for visbreaker, coker or hydroconversion unit

The distillation profiles of oil sands bitumen are continuous. As shown in Figure 2.4, Boduszynski proposed that the illustrated oil samples have continuous distillation profiles when reaching the

highest temperatures of the distillation and that as an approximation the distillation curve may be extrapolated.^{21, 22} From the distillation curve the comparison to conventional oil brands can be made, where can be seen that bitumen has a comparable profile for heavier boiling material, with the main difference being the shortage of lighter boiling materials.²¹

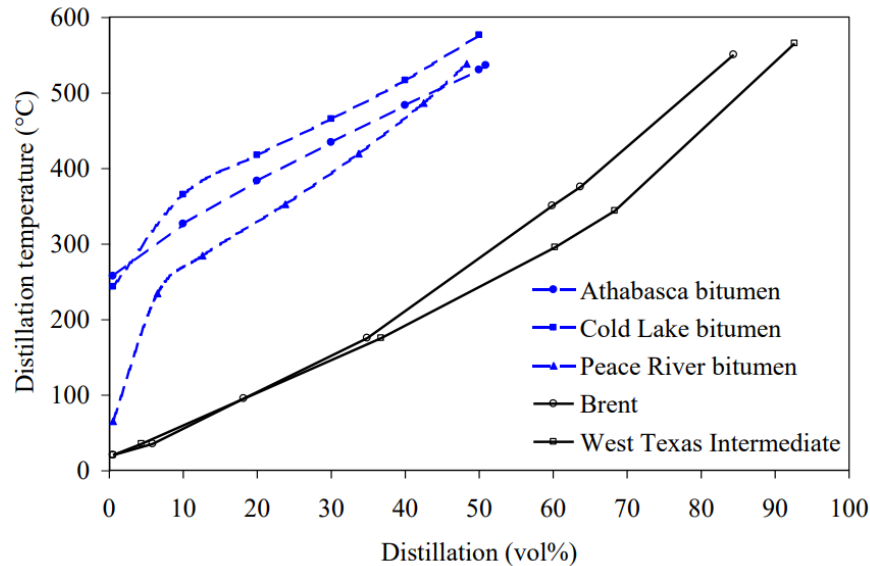


Figure 2.4 Distillation profiles of oilsands bitumen and other oil samples.²¹

(Reprinted from de Klerk, A. Unconventional Oil: Oilsands. In Future Energy; Letcher, T., Ed.; Elsevier, 2020; pp 49–65, with permission from Elsevier).

2.7.1 Industrial distillation of bitumen

If an oil refinery was designed in a way to process bitumen directly, it does not require the bitumen to be upgraded. It separates the feed by individual boiling fractions for treatment in the respective processing unit. Figure 2.5 represents in a simplified form the process's streams. It shows in what way the feed is blended and treated by defined capacity limits of the boiling range.²¹

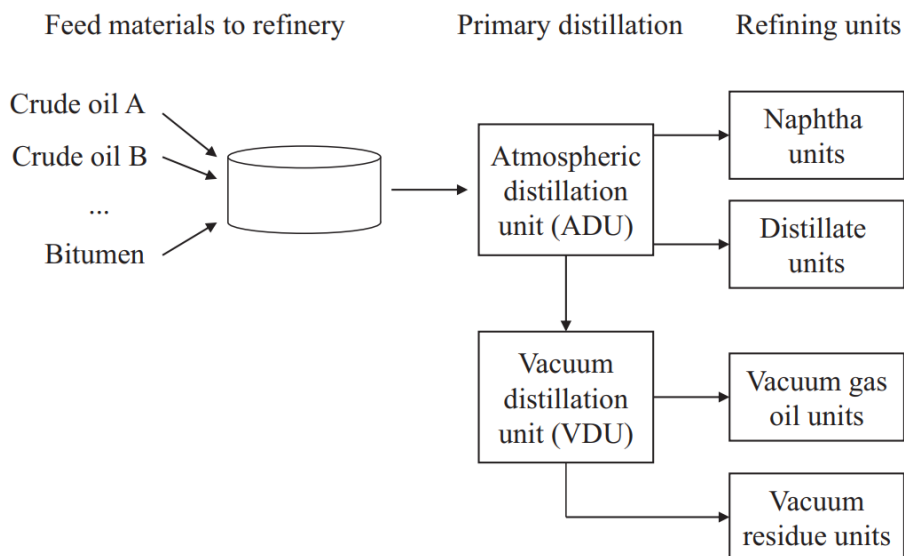


Figure 2.5 Outline of feed processing in a petroleum refinery.²¹

(Reprinted from de Klerk, A. Unconventional Oil: Oilsands. In Future Energy; Letcher, T., Ed.; Elsevier, 2020; pp 49–65. with permission from Elsevier).

As represented in Figure 2.5, about half of the bitumen feed is a vacuum residue with a boiling point higher than 525°C. Due to that, bitumen can only be marketed for processing to refineries with bitumen treatment capacity. It is processed with other petroleum feed to create a balanced blend considering the refinery units' capacity limits. In general, bitumen refining employs conventional crude oil processing technology with the main difference being the boiling point distribution of material.²¹

When employing bitumen upgrading, however, that process generates more light boiling fractions, reduced vacuum residue content and decreases heteroatom content (undesirable during refining). One of its main goals is to make bitumen fit the conventional petroleum distillation profile to a bigger extent. Upgrading makes bitumen more desirable for the market and lower viscosity allows pipeline transport. Boiling range distribution and decreased heteroatom content after upgrading compared to raw bitumen makes it less complicated for the refineries to process the bitumen and combine it with crude oil streams.²¹

2.7.2 Simulated distillation of bitumen

Distillation in a refinery distributes the process streams depending on the fractions' boiling ranges. Performing the distillation in practice resembles the refinery processes more accurately, but it is expensive and time-consuming for day-to-day quality checks. Simulated distillation (SimDist) by gas chromatography (GC) is an effective substitute for hands-on distillation in a distillation column. The operating principle of SimDist originates from the fact that hydrocarbons are eluted from the column in a boiling point range and full elution can be reached through a programmed temperature increase.²²

In general, a flame ionization detector acts in a way to detect a sample, while peak integration is completed through a predetermined time segment. Then, a mixture of standards is used to convert the time axis to a boiling point temperature range. Linear paraffin standards are most widely used for petroleum products to calibrate for temperature.²²

Due to the nature of GC methods, they are usually used when the collection of fractions is not necessary after the distillation curve is obtained. GC and distillation techniques are covered by ASTM standards. The most widely used SimDist methods are listed here:³

- ASTM D2887 involves simulated distillation by GC, with a sample size of ≤ 1 mL and is represented by a cumulative weight percent versus temperature that is based upon a calibration curve.
- ASTM D5307 is also a simulated distillation by GC, with a characteristic application being mainly for vacuum residue-rich samples. Here it means samples with boiling point temperatures higher than 524°C. The samples are injected two times with an added internal standard and by themselves.³

In the case of unachievable full elution, the boiling range distribution can be obtained from internal or external standards.²² Overall, the choice between SimDist and hands-on distillation depends on the implementation purpose, in general being if the focus on the distillation curve SimDist could be preferred and for the collection of fractions, physical distillation is preferred.

2.7.3 Vacuum distillation of bitumen

Atmospheric distillation techniques are able to cover only a small percentage of the bitumen distillation range. To extend the distillable fraction vacuum conditions are used (Figure 2.6).²³

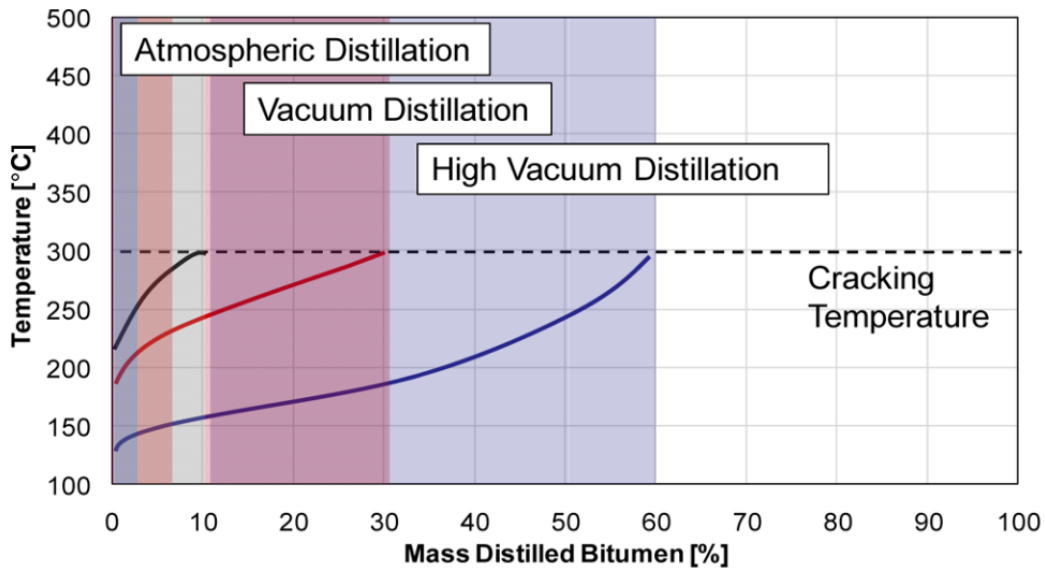


Figure 2.6 Bitumen distillation profile under conceptual different operating pressures.²³

(Reprinted with permission from Castellanos Díaz, O.; Sánchez-Lemus, M. C.; Schoeggel, F. F.; Satyro, M. A.; Taylor, S.D.; Yarranton, H. W. Deep-Vacuum Fractionation of Heavy Oil and Bitumen, Part I: Apparatus and Standardized Procedure. *Energy & Fuels* 2014, 28 (5), 2857–2865. Copyright 2014 American Chemical Society).

Figure 2.6 represents theoretical distillation curves of heavy oil under atmospheric, vacuum and high vacuum pressures. They stop before the temperature reaches the thermal cracking (about 300°C). After the cracking temperature chemical conversion takes place and the resulted compounds are different than the initial feed composition. Considering the limits, atmospheric distillation is usually able to reach 9 to 10 wt.% fractionation. By reducing the pressure, the boiling point temperatures of the feed are also decreased compared to their atmospheric equivalent boiling point temperatures. In that way, a larger portion of the sample can be distilled before the cracking temperature is passed. For example, following ASTM D1160 and the spinning band distillation, about 20-30 wt.% of heavy oil or bitumen can be fractionated at approximately 132 Pa (1 mmHg) absolute operating pressure.²³

2.8 Viscosity of bitumen

Viscosity is the frictional resistance that a moving fluid offers to an applied shearing force.⁸ Consequently, among all physical properties it can be called the most important for the movement

of liquids such as bitumen, oil and water. The viscosity behavior can be subdivided into Newtonian (when shearing force does not affect the frictional resistance) and non-Newtonian (the opposite).⁸

The characteristically high viscosity of bitumen prevents the application of conventional crude oil recovery methods and pipeline transport. Nevertheless, viscosity is highly dependent on temperature and decreases almost exponentially when the temperature increases. As was mentioned in the previous sections, another method to decrease the viscosity is with the addition of a solvent and partial upgrading. Also, colloidal dispersion in lower viscosity immiscible bulk matter can be applied for that purpose. In the Canadian oil sands industry, only dilution and upgrading are used as strategies to reduce bitumen viscosity to transport to the market.⁸

Dynamic (measurement unit Pa·s) and kinematic (measurement unit m²/s) are the viscosity types most widely used in the bitumen industry.

Another physical property that is important for the discussion in this thesis is the molecular weight which also increases with boiling point similar to viscosity and density.⁸ This thesis is concerned with physical properties affecting the relationship to find the best fitting explanation. For viscosity one of the best-known relationships between viscosity and the molecular weight is the empirical Mark-Houwink relationship:²⁴

$$\eta = KM^n \quad (\text{Equation 2.2})$$

where η is intrinsic viscosity, M is molecular weight, K and n are Mark-Houwink coefficients.²⁴

It is worthwhile to mention bitumen distillation fractions' physical properties separately from bitumen. The physical properties resemble that of crude oil distillation fractions. In this study, it was anticipated that the physical properties of the distillation fractions from bitumen and other crude oils would be comparable.

2.8.1 Practical Relationships in Viscosity of Bitumen

In engineering, practice viscosity is approached by applying predictive correlations. These correlations have been found empirically by conducting experiments. Seeton²⁵ gives an excellent review of the historical development of viscosity-temperature relations in the background of his paper.

Most commonly used in industry ASTM D341 – 20^{e1} presents the standard practice for predicting the viscosity of crude oil and bitumen cuts. The current viscosity-temperature equation derived by MacCoull has a general relationship as follows:²⁶

$$\log\log(Z) = A - B \log(T) \quad (\text{Equation 2.3})$$

where:

$$Z = v + 0.7 + \exp(-1.47 - 1.84 v - 0.51 v^2) \quad (\text{Equation 2.4})$$

and:

$$v = [Z - 0.7] - \exp(-0.7487 - 3.295 [Z - 0.7] + 0.6119[Z - 0.7]^2 - 0.3193[Z - 0.7]^3) \quad (\text{Equation 2.5})$$

where:

log = logarithm to base 10,

Z = defined in Equation 2.4,

A and B = constants,

T = temperature, K (or t + 273.15, where t is °C),

v = kinematic viscosity, mm²/s (or cSt).²⁶

This standard credits MacCoull with the log-log equation with an additive constant used in constructing his charts. The methodology of a chart based blending rule is presented as previously being applied to the MacCoull chart and an example of two hydrocarbons (gasoline and oil) is illustrated to determine a mixture viscosity.²⁵

Centeno et al.²⁷ summarized 26 mixing rules and divided them into distinctive groups by various properties.²⁸ They concluded that it is very challenging to predict viscosity for heavy feedstock and a better mixing rule is still needed.²⁷ In physical terms as opposed to a purely empirical description, Hildebrand employed molal (molar) volume for the calculation mixing rules with viscosity blending index.²⁹

$$1/\eta = B[(V - V_0)/V_0] \quad \text{Equation 2.6}$$

where η is the viscosity and V is the molal volume.²⁹

Hildebrand²⁹ commented that viscosity is possibly not directly related to temperature, but related to temperature through the change in molar volume. This would give some physical meaning to viscosity because a decrease in the molar volume would increase the frequency of interaction (sort of "friction") that would increase the viscosity. Thus, one would expect the temperature relationship to viscosity to be similar to the temperature relationship to the molar volume of the liquid.

These different viscosity relationships will be tested in this thesis, by viscosity versus temperature data and evaluation of different postulates/formulations of viscosity versus temperature and blending relationships. To make this possible, from density and the boiling range, an assumption has to be made about the average molar mass. For example, this is necessary if the goal is to test molar volume versus temperature dependence.

In this thesis, it was decided to use the equation by Riazi which can fit heavy hydrocarbon with a molecular weight of about 700 (Equation 2.6):³⁰

$$M = 4.965[\exp(2.097 \times 10^{-4}T_b - 7.78712SG + 2.08476 \times 10^{-3}T_bSG)]T_b^{1.26007}SG^{4.98308}$$

Equation 2.7

where M is molecular weight, T_b is the boiling point and SG is specific gravity.³⁰

2.8.2 Density

In this thesis, density will be used to evaluate the data along with the viscosity. The relationships will be checked with the goal to uncover additional physical meaning. It can be said that it is one of the main physical properties in bitumen upgrading along with viscosity.

The density measurement unit is g/cm³ or kg/m³.⁸ It is particularly important in the oil and gas industry (including bitumen) because oil is sold by volume rather than mass. Specific gravity is the main method of density measurement in the petroleum industry with the definition temperature 15.6°C. API (American Petroleum Institute) defined additional scale for the specific gravity calculation:¹

$$^{\circ}\text{API} = \frac{141.5}{\text{specific gravity at } 60^{\circ}\text{F}} - 131.5 \quad (\text{Equation 2.8})$$

API gravity is an inverse value to specific gravity.¹

Table 2.2 API gravity distribution.¹

Fraction	API gravity
Condensates	50–60°
Light Crudes	30–50°
Medium crude	20–30°
Conventional heavy crude	10–20°
Unconventional heavy crude/bitumen	<10°
Vacuum residue	<5°

Aromaticity and specific gravity (both important for upgrading of bitumen) are connected to API gravity by an increase with the API gravity decrease.¹

A deeper outlook into the density assumes that in general, paraffinic compounds in hydrocarbons tend to have lower density while aromatic hydrocarbons tend to have higher density. Density is also a function connected to pressure by increasing along with pressure. However, the rise in slow increasing pressure from 0.1 to 100 MPa results in a 4% density increase.⁸ Overall, it can be said that the density of bitumen is a function of its molecular composition. But the challenge is that the molecular composition of bitumen is very complex and very hard to determine.³

2.8.3 Refractive Index

Refractive Index will be employed in this thesis in various ways, for example, to provide additional validity of mixing different fractions and to check the correlation with other experimentally obtained physical properties.

The refractive index (abbreviated to RI or indicated as letter “n”) is defined as:¹⁹

$$RI = \frac{\text{speed of light in vacuum (or air)}}{\text{speed of light in the medium}}$$

Sanderson defines the process of refraction as “the key physical process that gives rise to the bending, or refraction, of the light beam, is the slowing down of the light as it enters the denser medium.”¹⁹ In the calculations the speed of light in a vacuum is 299,792,458 m/s.¹⁹

REFERENCES

- (1) Banerjee, D. K. *Oil Sands, Heavy Oil and Bitumen - From Recovery to Refinery*; PennWell Corporation: Tulsa, 2012.
- (2) Government of Alberta. Oil Production
<https://economicdashboard.alberta.ca/OilProduction> (accessed Jan 2, 2021).
- (3) Gray, M. *Upgrading Oilsands Bitumen and Heavy Oil*; University of Alberta Press: Edmonton, 2015.
- (4) Speight, J. G. Refining Heavy Oil and Extra-Heavy Oil. In *Heavy and Extra-heavy Oil Upgrading Technologies*; Gulf Professional Publishing: Boston, 2013; pp 1–13.
- (5) Speight, J. G. Thermal Cracking. In *Heavy and Extra-heavy Oil Upgrading Technologies*; Elsevier: Boston, 2013; pp 15–38.
- (6) Speight, J. G. Visbreaking: A Technology of the Past and the Future. *Sci. Iran.* **2012**, *19* (3), 569–573.
- (7) de Klerk, A. Thermal Conversion in Upgrading Part II: Visbreaking. University of Alberta: Edmonton 2020, p 29.
- (8) Lown, E.; Strausz, O. *The Chemistry of Alberta Oil Sands Bitumens and Heavy Oils*; Alberta Energy Research Institute publication: Calgary, 2003.
- (9) Khulbe, K. C.; Mann, R. S.; Lu, B. C.-Y.; Lamarche, G.; Lamarche, A.-M. Effects of Solvents on Free Radicals of Bitumen and Asphaltenes. *Fuel Process. Technol.* **1992**, *32* (3), 133–141.
- (10) Alili, A. Persistent Free Radicals in Asphaltenes and Their Reactions, University of Alberta, 2019.
- (11) Tannous, J. H.; de Klerk, A. Quantification of the Free Radical Content of Oilsands Bitumen Fractions. *Energy & Fuels* **2019**, *33* (8), 7083–7093.
- (12) de Klerk, A. Thermal Conversion in Upgrading Part I. University of Alberta: Edmonton 2020, p 32.

- (13) Villamena, F. A. EPR Spin Trapping. In *Reactive Species Detection in Biology: From Fluorescence to Electron Paramagnetic Resonance Spectroscopy*; Elsevier: Boston, 2017; pp 163–202.
- (14) Roberts, J. D.; Caserio, M. C. *Basic Principles of Organic Chemistry*, 2nd ed.; Addison-Wesley world student series; W. A. Benjamin, 1977.
- (15) Abragam, A.; Bleaney, B. *Electron Paramagnetic Resonance of Transition Ions*; Dover Books on Physics and Chemistry; Dover Publications, 1986.
- (16) Senesi, N.; Senesi, G. S. *Electron-Spin Resonance Spectroscopy*; Elsevier: Oxford, 2005; pp 426–437.
- (17) Eaton, G. R.; Eaton, S. S.; Barr, D. P.; Weber, R. T. *Quantitative EPR*; Springer Vienna: Vienna, 2010.
- (18) Eaton, G. R.; Eaton, S. S.; Barr, D. P.; Weber, R. T. Basics of Continuous Wave EPR. In *Quantitative EPR*; Springer Wien New York, 2010; pp 1–3.
- (19) Sanderson, J. *Understanding Light Microscopy*; RMS - Royal Microscopical Society; Wiley, 2019.
- (20) Boduszynski, M. M. Composition of Heavy Petroleums. 1. Molecular Weight, Hydrogen Deficiency, and Heteroatom Concentration as a Function of Atmospheric Equivalent Boiling Point up to 1400 °F (760 °C). *Energy & Fuels* **1987**, *1* (1), 2–11.
- (21) de Klerk, A. Unconventional Oil: Oilsands. In *Future Energy*; Letcher, T., Ed.; Elsevier, 2020; pp 49–65.
- (22) Barman, B. N.; Cebolla, V. L.; Membrado, L. Chromatographic Techniques for Petroleum and Related Products. *Crit. Rev. Anal. Chem.* **2000**, *30* (2–3), 75–120.
- (23) Castellanos Díaz, O.; Sánchez-Lemus, M. C.; Schoeggel, F. F.; Satyro, M. A.; Taylor, S. D.; Yarranton, H. W. Deep-Vacuum Fractionation of Heavy Oil and Bitumen, Part I: Apparatus and Standardized Procedure. *Energy & Fuels* **2014**, *28* (5), 2857–2865.
- (24) Rubinstein, M.; Colby, R. H. *Polymer Physics*; Oxford University Press: Oxford, 2003.
- (25) Seeton, C. Viscosity-Temperature Correlation for Liquids. *Tribol. Lett.* **2006**, *22*, 67–78.

- (26) ASTM D341. Standard Practice for Viscosity-Temperature Equations and Charts for Liquid Petroleum or Hydrocarbon Products. 2020, pp 1–6.
- (27) Centeno, G.; Sánchez-Reyna, G.; Ancheyta, J.; Muñoz, J. A. D.; Cardona, N. Testing Various Mixing Rules for Calculation of Viscosity of Petroleum Blends. *Fuel* **2011**, *90* (12), 3561–3570.
- (28) Zhang, L.; Zhang, L.; Xu, Z.; Guo, X.; Xu, C.; Zhao, S. Viscosity Mixing Rule and Viscosity–Temperature Relationship Estimation for Oil Sand Bitumen Vacuum Residue and Fractions. *Energy & Fuels* **2019**, *33* (1), 206–214.
- (29) Hildebrand, J. H. Motions of Molecules in Liquids: Viscosity and Diffusivity. *Science* **1971**, *174* (4008), 490–493.
- (30) Riazi, M. R. *Characterization and Properties of Petroleum Fractions*; ASTM manual series MNL 50; ASTM International, 2005.

CHAPTER 3 – SOLVENT EFFECT ON THE FREE RADICAL CONTENT IN BITUMEN IN THE ABSENCE OF REACTION

Abstract

In oil industries, free radical chemistry becomes crucial when dealing with non-catalytic processes. In contrast to polymer synthesis, in thermal cracking processes, conducted at temperatures $> 350\text{ }^{\circ}\text{C}$, bond cleavage is favored, whereas molecular growth via addition reactions to form heavier products is undesirable. Unfortunately, information is available only in the broader sense of how parameters, like temperature, affect the free radical pairs in dissociation and recombination equilibrium, which affects the free radical concentration. In addition, it is not clear how the free radical concentration of persistent radicals is affected at ambient temperature, which is important for the storage stability of thermally processed bitumen.

In this study, Electron Spin Resonance (ESR) spectroscopy was used to generate data on how different solvents will affect the free radical content in bitumen by changing the dissociation equilibrium of radical pairs. The solubility of bitumen was checked in the 54 different solvents considered for the study prior to analysis to evaluate solubility. The effect of the solvents on the free radical content in bitumen was determined exclusively for solvents that were capable of dissolving the bitumen.

The g -factor and analyte spin content generated from the quantitative analysis of the ESR spectra were correlated with the solvents' properties like the dipole moment, dielectric constant, ionization potential, molecular weight, density, dynamic and kinematic viscosities. The g -factor of dissociated radical pairs was shifted depending on the dipole moment of the solvent. The higher the dipole moment, the more shifted is the g -factor. Surprisingly, the ionization potential of sulfur containing, monoaromatic and diaromatic solvents was linearly proportional to the free radical concentration observed. Free radical concentration was poorly correlated with the other solvent properties.

3.1. Introduction

Free radical reactions are most commonly used in the synthesis of polymers.^{1,2} In oil industries, free radical chemistry becomes crucial when dealing with non-catalytic processes. In contrast to polymers synthesis, in thermal cracking processes, conducted at temperatures $>350^{\circ}\text{C}$, homolytic bond cleavage is desirable, whereas molecular growth via addition reactions is undesirable. Therefore, equilibrium must be shifted in a way to favor chain transfer reactions over chain growth during propagation to avoid coke formation. The formation of coke in thermal processes has long been recognized as a major drawback that causes an increase in viscosity of the product as well as fouling and product instability.^{3,4}

The domination of chain transfer vs. chain growth in a free radical network of reactions is a function of the operating temperature, the free radical concentration in the solution, and the viscosity of the bulk liquid.

The effect of temperature on the formation of heavy compounds is well established in the literature.^{5, 6, 7, 8, 9, 10, 11} This, as well, reflects how the temperature plays a role in shifting the balance of reactions to favor either chain transfer or chain growth. The importance of the reaction equilibrium between radical pairs and their dissociation is highlighted by the studies that employ high-temperature ESR to track the free radical concentration change as a function of temperature in petroleum and coal processes.^{12, 13, 14} The free radical concentration of Venezuelan residua increased with temperature and reached a local maximum at a temperature of 230°C before decreasing until around 330°C after which it increased again.¹⁴ Between the temperatures of 230 – 330°C , it seems that enough hydrogen transfer takes place capping the free radical formed below 230°C . This is reflected as a decrease in the free radical content in the solution. Once new molecules are formed, homolytic bond dissociation starts taking place beyond 330°C , typical thermal cracking temperatures, and forms new free radicals.

Independently of temperature, it is also possible to limit chain growth reactions by decreasing the free radical concentration in the bulk liquid.¹¹ In thermal processes, free radical concentration can be decreased by supplying hydrogen gas at high pressures. If transferable hydrogen or methyl groups are abundant, the probability of a reactive radical to add to another bulky reactive radical is diminished. However, incorporating hydrogen into reactions is costly. An alternative solution is the use of hydrogen donor solvents,^{9, 15, 16, 17, 18} additives¹⁹ or maltenes/resins.^{20, 21, 22}

In low viscosity liquids where the radical recombination is controlled by the diffusion rate, the lifetime of free radicals is on the order of microseconds.²³ When bituminous samples were stored at room temperature, the viscosity increased with the storage time, whereas the free radical content decreased.²⁴ This implies free radical chain growth.

In addition to viscosity, the free radical concentration during a chemical reaction depends on the type of the solvent.^{25, 26, 27, 28, 29} There was a mention of it in literature by Russell et al.^{30, 31, 32, 33, 34, 35, 36, 37} that the polarity, dielectric constant and kinematic viscosities of the solvents may have an effect on specific free radical reactions for specific compounds.

Unfortunately, the literature cited gave information only in the broader sense of how these parameters affected the free radical pairs in dissociation and recombination equilibrium. In addition, it is not clear how the free radical content is affected at ambient temperature and in the absence of chemical reactions by the nature of the bulk liquid.

In a previous study on the quantification of free radicals in oil samples, it was observed that the free radical content in solution, at room temperature, may be dependent on the bulk liquid properties.³⁸ It is, thus, speculated that it may be possible to manipulate the free radical content, in the absence of a reaction and independently of temperature, by using different solvents. The aim of this study is to generate data on how different solvents will affect the free radical content in bitumen.

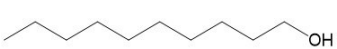
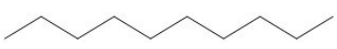
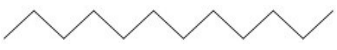
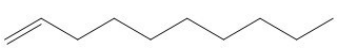
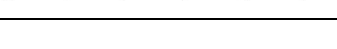
Prior to measuring the free radical content in bitumen, it was vital to identify what solvents are able to dissolve the bitumen. Hence, this study will also generate information on the solubility of bitumen in different randomly chosen solvents to represent a broad selection of compound classes. The effect of the solvents on the free radical content in bitumen was performed exclusively for solvents that were capable of dissolving the bitumen. Though this study may have implications for industrial applications, it was not tailored to answer such questions as to whether or not to co-feeding these solvents would be beneficial.

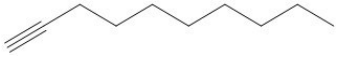
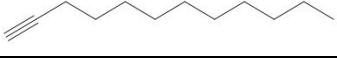
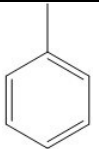
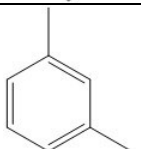
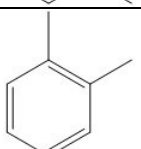
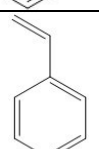
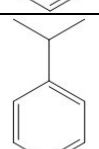
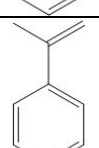
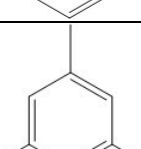
3.2. Experimental

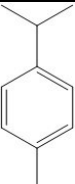
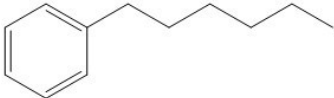
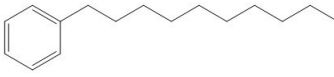
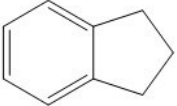
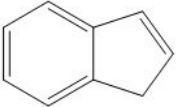
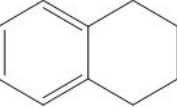
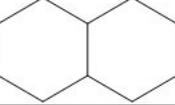
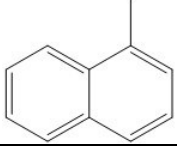
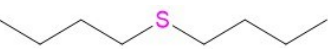
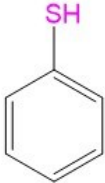
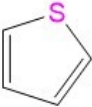
3.2.1 Materials

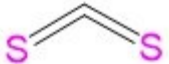
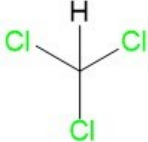
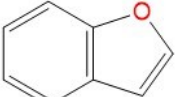
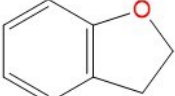
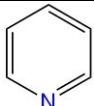
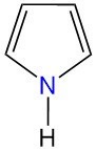
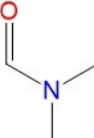
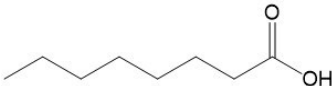
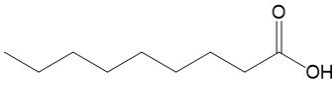
Several solvents were used for testing the change of free radical content in the ESR. The list of these solvents along with their purities and suppliers are listed in Table 3.1.

Table 3.1 Solvents used to dissolve the bitumen along with their purities and suppliers.

	Solvent Name	2-D Chemical Structure	Molecular Formula	CASRN ^a	Purity ^b	Supplier ^c
Alcohols	1-Hexanol		C ₆ H ₁₄ O	111-27-3	0.99	AA
	1-Heptanol		C ₇ H ₁₆ O	111-70-6	0.98	AO
	1-Octanol		C ₈ H ₁₈ O	111-87-5	0.99	SA
	1-Nonanol		C ₉ H ₂₀ O	143-08-8	0.98	SA
	1-Decanol		C ₁₀ H ₂₂ O	112-30-1	0.98	AA
Alkanes	Decane		C ₁₀ H ₂₂	124-18-5	0.99	SA
	Dodecane		C ₁₂ H ₂₆	112-40-3	0.99	SA
	Tetradecane		C ₁₄ H ₃₀	629-59-4	0.99	AA
	Pentadecane		C ₁₅ H ₃₂	629-62-9	0.99	SA
	Hexadecane		C ₁₆ H ₃₄	544-76-3	0.99	SA
Alkenes	1-Decene		C ₁₀ H ₂₀	872-05-9	0.94	SA
	1-Undecene		C ₁₁ H ₂₂	821-95-4	0.97	SA
	1-Dodecene		C ₁₂ H ₂₄	112-41-4	0.96	AA
	1-Tetradecene		C ₁₄ H ₂₈	1120-36-1	0.92	SA
	1-Hexadecene		C ₁₆ H ₃₂	629-73-2	0.94	AA

Alkynes	1-Decyne		C ₁₀ H ₁₈	764-93-2	0.98	SA
	1-Undecyne		C ₁₁ H ₂₀	2243-98-3	0.97	AA
	1-Dodecyne		C ₁₂ H ₂₂	765-03-7	0.98	SA
	1-Tetradecyne		C ₁₄ H ₂₆	765-10-6	0.97	SA
	1-Hexadecyne		C ₁₆ H ₃₀	629-74-3	0.9	AA
Monoaromatic hydrocarbons	Benzene		C ₆ H ₆	71-43-2	0.98	SA
	Toluene		C ₇ H ₈	108-88-3	0.999	FC
	<i>m</i> -Xylene		C ₈ H ₁₀	108-38-3	0.999	SA
	<i>o</i> -Xylene		C ₈ H ₁₀	95-47-6	0.99	FC
	Styrene		C ₈ H ₈	100-42-5	0.99	SA
	Cumene		C ₉ H ₁₂	98-82-8	0.98	AO
	α -Methylstyrene		C ₉ H ₁₀	98-83-9	0.99	SA
	Mesitylene		C ₉ H ₁₂	108-67-8	0.98	SA

	<i>p</i> -Cymene		C ₁₀ H ₁₄	99-87-6	0.99	SA
	n-Hexylbenzene		C ₁₂ H ₁₈	1077-16-3	0.98	AA
	1-Phenyldecane (Decylbenzene)		C ₁₆ H ₂₆	104-72-3	0.98	TCI
Diaromatic hydrocarbons	Indane		C ₉ H ₁₀	496-11-7	0.95	AO
	Indene		C ₉ H ₈	95-13-6	0.98	SA
	Tetralin		C ₁₀ H ₁₂	119-64-2	0.99	SA
	1,2-Dihydro-naphthalene		C ₁₀ H ₁₀	447-53-0	0.98	SA
Other hydrocarbons	Decalin		C ₁₀ H ₁₈	91-17-8	0.99	SA
	1-Methyl-naphthalene		C ₁₁ H ₁₀	90-12-0	0.95	SA
S compounds	Di- <i>n</i> -butyl sulfide		C ₈ H ₁₈ S	544-40-1	0.98	AA
	Benzenethiol		C ₆ H ₆ S	108-98-5	0.98	SA
	Thiophene		C ₄ H ₄ S	110-02-1	0.99	SA

	Tetrahydrothiophene		C ₄ H ₈ S	110-01-0	0.99	TCI
	Diphenyl sulfide		C ₁₂ H ₁₀ S	139-66-2	0.98	SA
	Carbon disulfide		CS ₂	75-15-0	0.999	FC
Cl compounds O compounds	Methylene chloride		CH ₂ Cl ₂	75-09-2	0.999	FC
	Chloroform		CHCl ₃	67-66-3	0.999	FC
	Tetrahydrofuran		C ₄ H ₈ O	109-99-9	0.996	FC
	2,3-Benzofuran		C ₈ H ₆ O	271-89-6	0.99	SA
	2,3-Dihydrobenzofuran		C ₈ H ₈ O	496-16-2	0.99	SA
	Pyridine		C ₅ H ₅ N	110-86-1	0.998	SA
N compounds	Pyrrole		C ₄ H ₅ N	109-97-7	0.975	SA
	N-methylpyrrolidine		C ₅ H ₁₁ N	120-94-5	0.97	SA
O+N comp.	N,N-dimethylformamide		C ₃ H ₇ NO	68-12-2	0.995	FC
Acids	Octanoic acid		C ₈ H ₁₆ O ₂	124-07-2	0.99	SA
	Nonanoic acid		C ₉ H ₁₈ O ₂	112-05-0	0.97	AO

^a CASRN = Chemical Abstracts Services Registry Number.

^b This is the purity of the material guaranteed by the supplier; the material was not further purified.

^c AA=Alfa Aesar; AO=Acros Organics; SA=Sigma Aldrich; FC=Fisher Chemicals; TCI= Tokyo Chemical Industry

These chemicals were used without further purification. The 54 solvents were chosen to be used in this study with the intent to ensure diversity. Solvents had different structures and belonged to different families: alcohols, alkanes, alkenes, alkynes, monoaromatic hydrocarbons, diaromatic hydrocarbons, other hydrocarbons as well as sulfur-containing compounds, chlorine-containing compounds, oxygen-containing compounds, nitrogen-containing compounds, oxygen- and nitrogen-containing compounds and acids. Alcohols, alkanes, alkenes, alkynes and acids were chosen to have at least 6 carbon atoms as bitumen may not be soluble in shorter chains.

The calibration of the ESR spectrometer was performed using 2,2-diphenyl-1-picrylhydrazyl (~90%, Sigma-Aldrich) in arabinose. Athabasca oilsands bitumen obtained from Suncor was used in this study. Water has been removed from the bitumen prior to conducting the ESR analyses. Water removal was part of another study performed and will not be discussed in the current work.

3.2.2 Equipment and procedures

In a 1 mL glass vial, around 30 mg of oilsands bitumen was weighed using a Mettler Toledo Balance XS105 with 0.01 mg readability. But the balance was set to 0.1 mg readability. Using a micropipette, 600 μ L of each solvent was added to the bitumen and the mixture was carefully shaken. Table 3.2 reflects the exact masses of samples tested as well as the analyte concentration. The concentration is shown in terms of mg bitumen/ml solvent rather than weight percent since the free radical content measurements are on a volume basis.

Table 3.2 The concentration of the bitumen samples tested for solubility in different solvents.

	Solvent Name	Mass of bitumen diluted (mg)	Analyte concentration (mg bitumen/ml solvent)
Alcohols	1-Hexanol	35.6	59.3
	1-Heptanol	36.2	60.3
	1-Octanol	39.4	65.7
	1-Nonanol	35.0	58.3

	Solvent Name	Mass of bitumen diluted (mg)	Analyte concentration (mg bitumen/ml solvent)
	1-Decanol	36.9	61.5
Alkanes	Decane	24.6	41.0
	Dodecane	39.4	65.7
	Tetradecane	34.0	56.7
	Pentadecane	31.3	52.2
	Hexadecane	33.2	55.3
Alkenes	1-Decene	31.9	53.2
	1-Undecene	39.0	65.0
	1-Dodecene	33.4	55.7
	1-Tetradecene	36.2	60.3
	1-Hexadecene	37.8	63.0
Alkynes	1-Decyne	31.9	53.2
	1-Undecyne	37.1	61.8
	1-Dodecyne	30.2	50.3
	1-Tetradecyne	30.5	50.8
	1-Hexadecyne	36.0	60.0
Monoaromatic hydrocarbons	Benzene	36.9	61.5
	Toluene	35.0	58.3
	<i>m</i> -Xylene	30.0	50.0
	<i>o</i> -Xylene	35.8	59.7
	Styrene	35.7	59.5
	Cumene	30.0	50.0
	α -Methylstyrene	32.3	53.8
	Mesitylene	31.0	51.7
	<i>p</i> -Cymene	39.9	66.5
	n-Hexylbenzene	33.5	55.8
	1-Phenyldecane	36.2	60.3
	Indane	33.9	56.5

	Solvent Name	Mass of bitumen diluted (mg)	Analyte concentration (mg bitumen/ml solvent)
Diaromatic hydrocarbons	Indene	38.2	63.7
	Tetralin	35.9	59.8
	1,2-	36.0	60.0
Other hydrocarbons	Decalin	31.7	52.8
	1-Methylnaphthalene	31.1	51.8
S compounds	Di- <i>n</i> -butyl sulfide	33.5	55.8
	Benzenethiol	31.1	51.8
	Thiophene	30.4	50.7
	Tetrahydrothiophene	30.4	50.7
	Diphenyl sulfide	37.9	63.2
	Carbon disulfide	32.8 ^a	54.6
Cl compounds	Methylene chloride	31.6 ^a	52.7
	Chloroform	37.1 ^a	61.9
O comp.	Tetrahydrofuran	33.3	55.5
	2,3-Benzofuran	30.8 ^a	51.3
	2,3-Dihydrobenzofuran	37.4	62.3
N compounds	Pyridine	31.5 ^a	52.4
	Pyrrole	35.5 ^a	59.1
	N-methylpyrrolidine	39.8	66.3
O+N comp.	N,N-dimethylformamide	31.2 ^a	52.0
Acids	Octanoic acid	38.1	63.5
	Nonanoic acid	34.2	57.0

^asamples were weighted with 0.01 mg readability and rounded to 0.1 mg readability.

A solubility check was performed prior to each analysis. The solubility of the bitumen in the solvent was first checked using the naked eye. The solvents that could not dissolve bitumen, and that could be seen to be insoluble by the naked eye, were not considered for analyses. The solvents in which bitumen appeared to be soluble were further inspected to confirm solubility using a Stereo Microscope. A drop of the mixture was placed on a glass microscope slide and examined under the light. Since the samples were mainly dark in color (bituminous mixture), a white background was used for better visualization of the solubility. Samples that were seen to be homogeneous under the microscope, were marked as soluble in the solvent and were further tested for free radical content. Those that showed insoluble matters were marked as partially soluble but were not further tested in the ESR.

Soluble samples were transferred with Fisherbrand® 9” Disposable Pasteur Pipets to PQ tubes: 5 mm-diameter medium wall quartz, 18 cm (7 inches) long, concentricity ± 0.0102 mm, camber ± 0.102 mm. In all instances, care was taken to fill the ESR tube used for analysis to a level that would ensure that the resonant cavity of the ESR was presented with the sample throughout the length of the tube in the resonant cavity.

3.2.3 Analyses

The free radical content in the products was measured using Active Spectrum benchtop extended range (Xband, 7000 Gauss) Micro-ESR. All measurements were performed at a microwave frequency of 9.68×10^9 Hz, 1.2 Gauss coil amplitude, a digital gain of 12 dB, and a microwave power of 15 mW. The analyses were the average of 7 scans with a sweep delay of 30 milliseconds between each scan. Analyses were conducted at the ambient temperature of 20 °C. All measurements were performed way below power saturation, where the relationship between power and response of the ESR is no longer linear. The phenomenon of saturation should be avoided during measurements in order to make sure quantification is valid. If the measurement time is less than the relaxation time of the radical, the radical will be saturated and thus, not detected.

The quantification of the free radical content into the number of spins per gram of sample was possible by the double integration of the first derivative ESR peak (i.e., the single integration of the absorption peak) using different calibration curves. The double integration was done using microESR software without base correction but with filtering done using Savitzky-Golay with a Gauss width of 4 and a polynomial order of 3.

ZEISS SteREO Discovery.V20 Motorized Stereo Microscope with 20:1 Zoom Range and a maximum resolution of up to 1000 LP/mm with PlanApo S 2.3x objective was used to check solubility. A snapshot of the mixture was taken and AxioVision Release 4.8.2 (06-2010) software by Carl Zeiss Microscopy was used to adjust the picture brightness and white level.

3.3 Results

3.3.1 Solubility of bitumen in different solvents

In order to check the effect of the bulk liquid on the free radical content, bitumen was chosen amongst the materials that are known to have large amounts of free radicals.³⁸ Unfortunately, the literature provides information only on some of the solvents that are able to dissolve bitumen or bituminous samples.³⁹ It was, thus, worthwhile generating data as a solubility check for bitumen.

Table 3.3 shows the solubility of bitumen in the different solvents used in this study. The concentration of bitumen in the solvents ranged between 50 and 60 mg bitumen/ml solvent as shown before (Table 3.2). This concentration was shown to be appropriate for the measurement of free radical content in our previous work.³⁸

Table 3.3 Solubility of bitumen in different solvents at a concentration of 50-60 mg bitumen/ml solvent.

	Solvent Name	Solubility Data		
		Completely soluble	Partially soluble	Insoluble
Alcohols	1-Hexanol			x
	1-Heptanol			x
	1-Octanol			x
	1-Nonanol			x
	1-Decanol			x
Alkanes	Decane			x
	Dodecane		x	
	Tetradecane		x	
	Pentadecane			x
	Hexadecane		x	
Alkenes	1-Decene		x	
	1-Undecene		x	
	1-Dodecene		x	
	1-Tetradecene			x

	Solvent Name	Solubility Data		
		Completely soluble	Partially soluble	Insoluble
	1-Hexadecene			x
Alkynes	1-Decyne		x ^b	
	1-Undecyne	x		
	1-Dodecyne	x		
	1-Tetradecyne		x ^b	
	1-Hexadecyne		x ^b	
Monoaromatic hydrocarbons	Benzene	x		
	Toluene	x		
	<i>m</i> -Xylene	x		
	<i>o</i> -Xylene	x		
	Styrene	x		
	Cumene	x		
	α -Methylstyrene	x		
	Mesitylene	x		
	<i>p</i> -Cymene	x		
	n-Hexylbenzene	x		
	1-Phenyldecane	x		
Diaromatic hydrocarbons	Indane	x		
	Indene	x		
	Tetralin	x		
	1,2-Dihydronaphthalene	x		
Other hydrocarbons	Decalin	x		
	1-Methylnaphthalene	x		
S comp.	Di- <i>n</i> -butyl sulfide	x		
	Benzenethiol	x		

	Solvent Name	Solubility Data		
		Completely soluble	Partially soluble	Insoluble
	Thiophene	x		
	Tetrahydrothiophene	x		
	Diphenyl sulfide	x		
	Carbon disulfide	x		
Cl compounds	Methylene chloride	- ^a		
	Chloroform	x		
O comp.	Tetrahydrofuran	x		
	2,3-Benzofuran	x		
	2,3-Dihydrobenzofuran	x		
N compounds	Pyridine	x		
	Pyrrole			x
	N-methylpyrrolidine	x		
O+N comp.	N,N-dimethylformamide			x
Acids	Octanoic acid			x
	Nonanoic acid			x

^aThe mixture seemed to be homogeneous under the microscope except for the droplets showing.

^bThe amount of insoluble matter in these samples is negligible.

Insoluble samples are samples that formed two phases and could be identified by the naked eye as a heterogeneous mixture.

Samples that, by the naked eye, seemed to form one phase but showed insoluble matter under the microscope, were classified as *partially soluble*. Figure 3.1 shows an example of two solvents in which bitumen was considered to be partially soluble.

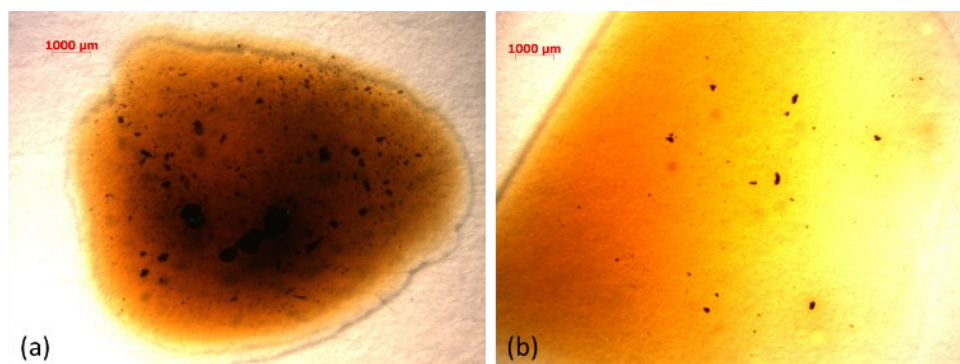


Figure 3.1 Snapshot from the stereomicroscope for a mixture of bitumen with (a) hexadecane and (b) 1-undecene showing insoluble matter.

Bitumen was considered to be *completely soluble* in samples that showed homogeneous texture under the microscope. Only samples that were completely soluble were further considered for free radical content measurements. Figure 3.2 shows an example of 5 solvents in which bitumen was considered to be completely soluble.

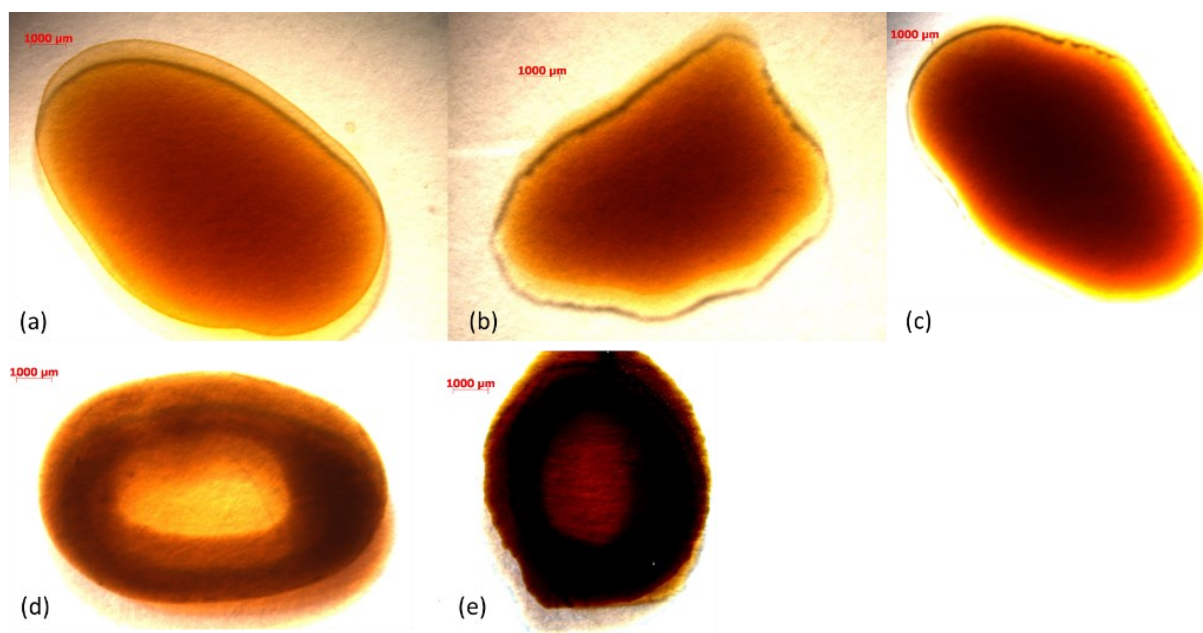


Figure 3.2 Snapshot from the stereomicroscope for a mixture of bitumen with (a) o-xylene, (b) indane, (c) benzenethiol, (d) tetrahydrofuran and (e) chloroform showing total solubility.

None of the alcohols or acids used in this study were able to dissolve the bitumen (Table 3.3). In addition to these two functional groups, it also seems that bitumen was not soluble in *n*-decane, *n*-

pentadecane, 1-tetradecene, 1-hexadecene, N,N-dimethylformamide and pyrrole. This will be further discussed in section 3.4.1.

Some of the alkanes, alkenes and alkynes were only able to dissolve the bitumen partially. This implies that a lower concentration of bitumen in these solvents may have formed a homogeneous mixture. However, this was not checked, because it was not within the scope of this study.

Solvents that were able to dissolve the bitumen only partially did not show consistent amounts of insoluble matter under the microscope. In other words, 1-decyne, 1-tetradecyne and 1-hexadecyne showed negligible amounts of insoluble matter (Figure 3.3) compared to other solvents in which bitumen was found to be partially soluble (see Figure 3.1).

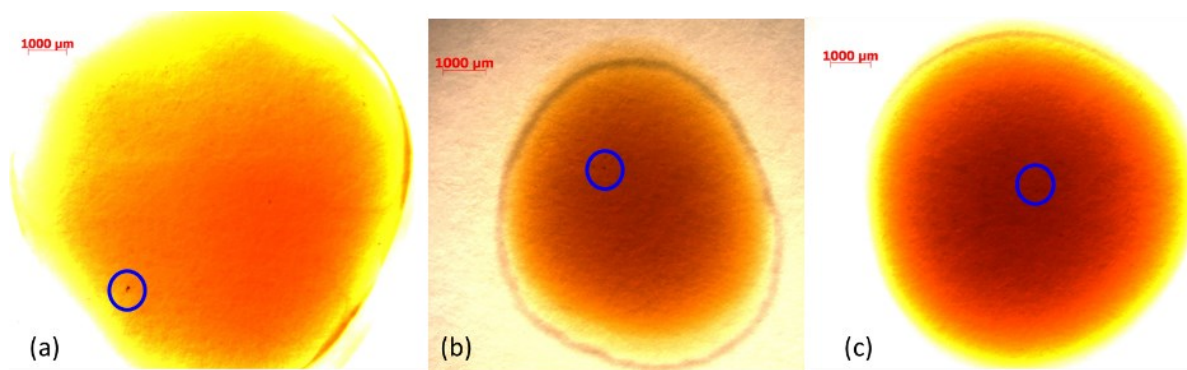


Figure 3.3 Snapshot from the stereomicroscope for a mixture of bitumen with (a) 1-decyne, (b) 1-tetradecyne, and (c) 1-hexadecyne showing negligible amounts of insoluble matters.

When we take a drop of a sample to be tested under the microscope, we are assuming that this drop represents the whole sample. Since the current study was not tailored to measure solubility, this assumption is made. It was, thus, worthwhile noting that the above-mentioned 3 solvents had minor insoluble matters compared to other solvents. However, this was not further investigated during the study.

Table 3.3 shows that all monoaromatic hydrocarbons, diaromatic hydrocarbons, other cyclic hydrocarbons and sulfur-containing compounds chosen in this study were able to dissolve the bitumen by forming a homogeneous mixture. In addition, methylene chloride, chloroform, tetrahydrofuran, 2,3-benzofuran, 2,3-dihydrobenzofuran, pyridine and N-methylpyrrolidine are solvents in which bitumen was completely soluble at the tested concentrations.

3.3.2 Effect of solvent properties on the g -factor

Solvents in which bitumen was completely soluble, as confirmed by the snapshots taken under the microscope, are considered for measurements in the ESR. Homogeneity of the sample is one of the requirements for ESR analyses for two reasons: (i) in the case of anisotropy, the sample cannot be tuned to adjust the phase of the magnetic field. Thus, a heterogeneous sample will fail to reflect similar properties in different directions and the instrument will not be able to tune; (ii) calculations of the free radical content are done on a volume basis such that the density of the mixture is assumed to be that of the solvent at low analyte concentrations. A heterogeneous sample will tend to form two phases that will make the density higher at the bottom of the tube and non-homogenous throughout.

For a valid comparison amongst the samples, the g -factor, which is independent of the microwave frequency, was calculated as described in Section 3.2.4.

Before quantification of the number of free radicals, the spectra collected for the various solvents were plotted. Figure 3.4 shows only 3 random solvents, namely styrene, tetrahydrofuran and methylene chloride. Upon inspection of the spectra obtained (Figure 3.4), three observations were made.

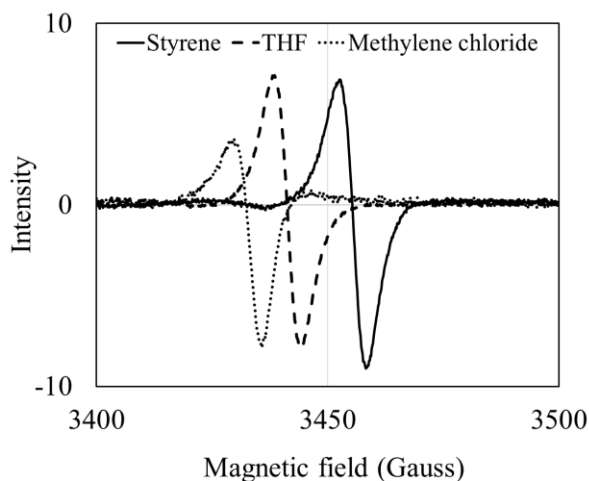


Figure 3.4 Electron spin resonance spectra of bitumen dissolved in three different solvents: styrene, THF (tetrahydrofuran) and methylene chloride.

The first observation was the broadness of the signal and the absence of hyperfine splitting. Though the signal reflects the interaction between the external magnetic field and the unpaired electron, the hyperfine splitting is due to the interaction between the nuclei and the unpaired electron. The absence of hyperfine splitting means that it is not possible to obtain information about the identity of the molecules.⁴⁰ The signal broadening is due to the overlap of different signals since bitumen is a complex mixture that contains a large amount of carbon-centered free radicals with different neighborhoods. Several factors including the molecular tumbling of micelles, the occurrence of *g*-anisotropy and the electron dipole-dipole interactions may lead to a lack of hyperfine splitting.⁴¹

The second observation is that all *g*-values were in the range of 2.002-2.020 that is characteristic of carbon-centered radicals. They usually have a *g*-factor value close to that of the “free electron” which is 2.0023 with a possible shift due to heteroatom content.⁴⁰ This outcome was anticipated since carbon-centered radicals are dominating in oil samples despite the presence of other free radical species like vanadium.^{38,41}

The third observation was that there was a shift in the value of the Landé *g*-factor for the different samples. This was noteworthy. Though the analyte was not modified in different samples (i.e. bitumen), there was an observable shift in the *g*-factor value of the samples with different solvents. Normalized values of the *g*-factor were calculated based on the *g*-factor value of the DPPH used as standard. The normalized values of the *g*-factor show that the shift in the *g*-factor was not attributed to an instrument artifact. Since the same analyte was used in all samples, the shift must be attributed to the properties of the solvent used. When the *g*-factor values were fitted against the dipole moment of the solvent, it was shown that these properties may be correlated (Figure 3.5). This correlation was independent of the category of the solvent as solvents in this graph were not sub-classified based on their functional groups.

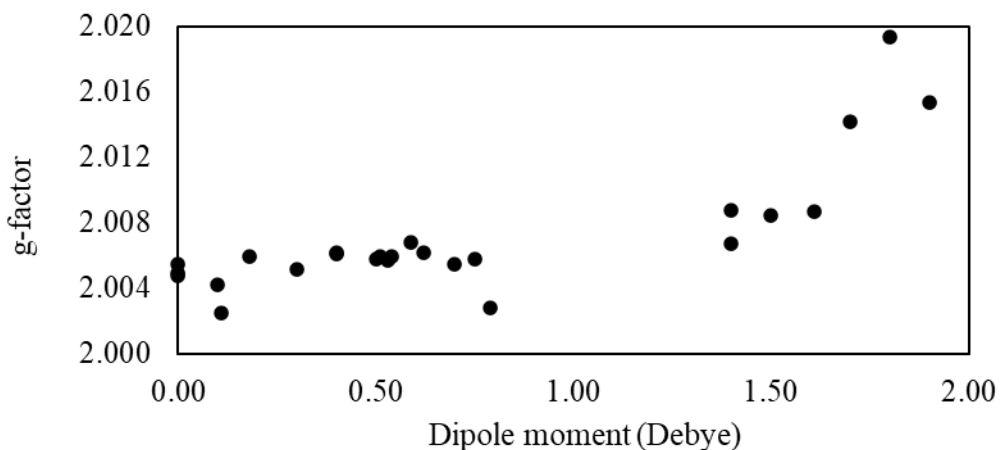


Figure 3.5 Correlation of the g-factor of the bitumen sample dissolved in various solvents with the dipole moment of the solvent.

3.3.3 Effect of solvent properties on the free radical content

The quantification of the free radicals in paramagnetic samples is possible by performing a single integration of the absorption peak to find the area underneath the curve. The signal in Figure 3.5 is the derivate of the absorption peak and hence requires a double integration. The quantification of the free radicals was done using DPPH as standard and using the calibration curves and equations (Equation 3.1) used in our previous study:³⁸

$$A_{\text{ESR}} = 0.26 \times 10^6 \cdot C_{\text{DPPH}}, r^2 = 0.993 \quad \text{Equation 3.1}$$

where A_{ESR} is the double integral value, and C_{DPPH} is the concentration of the calibration substance in $\mu\text{mol/mL}$.

It was found that the number of free radicals in the bituminous sample dissolved in different solvents was different (Table 3.4). All factors that may affect the signal like temperature as well as operating microwave power, microwave frequency and other properties were fixed amongst measurements. It is worthwhile noting that the spectrometer was not turned off or on before or after measurements since the measurements during the first hour of bridge warm-up are unreliable. Temperature largely affects the output of the detector crystal of the spectrometer which will affect the signal amplitude. In addition, there was no change in the microwave power before or after measurements to ensure an equilibrium response. Such change may affect the detector crystal temperature that may require extra time to reach the set value.⁴⁰

Since the analyte concentration and nature are not changed throughout the measurements, the change of free radical content must be attributed to the type of solvent used. In order to understand the reason for the difference of free radical content when varying the solvent, the properties of the various solvents including molecular weight, dipole moment, ionization potential, dielectric constant, dynamic viscosity, kinematic viscosity, density and refractive index were tabulated (Table 3.4). Some solvents characteristics were not available in the literature, though the solvents used in this study are common.

One of the important dielectric properties of the solvent is the loss tangent, also called the dissipation factor. The dissipation factor is related to the electrical properties of the material. It was, thus, clear from the literature that there was less interest in measuring such property for solvents. The dissipation factor was found to be 0.04 for toluene,⁴² 0.018 for *o*-xylene,⁴³ 0.091 for chloroform⁴⁴ and 0.047 for tetrahydrofuran.⁴⁴ There were no measured values for the rest of the solvents. The relation between the dissipation factor for the solvent and the free radical content will be further elaborated in Section 3.4.2.

Though bitumen appeared to be completely soluble in chloroform, 2,3-dihydrobenzofuran and pyridine, the samples did not lock on the ESR, reflecting anisotropy. This was a noteworthy observation reflecting that the ability of a solvent to dissolve the sample to be tested does not necessarily reflect isotropy.

Table 3.4 Solvents' characteristics and free radical content in bitumen sample dissolved in various solvents at the concentration of 50-60 mg bitumen/ml solvent.

Solvent Name		Solvent characteristics: MW – Molecular Weight, DM – Dipole Moment, IP – Ionization Potential, DC – Dielectric constant, DV – Dynamic Viscosity, RI – Refractive Index, n – Free Radical Content.							
		MW (g/mol)	DM (Debye)	IP (eV) ^d	DC (at 20- 25°C)	DV (cP)	Density (g/cm ³)	RI (nD)	n (×10 ¹⁸) (spins/g)
Alkyne	1-Undecyne	152	0.70	9.90	- ^a	2.00	0.773	1.431	0.85
	1-Dodecyne	166	0.70	9.90	- ^a	0.97	0.778	1.434	0.82
	Benzene	78	0.00[45]	9.23	2.40	0.61	0.876	1.497	0.81

Monoaromatic hydrocarbons	Toluene	92	0.40[45]	8.82	2.33	0.55	0.867	1.496	0.76
	<i>m</i> -Xylene	106	0.30[45]	8.56	2.30	0.58	0.860	1.497	0.94
	<i>o</i> -Xylene	106	0.50[45]	8.56	2.55	0.76	0.879	1.505	0.78
	Styrene	104	0.18[46]	8.48	2.42	0.71	0.909	1.546	0.77
	Cumene	120	0.40[47]	8.71	2.40	0.74	0.862	1.491	0.92
	α -Methylstyrene	118	0.75[48]	8.50	2.44	0.94	0.910	1.499	0.86
	Mesitylene	120	0.10[45]	8.42	2.40	0.62	0.864	1.497	0.91
	<i>p</i> -Cymene	134	0.00[45]	8.29	2.50	0.82	0.857	1.490	0.67
	<i>n</i> -Hexylbenzene	162	- ^c	9.80	2.30	1.64	0.861	1.486	0.90
	1-Phenyldecane	218	0.23	- ^a	2.40	2.47	0.858	1.482	0.85
Diaromatic	Indane	118	0.53[49]	8.50	2.30	0.97	0.965	1.537	0.81
	Indene	116	0.62[50]	8.14	2.87	1.76	0.997	1.595	0.68
	Tetralin	132	0.59[51]	8.45	2.77	1.98	0.970	1.541	0.80
	1,2-Dihydronaphthalene	130	1.40	8.26	- ^a	- ^a	0.997	1.582	0.70
Other	Decalin	138	0.00[45]	9.35	2.23	2.51	0.896	1.474	0.80
	1-Methylnaphthalene	142	0.51[51]	8.01	2.92	2.91	1.001	1.615	0.78
S compounds	Di- <i>n</i> -butyl sulfide	146	1.61	8.20	4.41	0.99	0.838	1.453	0.74
	Benzenethiol	110	1.40	8.30	4.38	1.25	1.073	1.588	0.72
	Thiophene	84	0.54	8.85	2.57	0.61	1.051	1.529	0.89
	Tetrahydrothiophene	88	1.90[45]	8.40	8.61	0.97	0.999	1.504	0.76
	Diphenyl sulfide	186	1.50	7.88	5.43	- ^a	1.113	1.633	0.63
	Carbon disulfide	76	0.11	10.08	2.64	0.37	1.266	1.627	1.44
Cl	Methylene chloride	85	1.80[45]	11.32	9.02	0.41	1.325	1.424	0.74
	Chloroform	119	1.10[45]	11.48	4.89	0.52	1.492	1.445	- ^b
O compounds	Tetrahydrofuran	72	1.70[45]	9.71	7.47	0.47	0.888	1.407	0.81
	2,3-Benzofuran	118	0.79	8.37	- ^a	- ^a	1.072	1.566	0.99
	2,3-Dihydrobenzofuran	120	- ^a	8.02	4.41	0.99	1.065	1.549	- ^b
N	Pyridine	79	2.30[45]	9.27	13.22	0.88	0.978	1.509	- ^b
	N-methylpyrrolidine	85	0.57	8.41	32.2	0.48	0.819	1.427	0.76

^[n] indicates source in the literature

^aValue not available in the literature.

^bSamples showing anisotropy and free radical content cannot be measured.

^cValue of 0.61 ± 1.08 Debye was reported in the literature⁵² reflecting uncertainty in the value of dipole moment for this compound.

^dAll ionization potential values were obtained by measurement using the photoelectron spectroscopy method except for alkynes that used photoionization electron spectroscopy and for 1,2-dihydronaphthalene that used the electron impact.

3.4. Discussion

3.4.1 Effect of the feed bulk liquid properties

The large difference in free radical content for the same analyte, that is bitumen, dissolved in different solvents was an interesting outcome. In addition, the shift in the g -factor had to be attributed to the type of solvent used. The effect of the solvent on the ESR signal, in general, was a topic discussed in the literature. There were differences observed in the nitrogen splitting for nitrobenzene anion radical when changing acetonitrile solvent to dimethylformamide or upon addition of water.⁵³ In another study, the proton splitting was remarkably affected when changing the nature of the solvent from ethanol-water solution to dimethyl sulfoxide (DMSO) solution. This was attributed to the shift from a protic to an aprotic solvent.⁵⁴

Hyperfine splitting was ascribed to the nature and strength of the radical-solvent interaction. It is well established that the unpaired electron does not only interact with the external magnetic field provided by the spectrometer but also with neighboring nuclei that have a magnetic moment. Since two different solvents will create two different radical-solvent complexes, the nature of the nucleus with which the radical is interacting is different.⁵⁴ The hyperfine splitting, which reflects the interaction between the radical and the nucleus is, thus, directly related to the electron spin density at the nuclei that have a nuclear spin.

Few other studies highlighted the effect of the solvent on the hyperfine splitting, e.g.^{55, 56, 57, 58, 59, 60}. In all these studies, the samples used were pure compounds and not complex mixtures like in the case of oilsands bitumen. Hyperfine splitting, in those cases, is visible and could be interpreted.

The hyperfine splitting is directly linked to the shift in the g -factor of the solvent. The analyte used in this study is a complex mixture of hydrocarbons. The single broad peak reflects several hyperfine lines overlapped. The correlation of dipole moment with the g -factor value (Figure 3.5) is thus now unambiguous with the explanation provided in the above-cited literature. The dipole moment, which arises from the differences in electronegativity, is a measure of the polarity of the solvent. The hyperfine coupling constant, which is a direct reflection of the extent of the delocalization of the unpaired electron over the molecule, was found to be affected by the polarity of the solvent used.⁶¹

However, the ability of the solvent to modify the ESR spectrum of the molecule seems to be exclusive to polar radicals. Non-polar radicals are not affected by the type of solvent used.⁶² In the current study, bitumen may contain both polar and non-polar radicals.

3.4.2 Effect of the feed bulk liquid properties on the free radical content

Table 3.4 illustrates the change of the free radical content of bitumen with the change of the solvent in the absence of a chemical reaction and at ambient conditions. Unfortunately, the body of literature used to explain the change in g-value in Section 3.4.1 did not specify whether the nature of the solvent affected the quantification of free radicals. A change in the g-value or hyperfine splitting does not necessarily imply a different amount of free radicals as the total integrated area, used for quantification, might stay intact.

For better visualization of the results and numbers in Table 3 and to better understand the reason for the variance in the free radical content for the same sample at ambient conditions and in the absence of a chemical reaction, graphs were plotted. There was no observable relationship between the free radical content in the bitumen sample and the molecular weight of the solvent used (Figure 3.6), nor with the dipole moment (Figure 3.7), dielectric constant (Figure 3.8), density (Figure 3.9), the dynamic viscosity (Figure 3.10) and the kinematic viscosity (Figure 3.11). The refractive index of the solvent showed no correlation with the free radical content (Figure 3.12) except for the diaromatic hydrocarbon solvents.

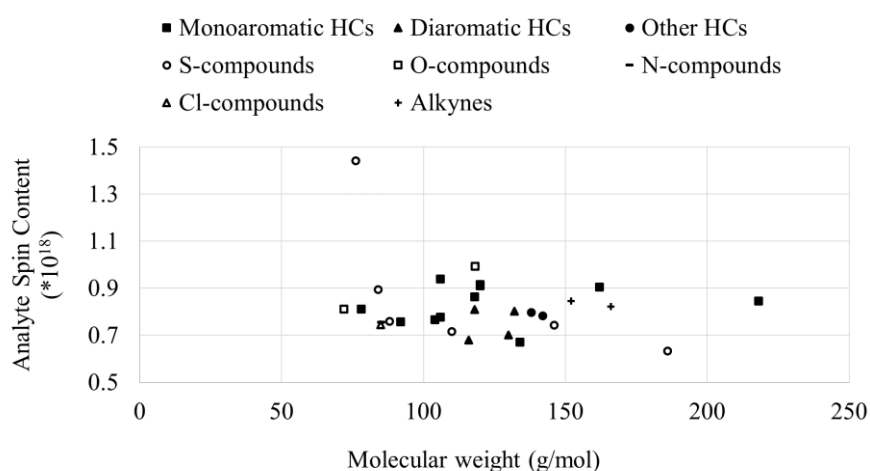


Figure 3.6 Correlation of the free radical content of the bitumen sample dissolved in various solvents with the molecular weight of the solvent.

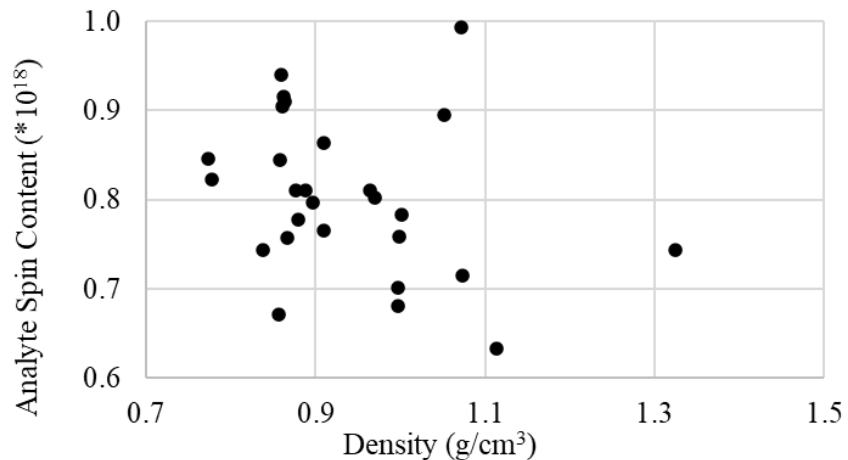


Figure 3.9 Correlation of the free radical content of the bitumen sample dissolved in various solvents with the density of the solvent.

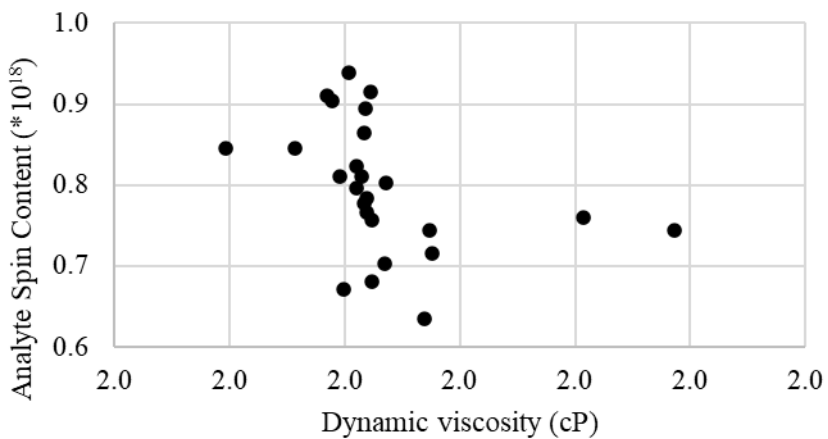


Figure 3.10 Correlation of the free radical content of the bitumen sample dissolved in various solvents with the dynamic viscosity of the solvent.

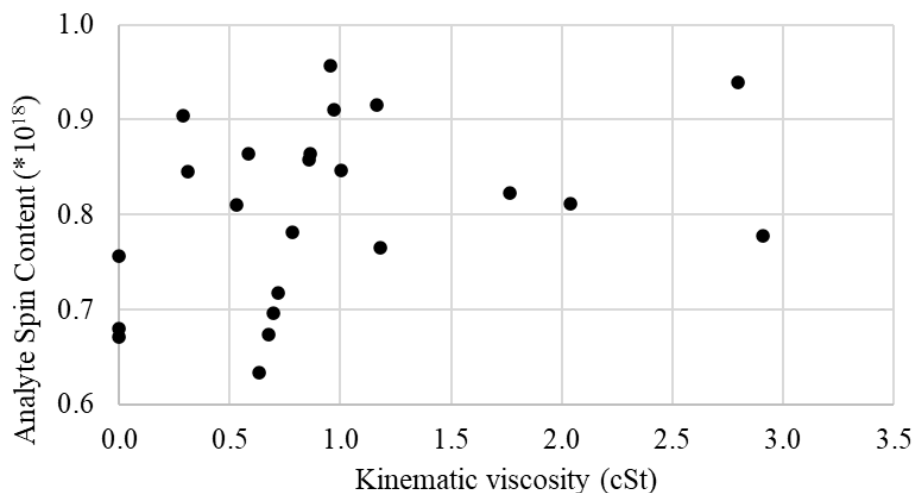


Figure 3.11 Correlation of the free radical content of the bitumen sample dissolved in various solvents with the kinematic viscosity of the solvent.

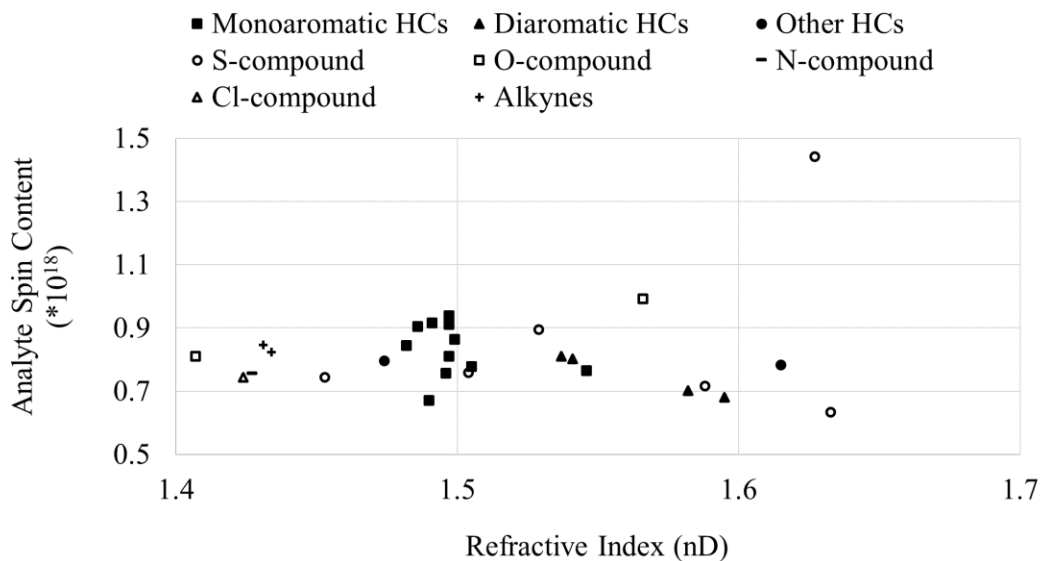


Figure 3.12 Correlation of the free radical content of the bitumen sample dissolved in various solvents with the refractive index of the solvent.

On another hand, when the free radical content of the bitumen was a plot against the ionization potential of the solvent, there was not one trend that could fit the data points for all the solvents (Figure 3.13a). However, there was an observable trend with sulfur containing solvents and diaromatic hydrocarbon solvents (Figure 3.13b and 3.13c).

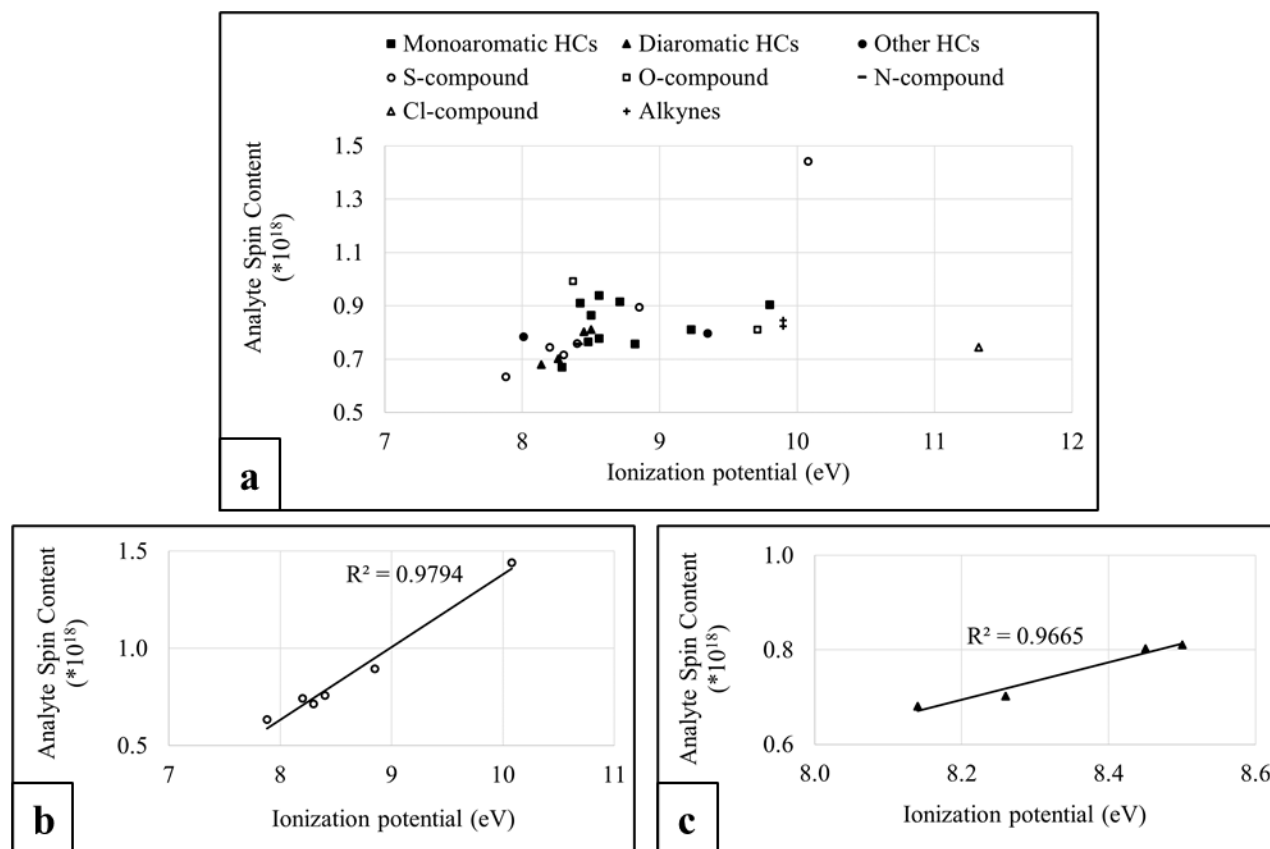


Figure 3.13 Correlation of the free radical content of the bitumen versus the ionization potential of (a) all the solvents; (b) sulfur containing solvents. (c) diaromatic hydrocarbon solvents.

The lines are indicative of the trend.

When tetramethyl-*p*-phenylenediamine and chloranil were mixed in the absence of a chemical reaction, it has been shown that the change of the bulk liquid properties from non-polar to more polar solvent lead to two different results; when a polar solvent was used with the mixture, Wurster's blue and chloranil free radicals were formed. Whereas this was not the case in the presence of a non-polar solvent.⁶³ However, the conclusions were elucidated based on a qualitative analysis that was grounded on the color change. In the case of bitumen, the dipole moment, which reflects the polarity of the solvent was not found to be correlated with the amount of free radicals present (Figure 3.7).

One of the factors that are known to affect the signal intensity is the dielectric properties of the solvent.⁴⁰ The dielectric properties include the dielectric constant and the dielectric loss tangent, also called the dissipation factor. It is postulated that the solvent's dielectric loss affects the

resonator quality factor (Q). While the solvent dielectric loss is related to the molecular motion, Q is characteristic of the ESR cavity and reflects how efficiently the microwave energy is stored in the cavity. A very interesting work by Dalal et. al⁶⁴ illustrates how the quality factor Q is affected by modifying the bulk liquid. 12 different solvents with different dielectric properties up to values of 37 were employed. It was found that lossy solvents (i.e. solvents with a high dielectric constant value) will lead to a shift in the detector current that, in turn, affects the amplitude of the hyperfine line resulting in significant errors in quantification. The dielectric properties of the solvent and the quality factor of the ESR resonator were found to be inversely proportional. There was also some relation between the quality factor Q and the integrated area of the signal intensity.⁶⁴ In the current study, tetrahydrothiophene, methylene chloride, tetrahydrofuran, pyridine and N-methylpyrrolidine have a large value of dielectric constant (>8) at 20-25°C. All other solvents used in this study have a dielectric constant of less than 5.5 (Table 3.4). Though the dielectric constant of the solvent could not be correlated with the free radical content in bitumen (Figure 3.8).

3.5 Conclusions

The qualitative conclusion of this study is that different solvents do affect free radical concentration in bitumen at ambient temperature, solvents addition to bitumen largely affects free radical content. In the same bitumen depending on added solvent analyte spin content ranges from 6×10^{17} to 1.5×10^{18} in the same bitumen sample. There is a general increase in g-factor which can be attributed to the solvent's dipole moment. The ionization potential of the solvents rises along with analyte spin content for sulfur and diaromatic hydrocarbons. It is important to note that physical properties such as dielectric constant, dipole moment, dynamic viscosity, kinematic viscosity, density, molecular weight were revealed to not correlate with the free radical content.

REFERENCES

- (1) Subramanian, H.; Landais, Y.; Sibi, M. P. Radical Addition Reactions. *Comprehensive Organic Synthesis: Second Edition* **2014**, *4*, 699–741. <https://doi.org/10.1016/B978-0-08-097742-3.00418-3>.
- (2) Giese, B. Synthetic Applications of Radical C-C Bond Forming Reactions. *Research on Chemical Intermediates* **1986**, *7* (1), 3–11.
- (3) León, A. Y.; Guzman, A.; Laverde, D.; Chaudhari, R. V.; Subramaniam, B.; Bravo-Suárez, J. J. Thermal Cracking and Catalytic Hydrocracking of a Colombian Vacuum Residue and Its Maltenes and Asphaltenes Fractions in Toluene. *Energy and Fuels* **2017**, *31* (4), 3868–3877. <https://doi.org/10.1021/acs.energyfuels.7b00078>.
- (4) Raseev, S. *Thermal and Catalytic Processes in Petroleum Refining*; Marcel Dekker: New York, 2003.
- (5) Thiyagarajan, P.; Hunt, J. E.; Winans, R. E.; Anderson, K. B.; Miller, J. T. Temperature-Dependent Structural Changes of Asphaltenes in 1-Methylnaphthalene. *Energy and Fuels* **1995**, *9*, 829–833. <https://doi.org/10.1021/ef00053a014>.
- (6) Nielsen, B. B.; Svrcek, W. Y.; Mehrotra, A. K. Effects of Temperature and Pressure on Asphaltene Particle Size Distributions in Crude Oils Diluted with N-Pentane. *Ind. Eng. Chem. Res.* **1994**, *33*, 1324–1330. <https://doi.org/10.1021/ie00029a031>.
- (7) Rahimi, P.; Gentzis, T.; Fairbridge, C.; Khulbe, C. Chemistry of Petroleum Residues in the Presence of H-Donors. *Preprints-American Chemical Society. Division of Petroleum Chemistry* **1998**, *43* (4), 634–636.
- (8) Harmony, J. A. K. Molecule-Induced Radical Formation. In *Methods in free-radical chemistry vol. 5*; Huyser, E. S., Ed.; Marcel Dekker, Inc: New York, 1974; pp 101–176.
- (9) Guo, A.; Wang, Z.; Feng, J.; Que, G. Mechanistic Analysis on Thermal Cracking of Petroleum Residue Using H-Donor as a Probe. *Preprints-American Chemical Society. Division of Petroleum Chemistry* **2001**, *46* (4), 344–347.

- (10) Guo, A.; Wang, Z.; Zhang, H.; Zhang, X.; Wang, Z. Hydrogen Transfer and Coking Propensity of Petroleum Residues under Thermal Processing. *Energy and Fuels* **2010**, *24* (5), 3093–3100. <https://doi.org/10.1021/ef100172r>.
- (11) Rahimi, P. M.; Gentzis, T. Thermal Hydrocracking of Cold Lake Vacuum Bottoms Asphaltene and Their Subcomponents. *Fuel Processing Technology* **2003**, *80* (1), 69–79. [https://doi.org/10.1016/S0378-3820\(02\)00223-0](https://doi.org/10.1016/S0378-3820(02)00223-0).
- (12) Yokono, T.; Obara, T.; Sanada, Y.; Shimomura, S.; Imamura, T. Characterization of Carbonization Reaction of Petroleum Residues by Means of High-Temperature ESR and Transferable Hydrogen. *Carbon* **1986**, *24* (1), 29–32.
- (13) Zhou, B.; Liu, Q.; Shi, L.; Liu, Z. Electron Spin Resonance Studies of Coals and Coal Conversion Processes: A Review. *Fuel Processing Technology* **2019**, *188* (March), 212–227. <https://doi.org/10.1016/j.fuproc.2019.01.011>.
- (14) Hernández, M. S.; Coll, D. S.; Silva, P. J. Temperature Dependence of the Electron Paramagnetic Resonance Spectrum of Asphaltenes from Venezuelan Crude Oils and Their Vacuum Residues. *Energy and Fuels* **2019**, *33*, 990–997. <https://doi.org/10.1021/acs.energyfuels.8b03951>.
- (15) Langer, A. W.; Stewart, J.; Thompson, C. E.; White, H. T.; Hill, R. M. Hydrogen Donor Diluent Visbreaking of Residua. *Industrial and Engineering Chemistry Process Design and Development* **1962**, *1* (4), 309–312. <https://doi.org/10.1021/i260004a014>.
- (16) Alemán-Vázquez, L. O.; Cano-Domínguez, J. L.; García-Gutiérrez, J. L. Effect of Tetralin, Decalin and Naphthalene as Hydrogen Donors in the Upgrading of Heavy Oils. *Procedia Engineering* **2012**, *42*, 532–539. <https://doi.org/10.1016/j.proeng.2012.07.445>.
- (17) Ignasiak, T. M.; Strausz, O. P. Reaction of Athabasca Asphaltene with Tetralin. *Fuel* **1978**, *57* (10), 617–621. [https://doi.org/10.1016/0016-2361\(78\)90191-6](https://doi.org/10.1016/0016-2361(78)90191-6).
- (18) Rahimi, P.; Gentzis, T.; Kubo, J.; Fairbridge, C.; Khulbe, C. Coking Propensity of Athabasca Bitumen Vacuum Bottoms in the Presence of H-Donors - Formation and Dissolution

of Mesophase from a Hydrotreated Petroleum Stream (H-Donor). *Fuel processing technology* **1999**, *60* (2), 157–170. [https://doi.org/10.1016/S0378-3820\(99\)00038-7](https://doi.org/10.1016/S0378-3820(99)00038-7).

(19) Clarke, P. F.; Pruden, B. B. Asphaltene Precipitation from Cold Lake and Athabasca Bitumens. *Petroleum Science and Technology* **1998**, *16* (3–4), 287–305. <https://doi.org/10.1080/10916469808949784>.

(20) Gould, K. A.; Wiehe, I. A. Natural Hydrogen Donors in Petroleum Resids. *Energy and Fuels* **2007**, *21* (3), 1199–1204. <https://doi.org/10.1021/ef060349t>.

(21) Wiehe, I. A.; Yarranton, H. W.; Akbarzadeh, K.; Rahimi, P. M.; Teclemariam, A. The Paradox of Asphaltene Precipitation with Normal Paraffins. *Energy and Fuels* **2005**, *19* (4), 1261–1267. <https://doi.org/10.1021/ef0496956>.

(22) Jamaluddin, A. K. M.; Nazarko, T. W.; Sills, S.; Fuhr, B. J. Deasphalted Oil - A Natural Asphaltene Solvent. *SPE Production & Facilities* **2007**, *11* (3), 161–165. <https://doi.org/10.2118/28994-pa>.

(23) Sosnovsky, D. V; Morozova, O. B.; Yurkovskaya, A. V; Ivanov, K. L. Relation between CIDNP Formed upon Geminate and Bulk Recombination of Radical Pairs. *J. Chem. Phys.* **2017**, *147*, No. 024303.

(24) Yan, Y.; Prado, G. H. C.; De Klerk, A. Storage Stability of Products from Visbreaking of Oilsands Bitumen.

(25) Sterck, B. De; Vaneerdeweg, R.; Prez, F. Du; Waroquier, M.; Speybroeck, V. Van. Solvent Effects on Free Radical Polymerization Reactions : The Influence of Water on the Propagation Rate of Acrylamide and Methacrylamide. *Macromolecules* **2010**, *43*, 827–836. <https://doi.org/10.1021/ma9018747>.

(26) Chen, H.; Wang, W.; Yang, Y.; Jiang, P.; Gao, W.; Cong, R.; Yang, T. Solvent Effect on the Formation of Active Free Radicals from H₂O₂ Catalyzed by Cr-Substituted PKU-1 Aluminoborate : Spectroscopic Investigation and Reaction Mechanism. *Applied Catalysis A, General* **2019**, *588*, 117283. <https://doi.org/10.1016/j.apcata.2019.117283>.

- (27) Herkes, F. E.; Friedman, J.; Bartlett, P. D. Peresters XIII. Solvent Effects in the Decomposition of t-Butylperoxy α -Phenylisobutyrate with Special Reference to the Cage Effect. *International Journal of Chemical Kinetics* **1969**, *1* (2), 193–207.
- (28) Bitzer, Z. T.; Goel, R.; Reilly, S. M.; Foulds, J.; Muscat, J.; Elias, R. J.; Richie, J. P. Effects of Solvent and Temperature on Free Radical Formation in Electronic Cigarette Aerosols. *Chem. Res. Toxicol.* **2018**, *31*, 4–12. <https://doi.org/10.1021/acs.chemrestox.7b00116>.
- (29) Holtomo, O.; Nsangou, M.; Fifen, J. J.; Motapon, O. DFT Study of the Effect of Solvent on the H-Atom Transfer Involved in the Scavenging of the Free Radicals \bullet HO₂ and \bullet O²⁻ by Caffeic Acid Phenethyl Ester and Some of Its Derivatives. *Journal of molecular modeling* **2014**, *20* (11), 2509. <https://doi.org/10.1007/s00894-014-2509-9>.
- (30) Russell, G. A. Solvent Effects in the Reactions of Free Radicals and Atoms. *Journal of the American Chemical Society* **1957**, *79* (11), 2977–2978.
- (31) Russell, G. A. Solvent Effects in the Reactions of Free Radicals and Atoms. II. Effects of Solvents on the Position of Attack of Chlorine Atoms upon 2,3-Dimethylbutane, Isobutane and 2-Deuterio-2-Methylpropane. *Journal of the American Chemical Society* **1958**, *80* (18), 4987–4996.
- (32) Russell, G. A. Solvent Effects in the Reactions of Free Radicals and Atoms. III. Effects of Solvents in the Competitive Photochlorination of Hydrocarbons and Their Derivatives. *Journal of the American Chemical Society* **1958**, *80* (18), 4997–5001.
- (33) Russell, G. A. Solvent Effects in the Reactions of Free Radicals and Atoms. IV. Solvents in Sulfuryl Chloride Chlorinations. *Journal of the American Chemical Society* **1958**, *80* (18), 5002–5003.
- (34) Russell, G. A. Solvent Effects in the Reaction of Free Radicals and Atoms. V. Effects of Solvents on the Reactivity of t-Butoxy Radicals. *The Journal of Organic Chemistry* **1959**, *24* (3), 300–302.
- (35) Russell, G. A. Solvent Effects in the Reactions of Free Radicals and Atoms. VI. Separation of Polar and Resonance Effects in the Reactions of Chlorine Atoms. *Tetrahedron* **1960**, *8* (1–2), 101–106.

- (36) Russell, G. A.; Ito, A.; Hendry, D. G. Solvent Effects in the Reactions of Free Radicals and Atoms. VIII. The Photochlorination of Aralkyl Hydrocarbons. *Journal of the American Chemical Society* **1963**, *85* (19), 2976–2983.
- (37) Hendry, D. G.; Russell, G. A. Solvent Effects in the Reactions of Free Radicals and Atoms. IX. Effect of Solvent Polarity on the Reactions of Peroxy Radicals. *Journal of the American Chemical Society* **1964**, *86* (12), 2368–2371.
- (38) Tannous, J. H.; De Klerk, A. Quantification of the Free Radical Content of Oilsands Bitumen Fractions. *Energy and Fuels* **2019**, *33* (8), 7083–7093.
- (39) Wiehe, I. A. *Process Chemistry of Petroleum Macromolecules*; CRC Press: Boca Raton, 2008.
- (40) Eaton, G. R.; Eaton, S. S.; Barr, D. P.; Weber, R. T. Basics of Continuous Wave EPR. In *Quantitative EPR*; Springer Wien New York, 2010; pp 1–3.
- (41) Strausz, O. P.; Lown, E. M. Spectroscopic Probes Into the Molecular Structure of Asphaltene. In *The chemistry of Alberta Oil Sands, Bitumens and heavy oils*; Alberta Energy Research Institute: Calgary, Alberta, Canada, 2003; pp 592–604.
- (42) Mello, P. A.; Barin, J. S.; Guarnieri, R. A. Microwave Heating. In *Microwave-Assisted Sample Preparation for Trace Element Analysis*; Elsevier, 2014; pp 59–75.
- (43) Hayes, B. L. *Microwave Synthesis: Chemistry at the Speed of Light*; Cem Corporation, 2002.
- (44) Kappe, C. O. Controlled Microwave Heating in Modern Organic Synthesis *Angewandte*. **2004**, 6250–6284. <https://doi.org/10.1002/anie.200400655>.
- (45) Poling, B. E.; Prausnitz, J. M.; O'Connell, J. P. *The Properties of Gases and Liquids*, 5th ed.; McGraw-Hill: New York, 2001.
- (46) Plamondon, J. E.; Buenker, R. J.; Koopman, D. J.; Dolter, R. J. The Dipole Moment of Styrene. *Proceedings of the Iowa Academy of Science* **1963**, *70* (1), 163–166.

- (47) Hassell, W. F.; Walker, S. Dielectric Studies. Part 4.—Relaxation Processes of Four Monoalkylbenzenes. *Transactions of the Faraday Society* **1966**, *62*, 861–873.
- (48) Briner, E.; Ryffel, K.; Perrottet, E. Ozonation de l'allyl-, Du Propényl-et Du Méthovinyln-benzène. Résultats de Déterminations Physico-chimiques (Spectres Raman, Spectres d'absorption Ultra-violette, Constantes Diélectriques et Moments Dipolaires). *Helvetica Chimica Acta* **1939**, *22* (1), 927–934.
- (49) Sidgwick, N. V.; Springall, H. D. 336. Dipole Moments and the Fixation of Aromatic Double Links: Bromohydrindenes and Bromotetralins. *Journal of the Chemical Society (Resumed)* **1936**, 1532–1537.
- (50) Caminati, W. Low-Energy Vibrations of Indene. *Journal of the Chemical Society, Faraday Transaction* **1993**, *89* (23), 4153–4155.
- (51) Rampolla, R. W.; Smyth, C. P. Microwave Absorption and Molecular Structure in Liquids. XXI. Relaxation Times, Viscosities and Molecular Shapes of Substituted Pyridines, Quinolines and Naphthalenes. *Journal of the American Chemical Society* **1958**, *80* (5), 1057–1061.
- (52) Pitt Quantum Repository pqr.pitt.edu.
- (53) Gendell, J.; Freed, J. H.; Fraenkel, G. K. Solvent Effects in Electron Spin Resonance Spectra. *The Journal of Chemical Physics* **1962**, *37* (12), 2832–2841.
- (54) Stone, E. W.; Maki, A. H. Electron Spin Resonance of Semiquinones in Aprotic Solvents. *The Journal of Chemical Physics* **1962**, *36* (7), 1944–1945.
- (55) Kokorin, A. I.; Tran, V. A.; Rasmussen, K.; Grampp, G. Effect of Solvent Nature on Spin Exchange in Rigid Nitroxide Biradicals. *Applied Magnetic Resonance* **2006**, *30* (1), 35–42.
- (56) Neugebauer, J.; Louwse, M. J.; Belanzoni, P.; Wesolowski, T. A.; Baerends, E. J. Modeling Solvent Effects on Electron-Spin-Resonance Hyperfine Couplings by Frozen-Density Embedding. *The Journal of Chemical Physics* **2005**, *123* (11), 114101.

- (57) Oakes, J.; Symons, M. C. R. Solvation Spectra Part 24.-Effect of Solvent on the Electron Spin Resonance Spectra of 2,6-Dimethyl and Related p-Benzosemiquinones. *Transactions of the Faraday Society* **1968**, *64*, 2579–2585.
- (58) Stone, E. W.; Maki, A. H. Solvent Effects on the Electron Spin Resonance Spectrum of P-Benzosemiquinone-1-C13. *Journal of the American Chemical Society* **1965**, *87* (3), 454–458.
- (59) Luckhurst, G. R.; Orgel, L. E. Solvent Effects in the Electron Spin Resonance Spectrum of Fluorenone Ketyl. *Molecular Physics* **1964**, *8* (2), 117–124.
- (60) Piette, L. H.; Ludwig, P.; Adams, R. N. Electron Paramagnetic Resonance of Aromatic and Aliphatic Nitro Anions in Aqueous Solution. *Journal of the American Chemical Society* **1962**, *84* (22), 4212–4215.
- (61) Sueishi, Y.; Isozaki, T.; Yamamoto, S.; Nishimura, N. ESR Study of Solvent Effects on the Electronic Structure of 2-(4'-dialkylaminophenyl) Indan-1, 3-dionyl Radicals. *Journal of physical organic chemistry* **1992**, *5* (4), 218–224.
- (62) Atherton, N. M.; Weissman, S. I. Association Between Sodium and Naphthalenide Ions. *Journal of the American Chemical Society* **1961**, *83* (6), 1330–1334.
- (63) Isenberg, I.; Baird, S. L. Solvent Effects in Radical Ion Formation. *Journal of the American Chemical Society* **1962**, *84* (20), 3803–3805.
- (64) Dalal, D. P.; Eaton, S. S.; Eaton, G. R. The Effects of Lossy Solvents on Quantitative EPR Studies. *Journal of Magnetic Resonance (1969)* **1981**, *44* (3), 415–428.
[https://doi.org/https://doi.org/10.1016/0022-2364\(81\)90276-6](https://doi.org/https://doi.org/10.1016/0022-2364(81)90276-6).

CHAPTER 4 – BITUMEN VACUUM DISTILLATION AND REFRACTIVE INDEX MEASUREMENTS OF THE FRACTIONS

Abstract

Distillation is a very important technique in bitumen upgrading and refining. It can assist with characterizing the bitumen without undergoing thermal cracking, and most importantly the fractions themselves can be refined to products that have a high market value. Hands-on distillation in a laboratory setting provides information about fractions mass yield and produces liquid fractions that can be further studied.

In this thesis chapter, bitumen atmospheric and vacuum fractional distillation were carried out. Atmospheric distillation was not practical due to the high initial boiling point of bitumen, which necessitates fractional distillation under a vacuum.

Vacuum distillation of bitumen was completed five times with an average liquid yield of 25 wt.% which is very typical for bitumen when the final cut point was 430°C. It resulted in about 15 fractions for each of the five distillations with a temperature range of 20°C for each cut.

In addition to the temperature range, the fractions were characterized by refractive index values. The intent behind this was to check that the same cut from different distillation runs was comparable. It showed a consistent result with an average difference of only 0.0025 nD.

4.1 Introduction

Fractional distillation of bitumen is an essential step of the bitumen characterization for the purposes of transportation, upgrading and refining. One of the ways to look deeper into the physical correlations and relationships in bitumen is hands-on distillation.

This work will employ practical distillation with the goal of determining the properties of the fractions, calculating the material balance and evaluating the results by comparing the refractive indexes (RI) of the fractions.

The distillation fractions, which were obtained, formed the starting materials for the work reported in Chapter 5.

4.2 Experimental

4.2.1 Prevention and Safety Measures during the work

Underwent Lab & Chemical Safety, Workplace Hazardous Materials Information System (WHMIS), Hazardous Waste Management, Respiratory Protective Equipment and respirator fitting test. I was trained by the authorized laboratory member on every piece of equipment that I used and followed standard operating procedures.

Laboratories, where I performed the experiments, follow strict safety protocols and provide access to the eye wash station, emergency shower, etc.

Personal protective equipment (PPE) used in the laboratory:

- Gloves: Kimberly-Clark Purple Nitrile Powder-Free exam gloves (double layered)
- Lab coat: A flame-resistant Bulwark FR lab coat
- Safety glasses: S-7022 Visitor Specs safety glasses
- Personal Clothes: long pants, closed-toe shoes
- Respirator: Honeywell Half-Face Respirator 7700-30M P/N 7700-11M
- Filters: Honeywell Safety N75003L N Series Organic Vapor & Acid Gas Cartridge

4.2.2 Materials

In this thesis, Athabasca oil sands bitumen from Suncor was used for the experiments as a feed. Penetration Characterization analyses were done by the procedures described in Chapter 5.

Table 4.1 Characterization of the feed: Athabasca oil sands bitumen from Suncor.

	Conditions	Value with units	Standard Deviation
Refractive Index	20°C	1.5758 nD	0
Viscosity	19.6°C	672.82 Pa*s	3.23
Density	19.99°C	1011 kg/m ³	0
Penetration	5 sec at 20°C	194 0.1mm	
ESR ^a	Solvent Toluene	0.76 × 10 ¹⁸ spins/g	
Elemental analysis	C	84.41%	
	H	10.44%	

	Conditions	Value with units	Standard Deviation
	N	0.54%	
	S	4.99%	

^aDetermined as a part of the project described in Chapter 3.

Throughout the study, toluene was used as a solvent for diluting and/or cleaning purposes. The descriptions: Toluene HPLC Grade Fisher Chemical >99.8% assay, CAS 108-88-3.

4.2.3 Equipment and Procedure

4.2.3.1 Crude Oil Distillation System

Suncor bitumen (about 650-850 g) from a barrel was poured into a 1 L glass beaker. The beaker with the bitumen inside was heated in the laboratory chamber furnace Carbolite CWF 11/13 at 60°C to allow the bitumen to flow. When the bitumen reached a less viscous state, it was poured into a round-bottom boiling flask (pot) and weighted at Mettler Toledo XP1203S balance with the maximum capacity of 1210 g and the readability of 0.001 g (exact mass of the bitumen during each distillation is provided in the material balance). Next, the stirrer and OMEGALUX thermocouple were put into the pot and placed into the Glas-Col 100B TEM108 1000 ml Aluminum Heating Mantle, which is a part of the B/R Instrument Corporation Crude Oil Distillation System Model 18 CODS with Edwards RV8 Rotary Vane Vacuum Pump. Consequently, the mantle was covered with an insulation jacket. The main elements of the distillation system are illustrated in Figure 4.1.

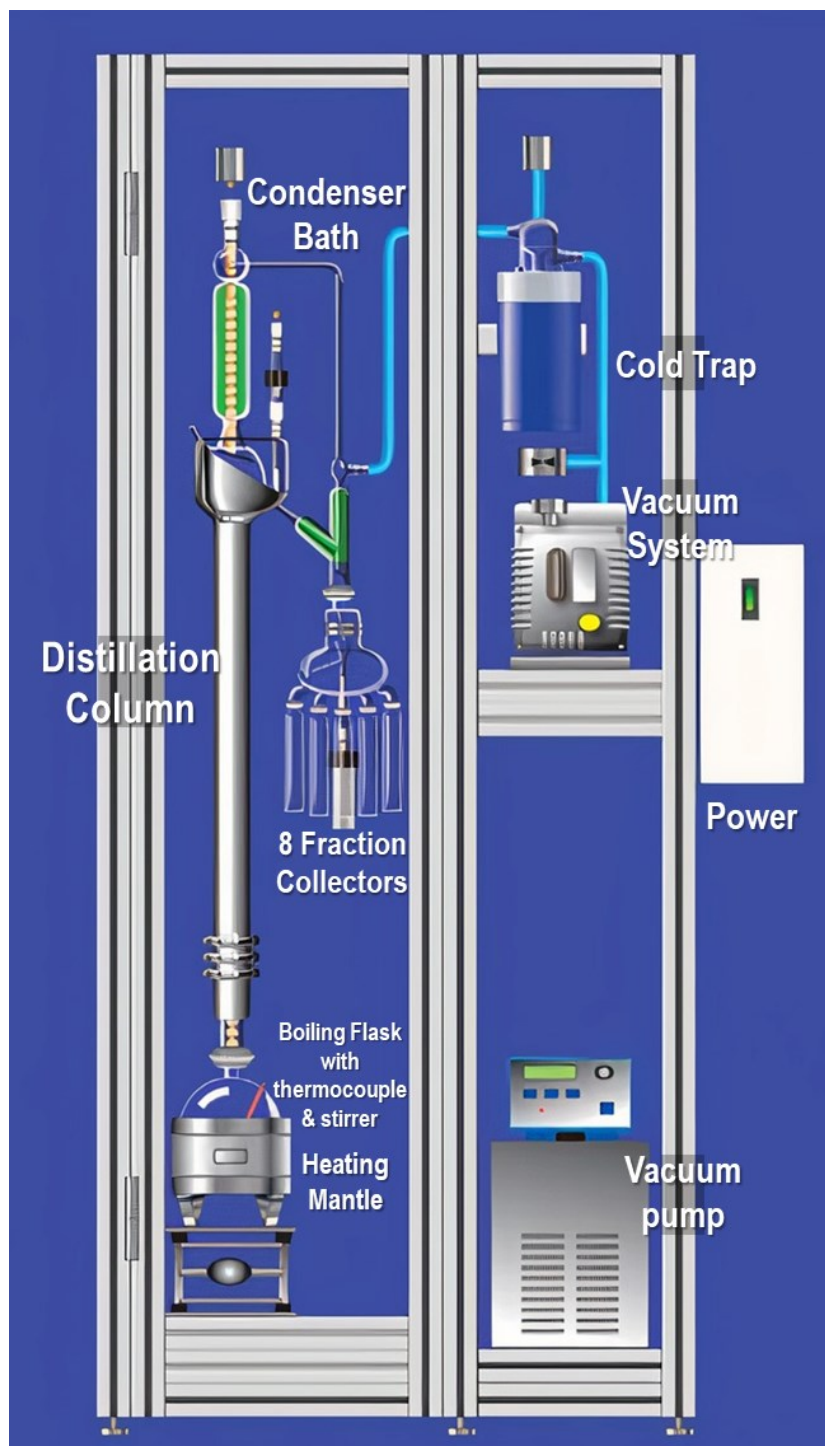


Figure 4.1 Mini Fractional Crude Oil Distillation System by B/R Instrument (edited)¹

The process was monitored from the computer screen on TempPro Distillation Data View Version 2.2.0.0.2.2.0.0, 2013, B/R Instrument Graphing Software for Distillation Results. Distillation was successfully performed five times overall. The first cut was opened at 25°C and

closed at 150°C. Next, the fractions were collected at 20°C intervals. To avoid cracking of the bitumen every distillation was set to stop when the pot reached 300°C.

During this project, atmospheric distillation was attempted twice. To improve the insulation of the column and decrease the heat loss, for the second attempt heater tape was installed covering the whole length of the distillation column. For the vacuum distillation pressure varied from 50 mm Hg to 0.1 mm Hg, exact values are given in the tables for the collected fractions from each distillation. Using vacuum distillation proved to be the most viable decision both theoretically and practically since bitumen has a high boiling point and, in this work, not allowing the bitumen to crack is one of the goals. A more detailed description of the whole process is graphically documented in Appendix A. The process is further described in Section 4.3.

4.2.3.1.1 Varying parameters during the distillation

1. Different mass of the bitumen (650-850 g) was used during each distillation run due to difficulty manipulating the amount of the viscous material such as bitumen especially inside the round-bottom flask (precise masses can be found in the material balance).
2. There was a problem of recovering stirrers after the runs since bitumen remaining after the distillation was non-flowing unless a high temperature was applied. Due to that, some of the stirrers were lost during the pot cleaning, thus, the lengths of the new stirrers were different.
3. The pressure was adjusted relative to the first runs and therefore was different for some of the cuts (exact values of the vacuum pressure are given in the Results section).
4. Cut point temperature ranges are reported as atmospheric equivalent boiling point temperature ranges and not the actual overhead temperatures at reduced pressure.

4.2.3.1.2 Pot cleaning procedure

After the distillation, the undistilled bitumen residue becomes almost solid. Because of that, in the case of the pot cool down, it was heated up again to 100°C in the laboratory chamber furnace Carbolite CWF 11/13. In that way, some of the remaining bitumen could be recovered, the rest is burned at 300°C for several hours. However, it is preferred to recover the bitumen right after the distillation, when the temperature in the pot goes down to about 100°C. At 100°C bitumen residue is still flowing which allows pouring into an amber bottle for storage.

4.2.3.1.3 Storage

The fractions were stored in a Fisherbrand Isotemp Flammable-Materials Storage Refrigerator No. 20FREEFSA at a temperature of 35°F (1.7°C). The fractions were obtained in the Summer of 2020 and the subsequent analyses were done over the course of the year.

4.2.3.1.4 Mixing

Fractions from the five distillations were mixed corresponding to the atmospheric equivalent boiling point temperature of the opening and closing cut. It was additionally checked by correlating the refractive index data (see Results section) to determine whether the cuts were near similar, as they were supposed to be.

Table 4.2 Assigned number (Fraction Identification Number (FIN)) and the temperature range of the mixed fractions.

Fraction Identification Number (FIN)	Atmospheric equivalent boiling point	
	Opening the cut, °C	Closing the cut, °C
1	25	150
2	150	170
3	170	190
4	190	210
5	210	230
6	230	250
7	250	270
8	270	290
9	290	310
10	310	330
11	330	350
12	350	370
13	370	390
14	390	410

Fraction Identification Number (FIN)	Atmospheric equivalent boiling point	
	Opening the cut, °C	Closing the cut, °C
15	410	430

4.2.4 Analyses

4.2.4.1 Refractive Index

Refractive Index (RI) was measured on an Abbemat 200 Refractometer from Anton Paar. Ethanol was used for cleaning the refractometer's cell after every sample and checking the equipment for functionality by measuring ethanol's RI at 20°C and comparing it to a literature value of 1.3610 nD.² The checking was done at the start of the day before the experiments. The sodium D-line (589nm) was used for the measurements. The range of the instrument is 1.30 to 1.72 nD and the accuracy is ± 0.0001 nD. The temperature probe accuracy of the instrument is $\pm 0.05^\circ\text{C}$.³

The volume of the samples used for analysis by the refractometer was in the range of 100-250 μL . Each measurement was conducted at the three temperatures: 20°C, 40°C, 60°C. To achieve an extra measure of certainty, each temperature was run twice in the order 20°C, 40°C, 60°C and 60°C, 40°C, 20°C.

4.2.4.2 Penetration Index

The measurements of each residue after the distillations and the feed bitumen were performed on The Humboldt Electric Automatic Penetrometer H-1240. H-1280 Standard hardened stainless-steel bituminous penetration needle with 40-45 mm exposed needle length and weight of 2.5 g were used during the measurements. Time length: 5 sec. All measurements were performed at room temperature of 20°C.

4.2.4.3 Estimated Level of Uncertainty

Most of the analyses in Chapters 4 and 5 were structured in a way to produce 3 values with a known constant interval. That allows creating a trendline with a coefficient of determination (R^2) to report a level of uncertainty of the measurements. R^2 is the square of the correlation coefficient that describes the proportion of the variation in y that is due to the variation in x.

The custom formula for “Average difference” was expressed as follows:

$$\text{Average Difference} = \frac{|A - RI_1| + |A - RI_2| + \dots + |A - RI_n|}{n} \quad (\text{Equation 4.1})$$

where RI – refractive index value of one measurement at 20°C, A – average value ($A = \frac{1}{n} \sum_{i=1}^n RI_i$).

In Excel, it looks as:

`= (ABS(AVERAGE(D7:H7)-D7)+ABS(AVERAGE(D7:H7)-E7)+ABS(AVERAGE(D7:H7)-F7)+ABS(AVERAGE(D7:H7)-G7)+ABS(AVERAGE(D7:H7)-H7))/Number of refractive index data points collected.`

4.3 Results

4.3.1 Distillation

Near atmospheric pressure distillation was attempted. The barometric pressure in Edmonton was around 698.5 mmHg (93.1 kPa),⁴ due to its altitude. The challenge with atmospheric pressure distillation was that the overhead temperature of the column only reached 21.4°C for the first attempt and 29.7°C for the second. Meanwhile, the temperature in the heating flask was 241.0°C and 285.7°C for the first and second atmospheric distillations respectively. This was at least partly due to heat loss, and partly due to the small amount of material in bitumen that is volatile at 300°C.

In an attempt to reduce heat loss, the outside of the column was wrapped in heating tape, before replacing the insulation on the outside of the column. The heating tape was operated at a heat rate of 30%. Both temperatures reached temperatures were below the initial boiling point of bitumen under a vacuum that was about 75°C (known from the vacuum distillation) and it was reckoned that it would not distort the temperature profile over the column.

The main reason why the pot was not heated to exactly 300°C was that during the second atmospheric distillation about 20 g of bitumen was spilled from the pot causing smoke where it touched hot surfaces. The spill was quickly cleaned. Two of the possible reasons:

1. About 100 g more bitumen than for the first attempt.
2. Remaining pressure in the column.

The spilling proved any further attempts to complete atmospheric distillation unproductive. Correspondingly, the decision was made to continue with vacuum distillation. In general, vacuum distillations were successful and were performed five times overall. The first droplets began to appear at around 75°C. More detailed values for the distillation process including reflux ratio and maximum boiling points are graphically presented in Appendix A.

Since distillations were performed five times, information about the collected fraction and material balances are summarized in the corresponding tables. Corresponding to Table 4.2, Fraction Identification Numbers (FIN) are given in the third column of Table 4.3.

Table 4.3 Collected fractions for Distillation 1.

Date	Pressure, mmHg	FIN	Fraction, °C	Fraction mass, g
2020-07-14	50	1	25-150	2.953
		2	150-170	0.876
		3	170-190	0.672
		4	190-210	1.715
		5	210-230	9.857
		6	230-250	3.601
		7	250-270	4.022
		8	270-290	17.462
2020-07-15	10	8	270-290	3.836
		9	290-310	68.22
2020-07-16	0.1	9	290-310	0.643
		10	310-330	0.632
		11	330-350	9.13
		12	350-370	3.435
		13	370-390	4.574
		14	390-410	9.871
		15	410-430	41.463
Total			25-430	182.962

From Table 4.3, it can be noticed that the first cut was opened in the same temperature window as the ending cut from the previous day. For example, cut 270-290°C from August 14, 2020, and cut 270-290°C from August 15, 2020. The reason behind it was to check if all the liquid yield was collected because the distillation stops once the pot reaches 300°C. It was done twice for Distillation 1 and 2. Information about the Distillation 2 is given in Table 4.5. Taking into account the negligible amount and the refractive index data, starting Distillation 3 all cuts were opened in the corresponding order regardless of the previous day's last cut temperature.

While collecting the fractions from the receivers, the rotten egg smell was present which might indicate the presence of hydrogen sulfide (odor threshold of hydrogen sulfide is <1 mg/m³).

Table 4.4 Material balance of the Distillation 1.

Input	Mass, g	Output	Mass, g	Comment
Bitumen in the pot	726.56	Bitumen in the pot after the distillation	527.501	Collected residue bitumen for further analysis 48.24 g
		Total mass of the fractions	182.962	
Overall	726.56	Overall	710.463	
		Loss	16.097	After every run, some bitumen stayed in the column
		Yield	25.182 wt.%	

Table 4.5 Collected fractions for the Distillation 2.

Date	Pressure, mmHg	FIN	Fraction, °C	Fraction mass, g	Comment
2020-07-21	50	1	25-150	1.206	
		2	150-170	0.803	
		3	170-190	0.710	
		4	190-210	10.067	Orange color
		5	210-230	0.475	
		6	230-250	1.811	
		7	250-270	13.991	Pink color
		8	270-290	17.284	
2020-07-22	5	8	270-290	0.345	
		9	290-310	10.500	
		10	310-330	63.551	
2020-07-23	0.1	10	310-330	0.072	
		11	330-350	2.693	

Date	Pressure, mmHg	FIN	Fraction, °C	Fraction mass, g	Comment
		12	350-370	5.238	Performed by Dr. Cibele Melo Halmenschlager, all the fractions, except the last one, were added to the flasks from the first distillation
		13	370-390	11.168	
		14	390-410	11.090	
		15	410-430	65.581	
Overall			25-430	216.585	

Table 4.6 Material balance of the Distillation 2.

Input	Mass, g	Output	Mass, g	Comment
Bitumen in the pot	817.968	Bitumen in the pot after the distillation	577.329	Collected 555.484 g
		Total mass of the fractions	216.585	
Overall	817.968	Overall	793.914	
		Loss	24.054	
		Yield	26.478 wt.%	

Table 4.7 Collected fractions for the Distillation 3.

Date	Pressure, mmHg	FIN	Fraction, °C	Fraction mass, g
2020-08-11	50	1	25-150	2.723
		2	150-170	0.747
		3	170-190	2.774
		4	190-210	7.583
		5	210-230	0.918
		6	230-250	0.911
		7	250-270	7.456

Date	Pressure, mmHg	FIN	Fraction, °C	Fraction mass, g
		8	270-290	14.974
2020-08-12	5	9	290-310	5.510
		10	310-330	52.582
2020-08-13	0.1	11	330-350	25.749
		12	350-370	32.124
Overall			25-370	154.051

Possible reasons for the small number of fractions:

- 1) 330 °C maximum pot temperature was introduced towards the end of the distillation.
- 2) Lower bitumen mass 649.452 g.
- 3) Smaller stirrer.

Table 4.8 Material balance of the Distillation 3.

Input	Mass, g	Output	Mass, g
Bitumen in the pot	649.452	Bitumen in the pot after the distillation	469.230
		Total mass of the fractions	154.051
Overall	649.452	Overall	623.281
		Loss	26.171
		Yield	23.720 wt.%

Table 4.9 Collected fractions for the Distillation 4.

Date	Pressure, mmHg	FIN	Fraction, °C	Fraction mass, g
2020-08-17	50	1	25-150	2.961
		2	150-170	0.664
		3	170-190	2.899
		4	190-210	0.900

Date	Pressure, mmHg	FIN	Fraction, °C	Fraction mass, g
		5	210-230	3.191
		6	230-250	7.664
		7	250-270	9.658
		8	270-290	15.338
2020-08-18	5	9	290-310	20.300
		10	310-330	60.421
2020-08-19	0.1	11	330-350	0.811
		12	350-370	66.910
		13	370-390	9.758
		15	390-410	26.376
Overall			25-410	227.851

Table 4.10 Material balance of the Distillation 4.

Input	Mass, g	Output	Mass, g	Comment
Bitumen in the pot	825.742	Bitumen in the pot after the distillation	593.127	Collected 574.808 g
		Total mass of the fractions	227.851	
Overall	825.742	Overall	820.978	
		Loss	4.764	
		Yield	27.593	

Table 4.11 Collected fractions for the Distillation 5.

Date	Pressure, mmHg	FIN	Fraction, °C	Fraction mass, g
2020-08-20	50	1	25-150	2.735
		2	150-170	3.755
		3	170-190	1.950
		4	190-210	2.567

Date	Pressure, mmHg	FIN	Fraction, °C	Fraction mass, g
		5	210-230	7.975
		6	230-250	12.121
		7	250-270	0.631
		8	270-290	5.500
2020-08-21	5	1	290-310	20.740
		2	310-330	58.718
2020-08-22	0.1	1	330-350	13.611
		2	350-370	5.098
		3	370-390	51.636
Overall			25-390	187.037

Table 4.12 Material balance of the Distillation 5.

Input	Mass, g	Output	Mass, g	Comment
Bitumen in the pot	773.659	Bitumen in the pot after the distillation	567.279	Collected 551.96 g
		Total mass of the fractions	187.037	
Overall	773.659	Overall	754.316	
		Loss	19.343	
		Yield	24.175	

The distillation curve summarizing all five distillations with individual lines and showing the general pattern is shown in Figure 4.2.

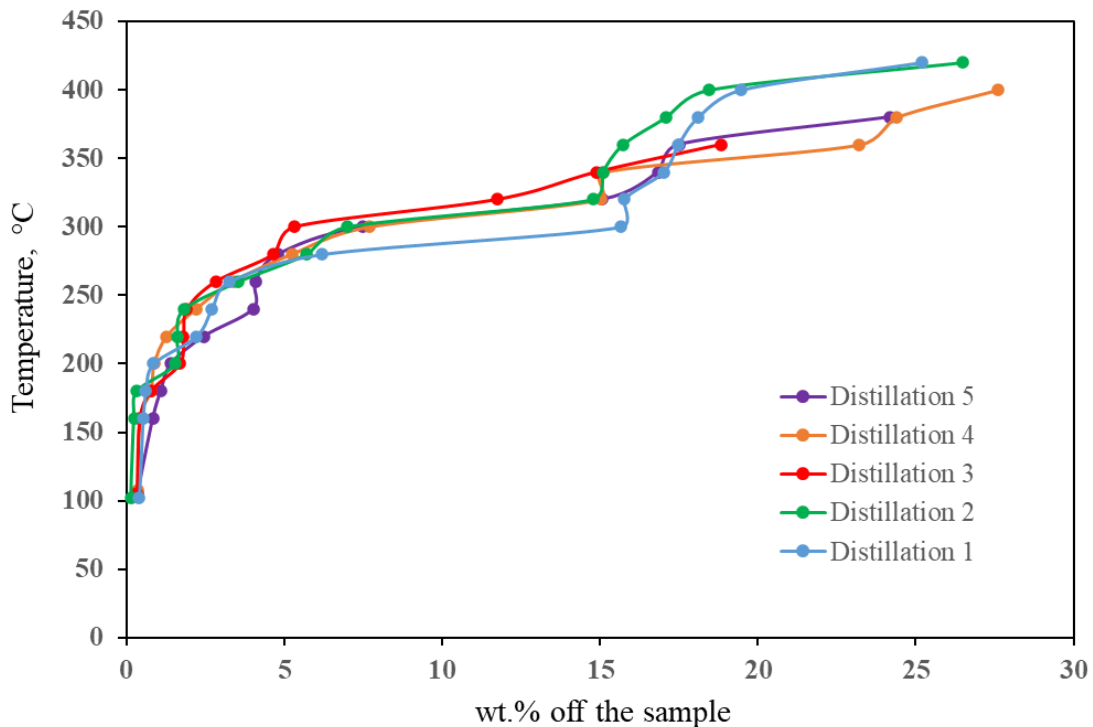


Figure 4.2 Distillation curve.

Table 4.13 illustrates summarized refractive index data from the 15 fractions from every distillation. The procedure is given in section 4.2.4.1. Only the measurements at 20°C are shown here. The complete data set is reported in Appendix B.

Table 4.13 Summarized refractive index data from every fraction from 5 distillations.

FIN	Refractive index values at 20 °C					Average R ² (from measurements at 20, 40, 60°C)	Average value	Average difference ^a
	Distillation Number							
	1	2	3	4	5			
1	1.4413	1.4431	1.4560	1.4508	1.4421	0.9998	1.4466	0.0054
2	1.4572	1.4512	1.4593	1.4552	1.4607	0.9999	1.4567	0.0028
3	1.4603	1.4563	1.4638	1.4620	1.4661	1.0000	1.4617	0.0027
4	1.4637	1.4659	1.4702	1.4661	1.4695	1.0000	1.4671	0.0022
5	1.4706	1.4735	1.4768	1.4681	1.4739	1.0000	1.4726	0.0026
6	1.4761	1.4746	1.4776	1.4722	1.4807	1.0000	1.4762	0.0023
7	1.4796	1.4786	1.4800	1.4786	1.4849	1.0000	1.4803	0.0018
8	1.4869	1.4873	1.4873	1.4855	1.4867	1.0000	1.4867	0.0005
9	1.4917	1.4954	1.4975	1.4956	1.4960	1.0000	1.4952	0.0014
10	1.5102	1.5101	1.5092	1.5105	1.5097	1.0000	1.5099	0.0004
11	1.5169	1.5169	1.5285	1.5197	1.5274	1.0000	1.5219	0.0048

FIN	Refractive index values at 20 °C					Average R ² (from measurements at 20, 40, 60°C)	Average value	Average difference ^a
	Distillation Number							
	1	2	3	4	5			
12	1.5255	1.5255	1.5319	1.5282	1.5270	1.0000	1.5276	0.0019
13	1.5280	1.5280		1.5368	1.5304	0.9999	1.5308	0.0030
14	1.5288	1.5288		1.5395		1.0000	1.5323	0.0048
15	1.5354	1.5342				1.0000	1.5348	0.0006

^aDescription of the Average difference is given in Equation 4.1.

Using the refractive index values from Table 4.13 was an additional tool for checking the degree to which the fractions correspond to each other. Respectively, a decision was made to mix the yield fractions from every distillation, resulting in 15 fractions overall. However, the main argument for the mixing was that essentially the temperature window of opening and closing the cuts were the same. Such a decision was necessary to receive a sufficient volume for the analyses.

4.3.2 Penetration Index

The penetration index was experimentally determined for the feed bitumen and for the vacuum residue that was left after every distillation (Table 4.14). The conditions of the measurements are stated in Part 4.2.4.4 Penetration Index.

Table 4.14 Penetration Index values for the feed bitumen and vacuum residue.

Sample	Penetration Index, 0.1mm
Feed bitumen	194
Vacuum residue from Distillation 1	116.5
Vacuum residue from Distillation 2	210.5
Vacuum residue from Distillation 3	178.5
Vacuum residue from Distillation 4	189
Vacuum residue from Distillation 5	207.5

4.4 Discussion

4.4.1 Analysis of the fractions mixing

Following the discussion of the arguments for mixing the fractions from every distillation, average values of the refractive index measured from the fractions from every distillation are compared to refractive index data measured from the resulting mixed 15 fractions in Figure 4.3

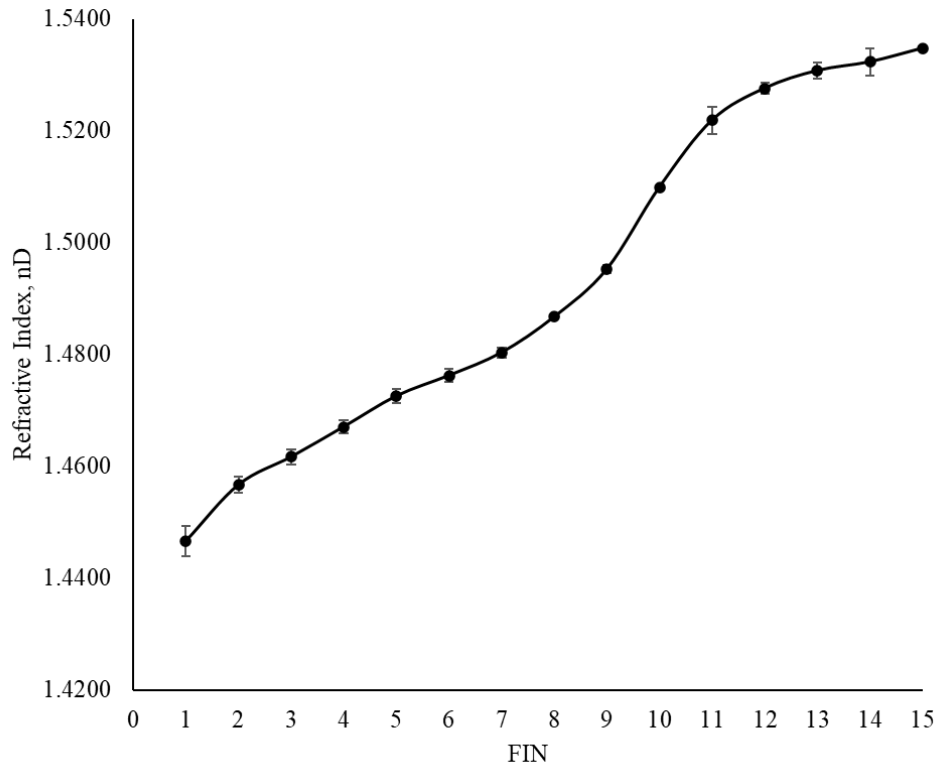


Figure 4.3 Refractive Index values with the average difference expressed by error bars.

The mathematical description of the Average difference is given in Equation 4.1. As can be seen from Figure 4.3, that difference is very small. On average, the difference was 0.0025 nD. This graph is meant to demonstrate that the fractions mixing was justified in terms of refractive index correlation.

After the mixing, it was immediately noticed that the fraction with Identification Number 10 of the temperature 310-330°C yielded the most with about 235.976 g. That information creates value for the industry since 310-330°C temperature range liquid product classified as Heavy gas oil

(HGO) and can be used as a feedstock for catalytic cracker or hydrocracker (from Table 2.1 in Chapter 2 Literature Review).

4.4.2 Penetration Index

In theory, once light boiling fractions are removed, the penetration values should decrease. However, it was not the case with the vacuum residue left after the distillation. The probable reason for the penetration index values to not decrease dramatically is related to the amount of time the residue spent at 250-300°C in the distillation pot.

4.5 Conclusion

In this chapter physical distillation of Suncor bitumen was conducted five times with the average yield of the liquid products equal to 25.430 wt.%, which corresponds to the numbers given in literature of 10-30 wt.%. Distillation fractions from the five distillations were mixed based on the same boiling range resulting in 15 fractions with boiling temperatures from about 70 to 430°C.

From bitumen distillation performed 5 times about 1 kg (968.486 g), the liquid yield was collected that was sufficient for the characterization and blending studies in Chapter 5.

REFERENCES

- (1) B/R Instrument. Mini Fractional Crude Oil Distillation Big Picture <https://brinstrument.com/fractional-crude-oil-distillation/Mini-Fractional-Crude-Oil-Distillation-Big-Picture>.
- (2) Hecht, E. *Optics*, 4th ed.; Pearson, 2002.
- (3) Turuga, A. S. S. Effect of Solvent Deasphalting Process on the Properties of Deasphalted Oil and Asphaltenes From Bitumen, University of Alberta, 2017.
- (4) Weather in Northeast Edmonton, July 13 world-weather.info/forecast/canada/northeast_edmonton/13-july/#2020 (accessed Oct 19, 2021).

CHAPTER 5 – RELATIONSHIPS IN PHYSICAL PROPERTIES OF BITUMEN FRACTIONS

Abstract

The physical properties of bitumen are manipulated to achieve targets of bitumen upgrading. Bitumen extracted from oil sands is naturally highly viscous. Most often reducing the viscosity is required. Fractional distillation can be one of the operations during bitumen upgrading. In this work, temperature correlations of viscosity and other physical properties (refractive index and density) will be experimentally determined and evaluated to find relationships in bitumen distillation fractions.

In this Chapter, the viscosity versus temperature relationship was evaluated through Hildebrand's postulate. Hildebrand argued that temperature viscosity relationships are influenced by a change in molar volume. The experimental results demonstrated that this might be true for the lighter fractions, but as the viscosity of the fractions goes up the linear trend turns to exponential. This might be due to the fact that Hildebrand's proposal was based on viscosity dependencies in pure compounds, while bitumen distillation fractions are a very complex mix of hydrocarbons.

Another approach taken in this Chapter was to test how different bitumen distillation fractions compare to each other by forming a blend. 14 blends were created with known ratios from 15 previously obtained bitumen distillation fractions. The blends were mostly made from higher boiling range fractions, for example, 270-290°C and 410-430°C, since they are producing the highest volume.

Refractive Index and density data demonstrated that the relationship between blends is related to weight composition, i.e. knowing the density of two pure distillation fractions, refractive index and density can be accurately estimated by only knowing wt.% of each. An assumption can be made that no chemical reaction is taking place and the blending is a purely physical phenomenon in the temperature range of 20-60°C. However, one blend consisting of 70 wt.% of bitumen distillation fraction with a boiling range of 310-330°C and 30 wt.% of 410-430°C deviated from that relationship.

Overall, it was found that the relationship between density and measurement temperature in a blend is linear over the range of 20-60°C, with density decreasing with an increase in temperature at the

rate of $-0.0007 \text{ g/cm}^3/\text{°C}$. The Refractive Index values also decreased with a temperature increase with a slope of the line equal to -0.0004 nD/°C .

The viscosity of the blends did not show a similar trend to refractive index and density relationships. As with the pure fractions, lighter blends had linear growth while heavier ones grow exponentially with respect to temperature. But it was found that adding a lighter boiling fraction with as little as 10 wt.% to a heavier fraction can dramatically decrease viscosity.

5.1 Introduction

In this work, the physical properties of bitumen distillation fractions will be experimentally determined to evaluate correlations that could characterize the physical properties relationships at a given temperature. Viscosity, density and refractive index were chosen as the main set of data points for the bitumen fractions.

Currently, the oil sands industry is mostly concerned with practical correlations for viscosity reduction. ASTM D341 – 20^{e1} gives excellent practical equations for the viscosity-temperature relations. Nevertheless, the majority of the relations are based on empirical data with little physical explanation behind it. Here, the standard will be checked based on obtained experimental data for the viscosity for different distillation cuts.

To evaluate the physical meaning behind the temperature viscosity relationship Hildebrand's molar volume postulate will be employed with molecular weight estimation derived from the Riazi-Daubert extended formula.

Lastly, blends of the bitumen distillation fractions will be created to investigate how viscosity, density and Refractive index change when two heavy oil products are blended at different ratios. It can be applied to interrogate the binary blending behavior of heavier fractions that cannot be fractionated by distillation without causing cracking.

5.2 Experimental

Prevention and Safety Measures during the work are covered in Chapter 4.2.1.

5.2.1 Materials

Mixed distillation fractions from Athabasca oil sands bitumen from Suncor (characterization is given in Table 4.1) were used during the work. The processes of distillation and mixing of the same cuts from different distillation runs are covered in Chapter 4.

To give a better perspective on how the fractions were designated, information from Table 4.2 is repeated here in Table 5.1.

Table 5.1 Assigned number (Fraction Identification Number (FIN)) and the temperature range of the mixed fractions.

Fraction Identification Number (FIN)	Atmospheric equivalent boiling point	
	Opening the cut, °C	Closing the cut, °C
1	25	150
2	150	170
3	170	190
4	190	210
5	210	230
6	230	250
7	250	270
8	270	290
9	290	310
10	310	330
11	330	350
12	350	370
13	370	390
14	390	410
15	410	430

5.2.2 Analyses

First, physical properties such as refractive index, density and viscosity were determined for each of the 15 mixed fractions. Then, a plan was made to blend several of them in specific ratios (wt.%). After that, refractive index, density and viscosity analyses were repeated for the resulting blends. In section 4.2.4.5 Estimated Level of Uncertainty, the procedure is given to get the coefficient of determination (R^2) value for the measurements uncertainty evaluation.

Results for Electron Spin Resonance (ESR) Spectroscopy, Nuclear Magnetic Resonance (NMR) Spectroscopy, Fluorescence and Elemental Analysis were determined only for the 15 straight run distillation fractions.

5.2.2.1 Refractive Index

The Refractive Index procedure was given in section – 4.2.4.1 Refractive Index.

5.2.2.2 Viscosity

5.2.2.2.1 Anton Paar Cold Properties Kinematic Viscometer

Fractions from number 1 to number 11 were analyzed on Anton Paar SVM 3001 Cold Properties kinematic viscometer. SVM 3001 Cold Properties kinematic viscometer is able to provide values for both density and viscosity in one run. But it has a consequence of being more delicate, so precautions had to be taken. It was dangerous to determine the viscosity of the fractions 1 (25-150°C) and 2 (150-170°) at 60°C due to the danger of rising pressure inside the instrument because of the vaporization. While RheolabQC rotational rheometer is not sensitive enough to show the viscosity values for light oil samples.

Anton Paar SVM 3001 Cold Properties kinematic viscometer has a viscosity repeatability of 0.1% and density repeatability of 0.0002 g/cm³. From three supported precision classes “Ultrafast, Fast and Precise,” Precise was selected to conduct the measurements. In addition, it shows specific gravity values at 15.6°C.

In the results section, “Approximate Cell Temp. °C” for the density and viscosity means that the actual cell temperature for Anton Paar SVM 3001 Cold Properties viscometer was slightly different: $\pm 0.002^\circ\text{C}$.

5.2.2.2 *RheolabQC rotational rheometer*

Fractions 12, 13, 14, 15 and all consequently prepared blends viscosity values were determined on Anton Paar rotational rheometer for quality control – RheolabQC No. 81143139. The temperature was manipulated with Julabo F25-HE Refrigerated/Heating Circulator No. 40054167 to the temperatures of 20°C, 40°C, 60°C. However, in practice, there was a slight deviation with the actual reading fluctuating at $\pm 0.5^\circ\text{C}$.

Each time about 4 g of the sample was placed to the Anton Paar Small Measuring Cup C-CC17/QC-LTD and Concentric Cylinder CC17 was inserted inside. When initially placed in the cup, a sample was left there for several minutes to achieve consistent temperature with the temperature setting. The same applies to increasing the temperature, every time the temperature value in the chiller was changed, the bitumen was left there for another 5 min before starting the actual measurement.

Depending on the estimated substance consistency, programs were created for the rheometer runs. In general, the analysed samples performed best with a shear rate set to 1,500 1/s. The reason for the Shear Rate value as high as 1500 1/s is that it could not produce results with any lower value. Lower shear rates of 10 1/s, 50 1/s, 100 1/s, 200 1/s, 500 1/s were attempted multiple times resulting in negative viscosity values or status messages with M- or M+ that show results which fall outside the lower torque range.¹

Data export was completed through the program RheolabQC – 1.50.9412.17. Toluene was used for cleaning the rheometer cup.

5.2.2.3 Density

Obtaining density values for the fractions from numbers 1 to 11 was described in part 5.2.3.2.1 Anton Paar Cold Properties Kinematic Viscometer. For the fractions 12, 13, 14, 15 and consequent blends Anton Paar Density Meter DMA 4500 M was employed. For it, the readability is 0.00005 g/cm³. It also shows specific gravity values for every density measurement.

Thermo Scientific Luer-Slip 5 mL Plastic Syringes were used to inject the samples. At the start of the day the density meter was checked with toluene at 20°C to determine if it functions correctly. The obtained value was compared to the literature value of 0.8669 g/cm³ for toluene density at

20°C.² In the case of the feed bitumen, the sample was preheated to achieve the flowing state. Each measurement was conducted at the three temperatures: 20°C, 40°C, 60°C.

5.2.2.4 Elemental Analysis

Performed at the Analytical and Instrumentation Laboratory of the Department of Chemistry Gunning/Lemieux Chemistry Centre of the University of Alberta. About 5 mg from each sample of interest was submitted for the analysis.

5.2.2.5 Electron Spin Resonance (ESR) Spectroscopy

In addition to the Electron Spin Resonance (ESR) spectroscopy procedure covered in Chapter 3, 15 fractions were analyzed twice: without adding a solvent and with adding about 50 vol.% toluene.

5.2.3 Blending procedure

15 mL Disposable Plastic Tubes Corning 430053 with Plug Seal Cap were used to blend the two fractions at a known ratio (exact ratios in Table 5.6) due to being convenient to weight, showing approximate volume and allowing seamless transfer of the liquid blend to the rheometer's cup. The ratios were calculated in mass percentage (wt.%). The samples were weighed on the Analytical Balance Mettler Toledo XS105 DualRange with a readability of 0.01 mg. They were vigorously shaken to achieve homogeneity.

Samples received from the blending were analyzed by the consequent techniques summarized in the following sections: 4.2.4.1 Refractive Index, 5.2.2.2 Viscosity (5.2.2.2.1 RheolabQC rotational rheometer), 5.2.2.3 Density.

It is important to note that due to the scarce volume of some of the fractions, analyses were performed in a way to decrease the sample loss. First, several drops were placed into the refractometer and about 4-3 mL of the sample were loaded into the rheometer directly from the tube. Second, after the viscosity analysis, the samples were recovered, and several drops were checked in the refractometer at 20°C for validation. Since the refractive index values did not demonstrate a large deviation, the liquid sample was further loaded to the Density Meter by the procedure described above.

Overall, the whole process of blending, refractive index, viscosity and density analysis took about three hours for a single ratio. Considerations included RheolabQC rheometer limitations that will show viscosity values ≤ 0.0004 Pa·s (determined experimentally) with negative values, low volume of particular fractions and Combination Number of 6435 (if we take 7 ratios from the 15 fractions by 5-95; 10-90; 30-70; 50-50; 70-30; 90-10; 90-5;). In the end, it was decided to analyse 14 blends (Table 5.6).

5.2.4 Coefficient of Determination (R^2)

Characterization of R^2 relative to this thesis is given in section 4.2.4.5 Estimated Level of Uncertainty.

5.3 Results

5.3.1 Physical properties of the 15 fractions

Table 5.2 demonstrates density values for the 15 fractions numbered by FIN from 1 to 15. Numbers were rounded up to four decimal places.

Table 5.2 Density of the 15 fractions.

	Density, g/cm ³ of the 15 fractions							
Approximate Cell Temp. °C	1	2	3	4	5	6	7	8
60	a	a	0.8239	0.8343	0.8422	0.8516	0.8547	0.8661
40	0.7938	0.8291	0.8386	0.8488	0.8565	0.8659	0.8686	0.8800
20	0.8095	0.8443	0.8531	0.8633	0.8708	0.8798	0.8826	0.8935
10	0.8173	0.8517	0.8606	0.8706	0.8779	0.8868	0.8896	0.9005
0	0.8250	0.8590	0.8678	0.8777	0.8849	0.8938	0.8965	0.9074
-5	0.8289	0.8627	0.8715	0.8812	0.8884	0.8972	0.9000	0.9107
-10	0.8326	0.8663	0.8750	0.8847	0.8919	0.9008	0.9035	0.9143
-20	0.8403	0.8736	0.8822	0.8918	0.8988	0.9077	0.9103	0.9210
<i>R</i> ²	0.9999	0.9999	1.0000	1.0000	1.0000	1.0000	1.0000	1.0000
<i>Slope</i> ($\times 10^4$)	-7.7441	-7.4045	-7.2961	-7.1931	-7.0869	-6.9990	-6.9608	-6.8632
<i>Standard error of the slope</i> ($\times 10^6$)	2.7505	2.7505	2.7505	2.7505	2.7505	2.7505	2.7505	2.7505
Approximate Cell Temp. °C	9	10	11	12	13	14	15	
60	0.8928	0.9033	0.9274	0.9314	0.9335	0.9431	0.9399	
40	0.9062	0.9165	0.9407	0.9446	0.9467	0.9560	0.9530	
20	0.9196	0.9300	0.9540	0.9579	0.9599	0.9689	0.9660	
10	0.9264	0.9367	0.9607	b	b	b	b	
0	0.9331	0.9434	0.9674	b	b	b	b	
-5	0.9364	0.9469	0.9707	b	b	b	b	
-10	0.9399	0.9502	0.9744	b	b	b	b	
-20	0.9466	0.9571	0.9812	b	b	b	b	
<i>R</i> ²	1.0000	1.0000	0.9999	1.0000	1.0000	1.0000	1.0000	
<i>Slope</i> ($\times 10^4$)	-6.7228	-6.7204	-6.7096	-6.6250	-6.6050	-6.4650	-6.5175	
<i>Standard error of the slope</i> ($\times 10^6$)	0.8512	1.4617	2.4971	0.2887	0.8660	1.7321	2.7424	

^a: It was hazardous to determine the properties of the fractions 25-150°C and 150-170°C at 60°C due to the danger of rising pressure inside the instrument because of the vaporization. In turn, the RheolabQC rheometer is not sensitive enough to determine the viscosities of the light fractions at 60°C.

^b: High viscosity of the last four samples prevented the analysis on Anton Paar SVM 3001 Cold Properties kinematic viscometer. They were measured as described in section 5.2.2.2 Density and viscosity.

An interesting aspect about the data in Table 5.2 is that density temperature coefficient $\text{g/cm}^3/\text{°C}$ (slope of the line) for density values for every FIN is -0.0007, except for FIN 1 and FIN 14 where it equals to -0.0008 and -0.0006 respectively.

The viscosity of the 15 mixed fractions is presented in Table 5.3. For the first 11 fractions analysed on Anton Paar SVM 3001, Cold Properties kinematic viscometer reproducibility is 0.35% and viscosity repeatability is 0.1%. For the fractions starting from number 12, from RheolabQC rotational rheometer, a Shear Rate of 200 1/s was implemented. The estimated maximum deviation, for example, at 1000 $\text{mPa}\cdot\text{s}$ is about 2 % [Anton Paar Service Representative (no external calibration was made)].

Table 5.3 Viscosity of the 15 fractions in $\text{mPa}\cdot\text{s}$.

Approximate Cell Temp., °C	1	2	3	4	5
60	^a	^a	1.0871	1.2926	1.5608
40	0.8034	1.2584	1.4875	1.8161	2.2625
20	1.0756	1.7941	2.1821	2.7735	3.6212
10	1.2745	2.2116	2.7405	3.5745	4.8252
0	1.5376	2.7968	3.5446	4.7799	6.7343
-5	1.7449	3.2232	4.128	5.6659	8.1808
-10	1.9509	3.7072	4.8171	6.7637	10.066
-20	2.4799	5.0564	6.8088	10.118	16.249
Approximate Cell Temp., °C	6	7	8	9	10
60	1.9336	2.1018	2.9205	6.4596	8.1695
40	2.9292	3.2436	4.8649	12.682	17.959
20	5.0091	5.713	9.6569	34.166	54.892
10	6.9933	8.1421	15.011	65.724	115.46
0	10.366	12.413	25.561	146.27	286.71
-5	13.070	15.907	35.053	235.21	491.24
-10	16.783	20.831	49.595	396.37	888.99
-20	30.181	39.391	113.05	1356.9	3577.8
Approximate Cell Temp., °C	11	12	13	14	15
60	17.933	31.26	39.051	72.616	73.857
40	49.811	109.067	136.934	294.079	302.453
20	218.69	547.3	739.78	2013.58	2097.08
10	584.96	^b	^b	^b	^b

0	1949.1	b	b	b	b
-5	3972	b	b	b	b
-10	8739.2	b	b	b	b
-20	56472	b	b	b	b

^a and ^b indications see under Table 5.2.

The numbers were deliberately not rounded to reflect the precision and avoid a rounding bias, because they were used in subsequent calculations.

Table 5.4 shows refractive index values that were averaged from the two measurements. Complete data set of the 15 mixed fractions is available in Appendix B.

Table 5.4 Refractive Index values for the 15 fractions.

FIN	Refractive Index, nD			R^2	Slope ($\times 10^4$)	Standard error of the slope
	at 20°C	at 40°C	at 60°C			
1	1.4470	1.4378	1.4288	1.0000	-4.5500	2.8868×10^{-6}
2	1.4590	1.4503	1.4416	1.0000	-4.3500	3.1893×10^{-18}
3	1.4630	1.4545	1.4460	1.0000	-4.2500	3.1279×10^{-18}
4	1.4675	1.4592	1.4509	1.0000	-4.1500	6.1332×10^{-20}
5	1.4715	1.4633	1.4551	1.0000	-4.1000	0
6	1.4764	1.4683	1.4602	1.0000	-4.0500	6.1332×10^{-20}
7	1.4789	1.4708	1.4628	1.0000	-4.0250	1.4434×10^{-6}
8	1.4866	1.4786	1.4707	1.0000	-3.9750	1.4434×10^{-6}
9	1.5038	1.4959	1.4881	1.0000	-3.9250	1.4434×10^{-6}
10	1.5108	1.5029	1.4952	0.9999	-3.9000	2.8868×10^{-6}
11	1.5276	1.5199	1.5121	1.0000	-3.8750	1.4434×10^{-6}
12	1.5304	1.5226	1.5147	1.0000	-3.9250	1.4434×10^{-6}
13	1.5319	1.5242	1.5166	1.0000	-3.8250	1.4434×10^{-6}
14	1.5338	1.5261	1.5185	1.0000	-3.8250	1.4434×10^{-6}
15	1.5351	1.5276	1.5200	1.0000	-3.7750	1.4434×10^{-6}

In Table 5.5 the results of elemental composition are given for each of the mixed 15 fractions numbered by FIN with the calculated sum. The complete set of data received from the Analytical and Instrumentation Laboratory is given in Appendix C.

Table 5.5 Elemental Analysis of the 15 fractions.

FIN	%C	%H	%N	%S	<i>Sum</i>
1	75.15	11.75	<0.2	0.78	87.69
2	81.87	12.74	<0.2	0.58	95.18
3	83.15	12.92	<0.2	0.63	96.71
4	83.80	13.02	<0.2	0.59	97.42
5	84.83	13.06	<0.2	0.75	98.63
6	85.09	12.98	<0.2	1.02	99.09
7	85.34	12.93	<0.2	1.22	99.49
8	85.62	12.69	<0.2	1.40	99.70
9	85.40	12.09	<0.2	2.05	99.55
10	85.20	11.79	<0.2	2.32	99.30
11	85.62	11.28	<0.2	3.11	100.00
12	85.13	11.32	<0.2	3.11	99.56
13	85.10	11.29	<0.2	3.08	99.47
14	85.08	11.17	<0.2	3.12	99.37
15	84.96	11.21	0.24	3.18	99.35

<0.2 indicates the quantification limit for Nitrogen at the analysis conditions.

Sum not being equal to 100% at some instances might be due to evaporation and/or additional undetected elements present.

5.3.1.1 Electron Spin Resonance (ESR) Spectroscopy

In the case of ESR, the results are better presented quantitatively. The presence of free radicals is detected. However, some of the peaks have a lot of noise (Figure 5.1, a). In Figure 5.1, b integrated results give double integral value of 184.62 (Gauss Width = 4; Polynomial Order = 3).

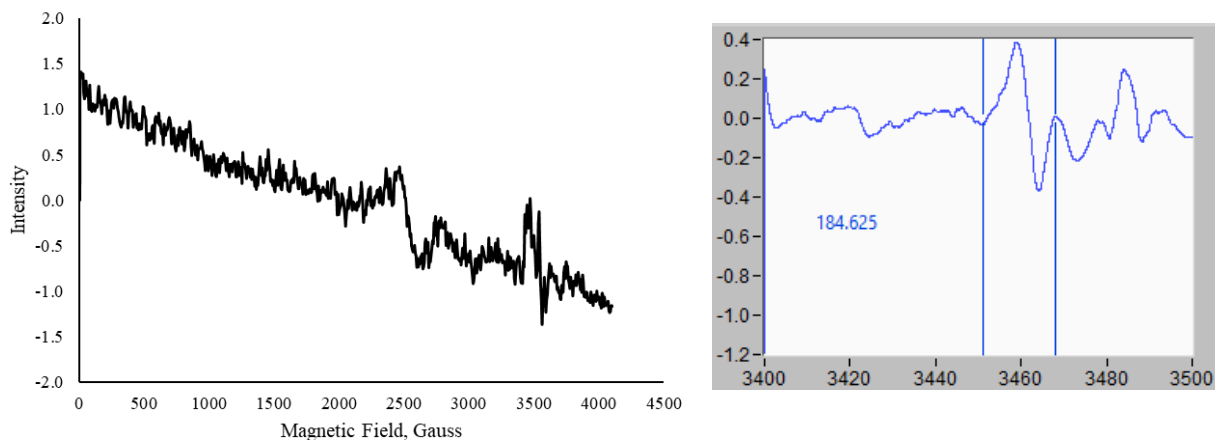
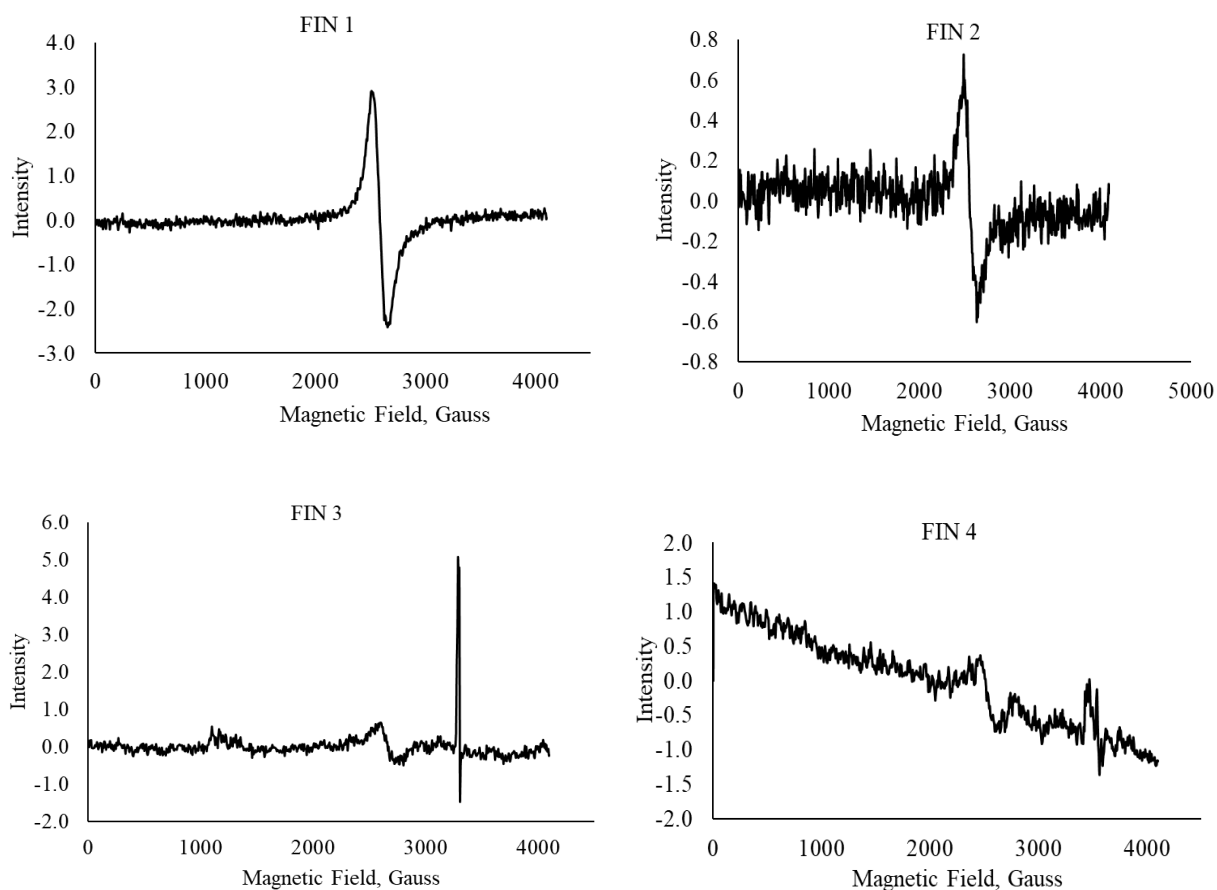
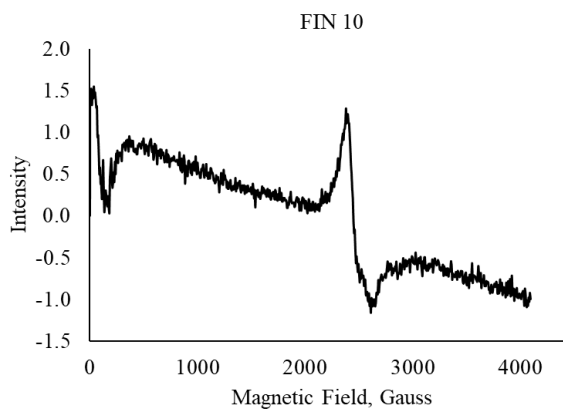
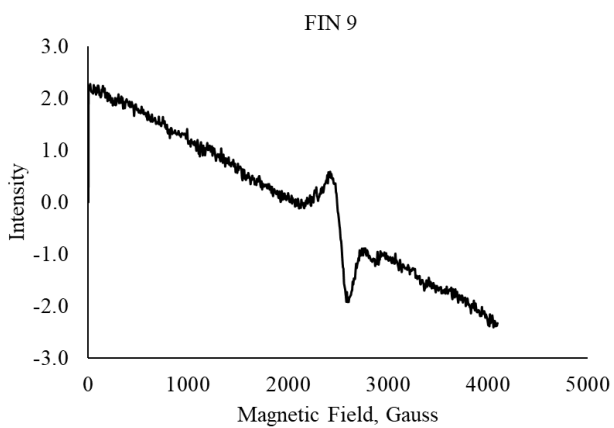
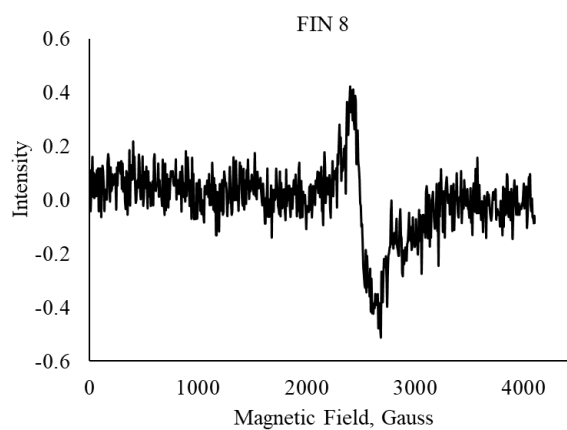
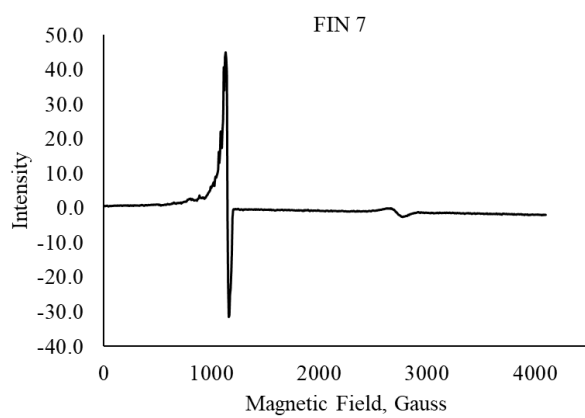
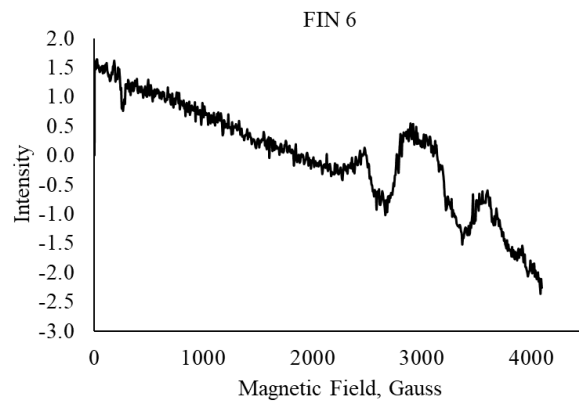
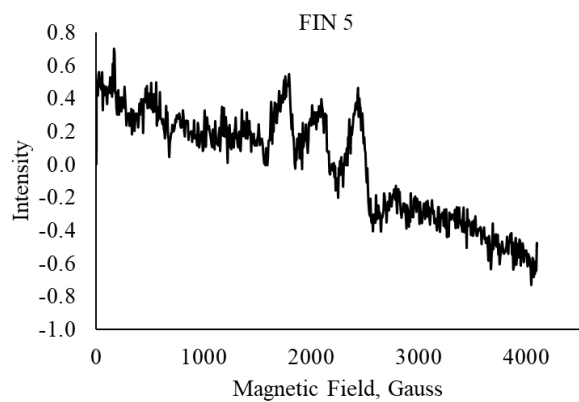


Figure 5.1 ESR spectrum of FIN 4.

Although the value of the double integral is as small as 184.62 (in Chapter 3 for bitumen it's about 5000), it still indicates that free radicals are present. But as can be seen from Figure 5.1, the error might be too high for reliable quantification.

ESR spectra of all 15 fractions are presented below in Figure 5.2.





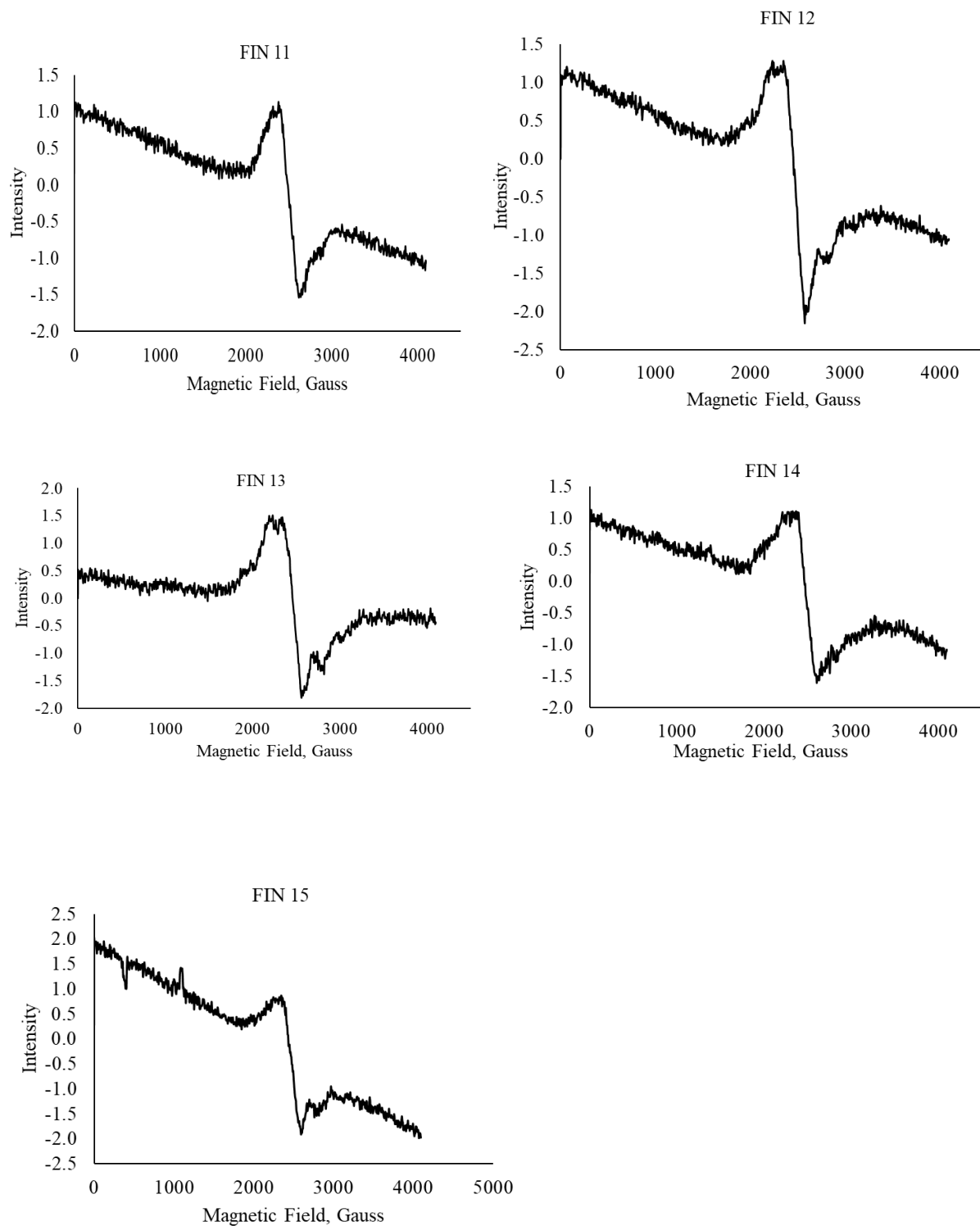


Figure 5.2 ESR spectra of the 15 fractions. The organic radicals are between 3400 and 3500 G.

5.3.2 Blending results

Table 5.6 Blended fractions with assigned Blend Identification Number (BIN) expressed by wt.% of the two blended FIN.

BIN	1		2		3		4		5	
FIN	8	15	8	15	8	15	10	15	10	15
wt.%	5	95	70	30	90	10	50	50	90	10
m, g	0.2022	3.8380	2.8115	1.2053	3.5897	0.4009	2.0049	1.9975	3.7397	0.3981
BIN	6		7		8		9		10	
FIN	5	10	5	10	10	12	8	15	8	15
wt.%	10	90	50	50	50	50	50	50	30	70
m, g	0.4180	3.6043	2.0060	1.9955	1.9974	1.9923	2.1847	2.1522	1.2010	2.7996
BIN	11		12		13		14			
FIN	10	15	10	15	5	15	5	15		
wt.%	30	70	70	30	10	90	30	70		
m, g	1.2340	2.8118	2.8798	1.2635	0.4030	3.6084	1.4995	3.5280		

m – exact measured mass.

The order of BIN in Table 5.6 is based on the time the blend was prepared with the BIN 1 being the earliest. As can be noticed from Table 5.6, FIN 15 is the most used one. FIN 15 was chosen as often due to being the heaviest fraction and producing a high volume from the distillation performed during Chapter 4. In theory, at a temperature of 20°C viscosity of 2097.08 mPa·s, FIN 15 can severely affect viscosity distribution, thus clearly demonstrating the contribution of the high viscosity sample and the influence of the lower viscosity sample during blending.

Other practical reasons for choosing that specific bitumen fractions for blending:

1. The volume of the low-boiling fractions (FIN 1-3) produced during work in Chapter 4, was not sufficient to create a blend for loading to the rheometer and density meter.
2. RheolabQC rheometer lacks sensitivity to determine the viscosity of light samples, especially at 60°C.

Consequently, there was both a practical and a scientific reason for the prevalence of blends with FIN 15.

5.3.3 Analyses of the blends

Table 5.7 presents RI values of the blends averaged from 2 measurements (except BIN 3 that was measured once). The complete data set can be found in Appendix B.

Table 5.7 Refractive Index of the Blends designated by BIN with R² and slope of the line value.

RI of the Blends by BIN, nD							
T, °C	1	2	3	4	5	6	7
20	1.5333	1.5008	1.4913	1.5238	1.5174	1.5067	1.4910
40	1.5257	1.4929	1.4833	1.5159	1.5098	1.4988	1.4829
60	1.5182	1.4851	1.4754	1.5082	1.5017	1.4911	1.4748
<i>R²</i>	<i>1.0000</i>	<i>1.0000</i>	<i>1.0000</i>	<i>1.0000</i>	<i>0.9997</i>	<i>0.9999</i>	<i>1.0000</i>
<i>Slope (×10⁴)</i>	<i>-3.7750</i>	<i>-3.9250</i>	<i>-3.9750</i>	<i>-3.9000</i>	<i>-3.9250</i>	<i>-3.9000</i>	<i>-4.0500</i>
<i>Standard error of the slope</i>	<i>1.4434 ×10⁻⁶</i>	<i>1.4434 ×10⁻⁶</i>	<i>1.4434 ×10⁻⁶</i>	<i>2.8868 ×10⁻⁶</i>	<i>7.2169 ×10⁻⁶</i>	<i>2.8868 ×10⁻⁶</i>	<i>6.1332 ×10⁻²⁰</i>
RI of the Blends by BIN, nD							
T, °C	8	9	10	11	12	13	14
20	1.5205	1.5104	1.5201	1.5292	1.5177	1.5299	1.5158
40	1.5127	1.5026	1.5124	1.5216	1.5103	1.5217	1.5080
60	1.50505	1.4948	1.5049	1.5138	1.5032	1.5141	1.5003
<i>R²</i>	<i>1.0000</i>	<i>1.0000</i>	<i>0.9999</i>	<i>1.0000</i>	<i>0.9999</i>	<i>0.9993</i>	<i>1.0000</i>
<i>Slope (×10⁴)</i>	<i>-3.8625</i>	<i>-3.9000</i>	<i>-3.8000</i>	<i>-3.8500</i>	<i>-3.6250</i>	<i>-3.9500</i>	<i>-3.8750</i>
<i>Standard error of the slope</i>	<i>2.1651 ×10⁻⁶</i>	<i>6.1332 ×10⁻²⁰</i>	<i>2.8868 ×10⁻⁶</i>	<i>2.8868 ×10⁻⁶</i>	<i>4.3301 ×10⁻⁶</i>	<i>8.6603 ×10⁻⁶</i>	<i>1.4434 ×10⁻⁶</i>

For BIN 13, since two measurements were conducted, it can be seen that the first value at 20°C was equal to 1.5305 nD. This is the value responsible for the R² going down compared to other blends. In Appendix B Table B.7, it can be noticed that for the second measurement (temperature going in the reverse order 60°C, 40°C, 20°C) R² is equal to 0.9999. If the value was deviating on the second run after 60°C, some could argue that it might be happening because of some sort of chemical or physical transformation. But since it is the very first measurement, the reason is not clear.

In Table 5.8 density for every blend is presented, the designation is by BIN.

Table 5.8 Density of the Blends.

	Density of the Blends by BIN, g/cm ³						
T, °C	1	2	3	4	5	6	7
20	0.9624	0.9147	0.9008	0.9483	0.9336	0.9241	0.9001
40	0.9494	0.9012	0.8871	0.9349	0.9201	0.9106	0.8864
60	0.9363	0.8877	0.8735	0.9216	0.9067	0.8972	0.8727
R ²	1.0000	1.0000	1.0000	1.0000	1.0000	1.0000	1.0000
Slope ($\times 10^4$)	-6.5250	-6.7500	-6.8250	-6.6750	-6.7250	-6.7250	-6.8500
Standard error of the slope	1.4434×10^{-6}	0	1.4434×10^{-6}	1.4434×10^{-6}	1.4434×10^{-6}	1.4434×10^{-6}	1.7173×10^{-18}
	Density of the Blends by BIN, g/cm ³						
T, °C	8	9	10	11	12	13	14
20	0.9440	0.9287	0.9430	0.9550	0.9396	0.9562	0.9366
40	0.9305	0.9153	0.9267	0.9418	0.9262	0.9431	0.9232
60	0.9172	0.9019	0.9164	0.9286	0.9128	0.9299	0.9099
R ²	1.0000	1.0000	0.9826	1.0000	1.0000	1.0000	1.0000
Slope ($\times 10^4$)	-6.7000	-6.7000	-6.6500	-6.6000	-6.7000	-6.5750	-6.6750
Standard error of the slope	2.8868×10^{-6}	1.2266×10^{-19}	8.6603×10^{-5}	0	1.5946×10^{-18}	1.4434×10^{-6}	1.4434×10^{-6}

R² for density of BIN 10 is considerably lower than for all the other blends which are equal to 1 for each of the blends. If one would make a graph, the last value at 60°C is the one that makes the whole line deviate from the linear trend. The reason for that is unknown. In this case, it might be worthy to note that from the same measurements API gravity for the density of BIN 10 is equal to 17.97 at 20°C, 17.99 at 40°C and 17.98 at 60°C.

In Table 5.9 viscosity values of the prepared blends are presented. All of the values were determined on RheolabQC rotational rheometer since SVM 3001 Cold Properties kinematic viscometer is very sensitive and might be permanently contaminated if used for measuring material as heavy as bitumen distillation fractions.

Table 5.9 Viscosity of the Blends designated by BIN.

The viscosity of the Blends by BIN, mPa·s							
T, °C	1	2	3	4	5	6	7
20	1062.7710 ^b	25.8400	13.0070	191.3160	64.7840 ^b	37.3270	8.5080
40	197.9260 ^b	9.6820	5.4000	58.8480	20.2870	13.3240	1.4550
60	52.6480	^a	^a	18.2280	7.3490	3.2210	0.5370
The viscosity of the Blends by BIN, mPa·s							
T, °C	8	9	10	11	12	13	14
20	145.8360	64.3460	178.2120	165.0170	121.0230	170.6920	97.0980
40	38.8670	22.4670	46.1390	100.6210	31.9540	115.7050	28.3480
60	13.6050	8.8660	15.7890	31.6820	11.1830	34.3580	10.8060

^aOutside of the RheolabQC rheometer's range.

^bShear rate of 200 1/s. For all the others, Shear Rate is 1500 1/s.

5.4 Discussion

5.4.1 Processing of the experimental results from the 15 fractions

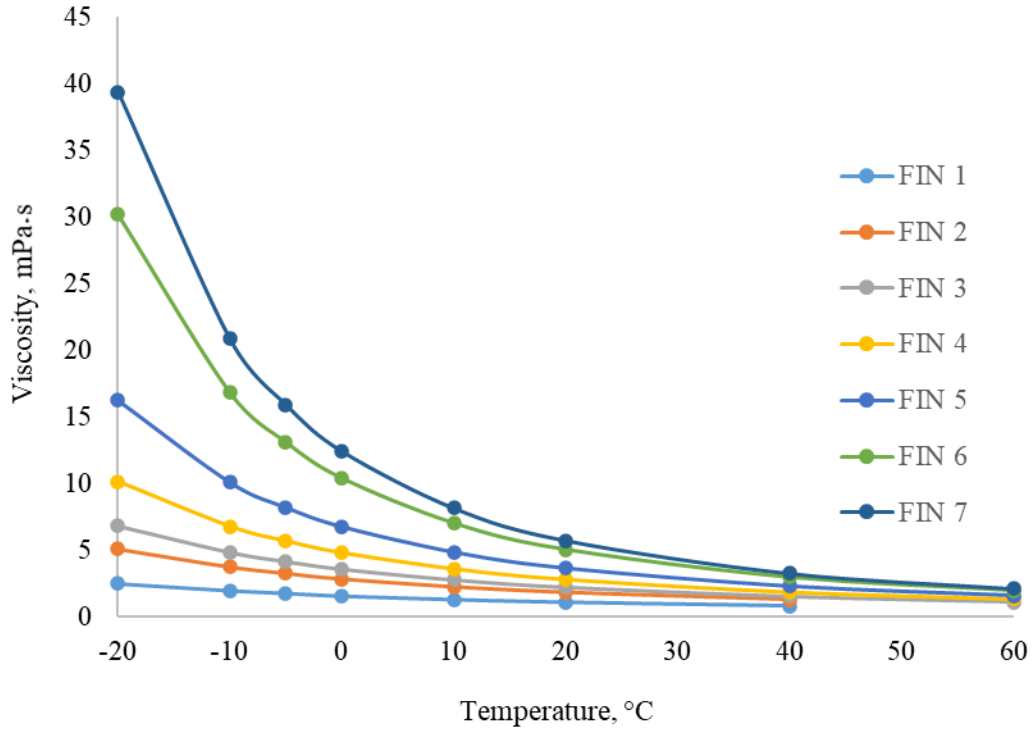


Figure 5.3 Temperature-Viscosity chart for the first 7 fractions.

As can be seen from Figure 5.3, that the viscosity increases exponentially with a decrease in temperature for the bitumen distillation fractions. In relation to the others, FIN 1 appears almost linear due to the scale, in the reality the relationship there still follows the exponential growth, which is presented in Figure 5.4.

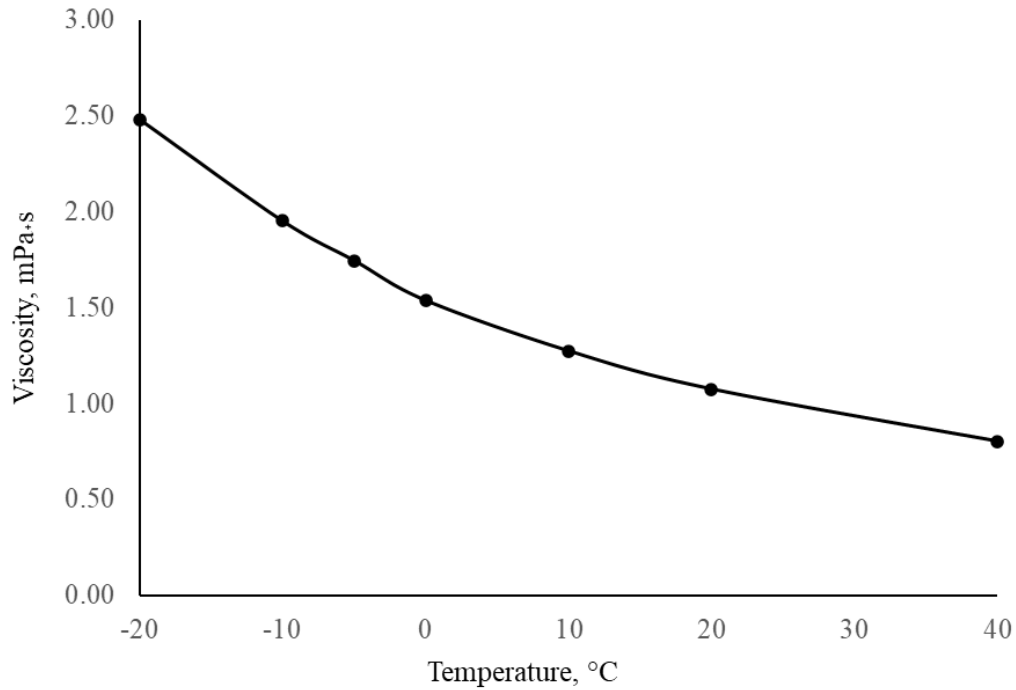


Figure 5.4 Temperature-Viscosity chart for FIN 1.

Observations of the exponential relationship between viscosity and temperature are still considered empirical.³ Nevertheless, this is also the form of the relationship given by ASTM D341 – 20^{e1}, which will be evaluated next.

5.4.2 ASTM D341 – 20^{e1} evaluation

First, ASTM D341 – 20^{e1} will be tested by comparing calculated results with experimental viscosity data. The formulas for the calculations are presented in Chapter 2 Literature Review Equations 2.3-2.5.

As can be seen from the previous sections, the viscosity relationship is strictly exponential, ASTM D341 – 20^{e1} can be used to linearize it.⁴ This is illustrated by showing the experimental and calculated values for one of the distillation fractions as a function in Figure 5.5.

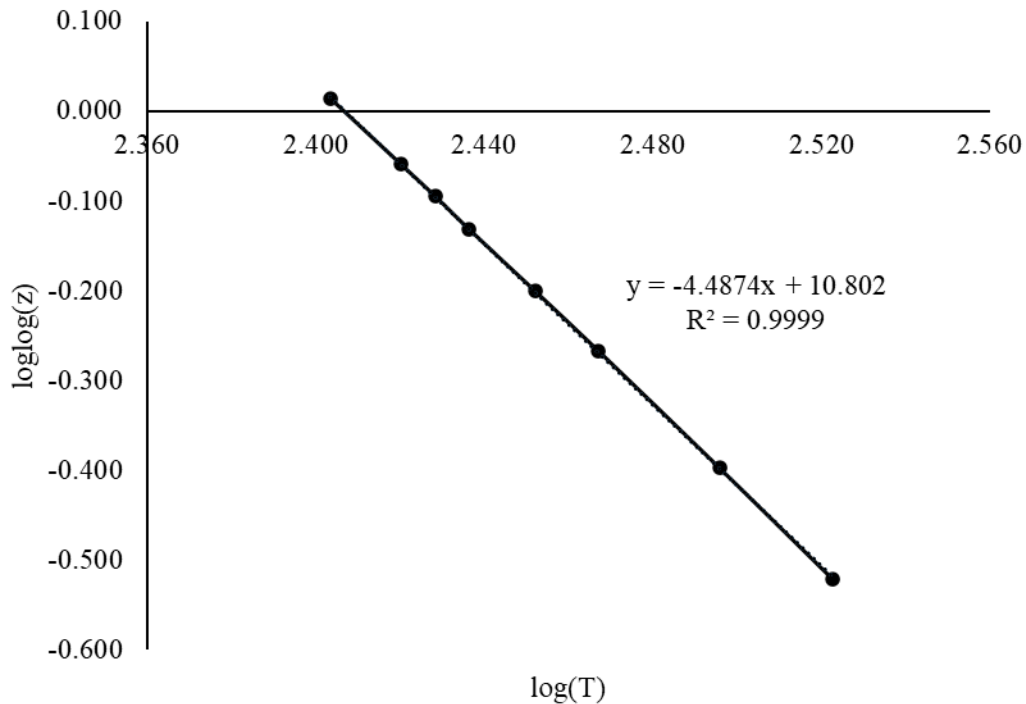


Figure 5.5 Linearization from ASTM D341 – 20^{e1} for FIN 4 as an example.

With R² value of 0.9999, the standard was very accurate in transforming the viscosity data to the linear form. In a mathematical sense, it allows using linear extrapolation for further viscosity prediction. A good fit was observed for essentially every fraction with R² ranging from 0.9992 to 1.0000. In more accurate terms, when calculating predicted viscosity at 40°C from 20°C and 60°C FIN 4 data, the results were 1.8103 mPa·s compared to the experimental value of 1.8161 mPa·s with an error of only 0.319%. The calculations showed similar accurate results for lower boiling fractions.

Trendline equation values for every fraction calculated through ASTM D341 – 20^{e1} are summarized in Table 5.10. In the last column, as an example, the error is calculated by comparing experimentally found viscosity at 40°C and calculated by ASTM D341 – 20^{e1} at the same temperature. 40°C was chosen because at this temperature the values are present for all of the fractions.

Table 5.10 Values calculated from ASTM D341 – 20^{e1}.

FIN	R ²	Slope	Offset	Example error at 40°C, % ^a
1	0.9996	-4.6591	10.9000	0.1195

FIN	R ²	Slope	Offset	Example error at 40°C, % ^a
2	0.9999	-4.4751	10.6390	0.1680
3	0.9999	-4.4787	10.7100	0.2817
4	0.9999	-4.4874	10.8020	0.3191
5	1.0000	-4.5153	10.9420	0.3258
6	1.0000	-4.5936	11.2120	0.2569
7	1.0000	-4.6352	11.3430	0.1548
8	0.9999	-4.7374	11.6960	0.1502
9	0.9998	-4.7484	11.9060	2.6350
10	1.0000	-4.8202	12.1350	0.6553
11	1.0000	-4.8085	12.2330	1.0174
12	0.9992	-4.6804	11.9870	7.1600
13	0.9998	-4.5688	11.7300	3.8602
14	0.9999	-4.4698	11.5470	2.2327
15	0.9999	-4.4808	11.5770	2.4330

^aExample error indicates the percentage error between experimentally found values and the viscosity values predicted from the standard $\frac{|\text{Predicted viscosity} - \text{Experimental viscosity}|}{|\text{Predicted viscosity}|} \times 100\%$.

Stating FIN 12, viscosity was measured on the RheolabQC rheometer as described in Section 5.2.2.2 Viscosity. From Table 5.3, which presents collected viscosity values for the fractions, it can be seen that starting FIN 12 viscosity values were collected only at three temperatures instead of eight or seven as for the previous fractions. That might be a reason for the high error and lower R² at FIN 12. However, for even heavier fractions (FIN 13, 14, 15) values collected at three temperatures seem to be sufficient for the accurate correlation.

5.4.3 Evaluating Hildebrand Molar Volume Postulate

Since empirical equations need to uncover more of the physical meaning behind viscosity relationships, one might want to take a step back and evaluate earlier theories. Here, Hildebrand's³ proposal will be evaluated to see if molal volume change is dependent on fluidity (reverse function of viscosity 1/η) and not only temperature.

In this work molar volume will be used for the calculations. Molal volume is in units of density (kg/m³), whereas molar volume is in units of m³/mol. For a non-reacting material, the relationship between these is constant and given by the molecular mass (kg/mol). Hildebrand argues that molecules are such proximate to each other, so they suppress self-diffusion, in the case of the molar volume at which fluidity approaches 0. And relative expansion is dependent on fluidity.³

To check Hildebrand's postulate, first, molecular weight has to be determined for every fraction, That can be done by Riazi-Daubert extended formula for heavy hydrocarbons⁵:

$$M = 42.965[\exp(2.097 \times 10^{-4}T_b - 7.78712SG + 2.08476 \times 10^{-3}T_bSG)]T_b^{1.26007}SG^{4.98308}$$

Formula 5.1

Where M is molecular weight (g/mol), T_b (°F) is the average boiling point and SG is specific gravity.

The resulting estimated molecular weight values are presented in Table 5.11.

Table 5.11 Molecular Weight calculated from the Riazi extended formula for heavy hydrocarbons.

FIN	Molecular Weight, g/mol
1	118.37
2	126.57
3	151.85
4	164.88
5	179.17
6	194.03
7	211.17
8	227.59
9	240.89
10	259.02
11	273.57
12	296.34
13	320.98
14	344.44
15	374.59

Now, inserting values to find Molar Volume ($M/\rho(\text{density})$) and fluidity, gives a graph illustrated in Figure 5.6.

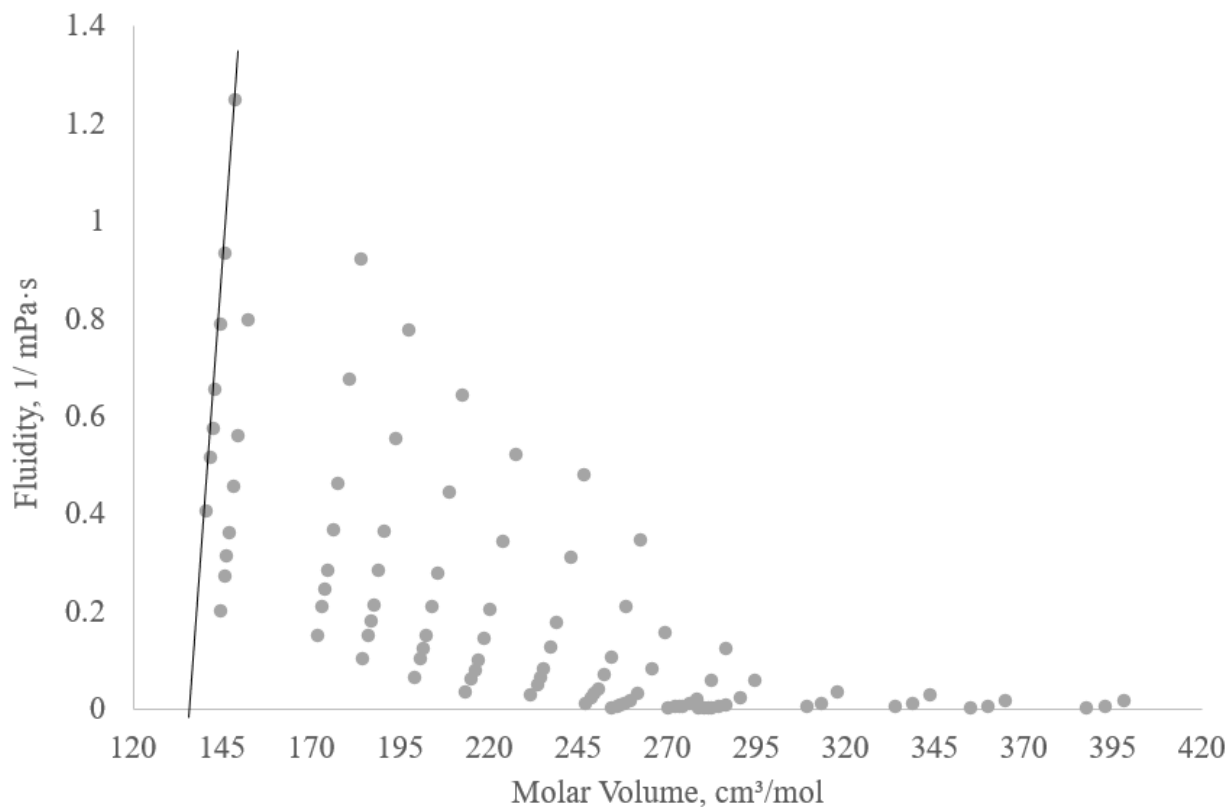


Figure 5.6 Fluidity dependence on molar volume (first 11 values were measured at 8 different temperatures, last four values were measured only at 3 temperatures, see Table 5.3).

In Figure 5.6, it can be seen that Hildebrand's proposed relationship demonstrates a good linear trend for low boiling fractions, but as the boiling temperature rises, so does the deviation from this linear trend. It could be dependent on the size of the molecules and the fact that Hildebrand used pure compounds in the evaluation, while here a complex mixture of hydrocarbons is used which is the distillation fractions of bitumen.

Derived from the experimental data, for FIN 1 the relationship does seem to be fitting, but not for the heavier fractions, for example, FIN 15 (Figure 5.6).

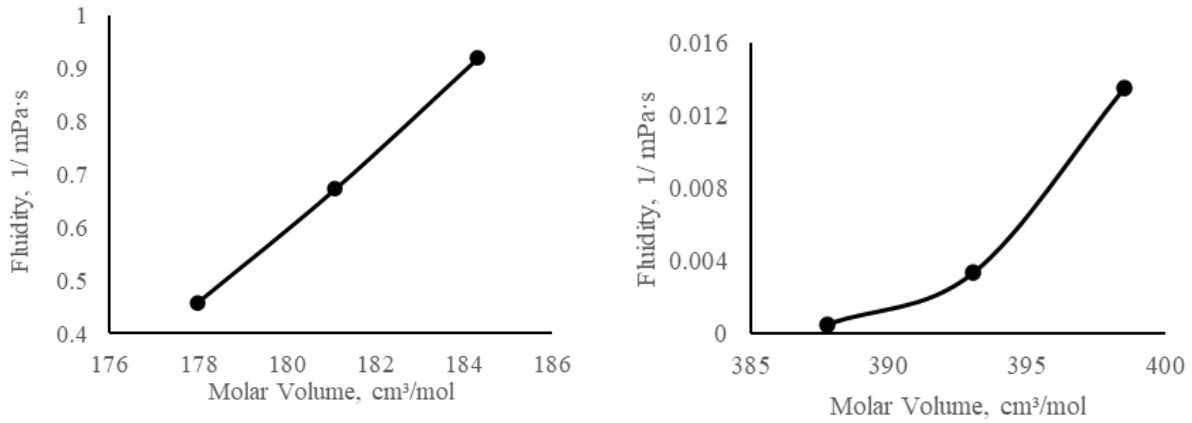


Figure 5.7 Molar Volume Fluidity relationship for FIN 3 and FIN 15.

5.4.4 Evaluating Refractive Index of Bitumen Distillation Blends

Blending correlations for the refractive index and density are very straightforward. Even from the visualization in Figure 5.8, it can be seen that a simple proportionality pattern is followed.

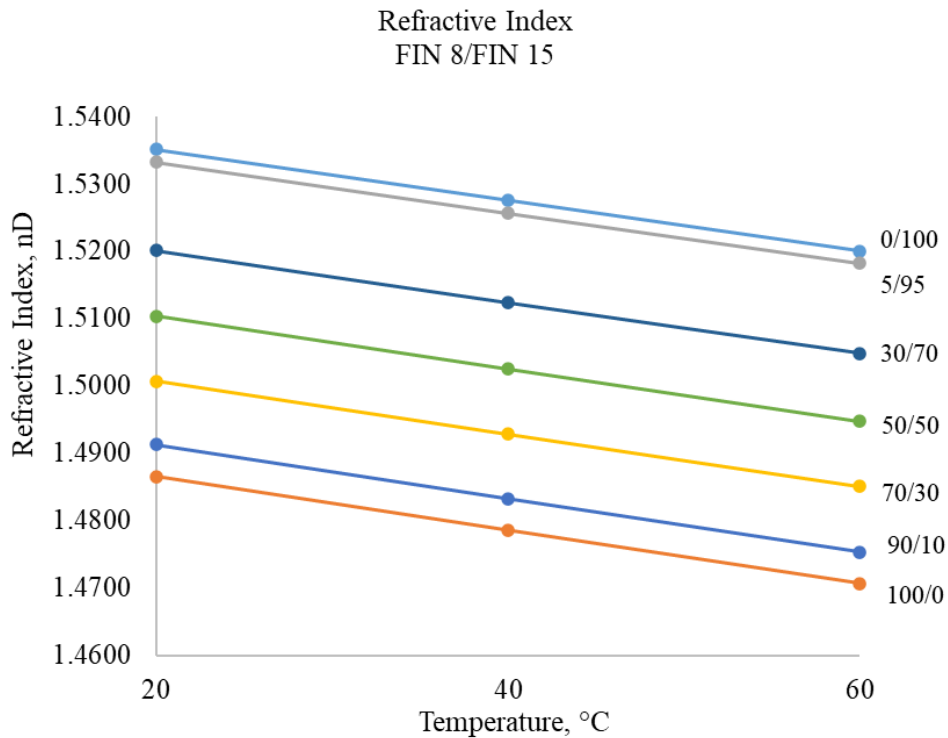


Figure 5.8 Refractive Index distribution for the FIN 8/FIN 15 blends.

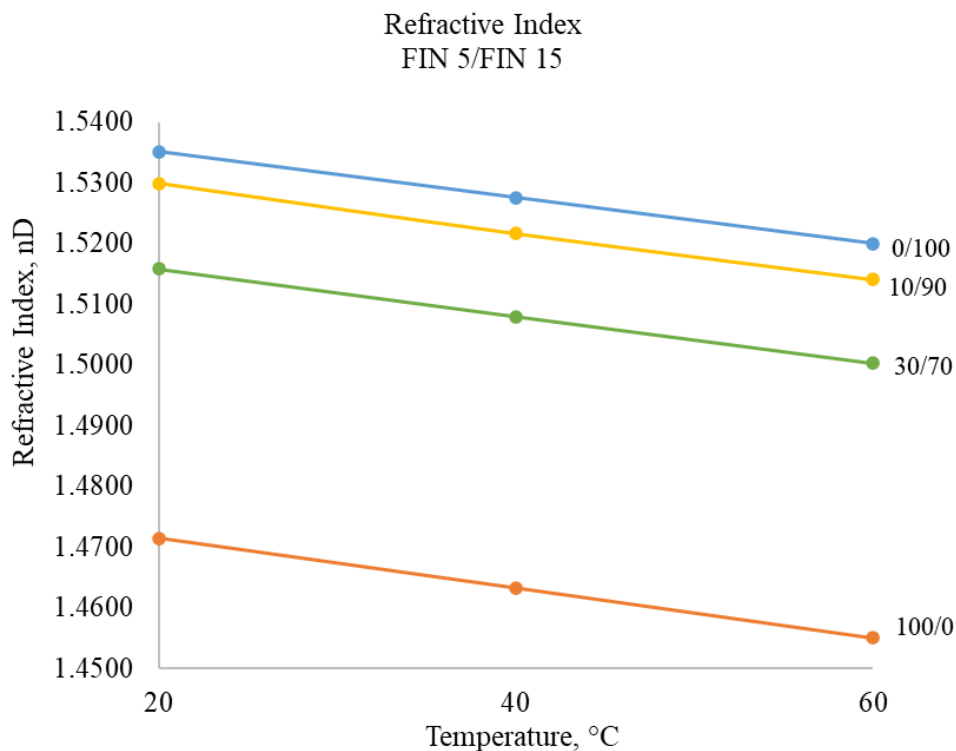


Figure 5.9 Refractive Index distribution for the FIN 5/FIN 15 blends.

For example, comparing the refractive index from Figure 5.9 to the experimental value, at FIN 5 (30 wt.)/FIN 15 (70 wt.) at 20°C, knowing only density data for FIN 5 and FIN 10, gives refractive index value of 1.51602 nD. The experimental value is 1.5158, the difference is 0.0002 nD. This difference is negligible and can appear during the experimental measurement of the refractive index.

However, one intriguing refractive index value is for BIN 12. At 70 wt.% of FIN 10 and 30 wt.% of FIN 15, the refractive index value did not follow the strictly proportional rule observed before. It might indicate a chemical reaction or physical change happening at that particular ratio at room temperature. To check the results the refractive index was measured again with a newly prepared blend of the same ratio (70 wt.% of FIN 10 and 30 wt.% of FIN 15). Two measurements show a similar trend, but one is much higher than 50 wt.% /50 wt.% and the other is lower (Figure 5.10 a and b). The reason for the variability in this specific combination of FIN 10 and FIN 15 remains unresolved.

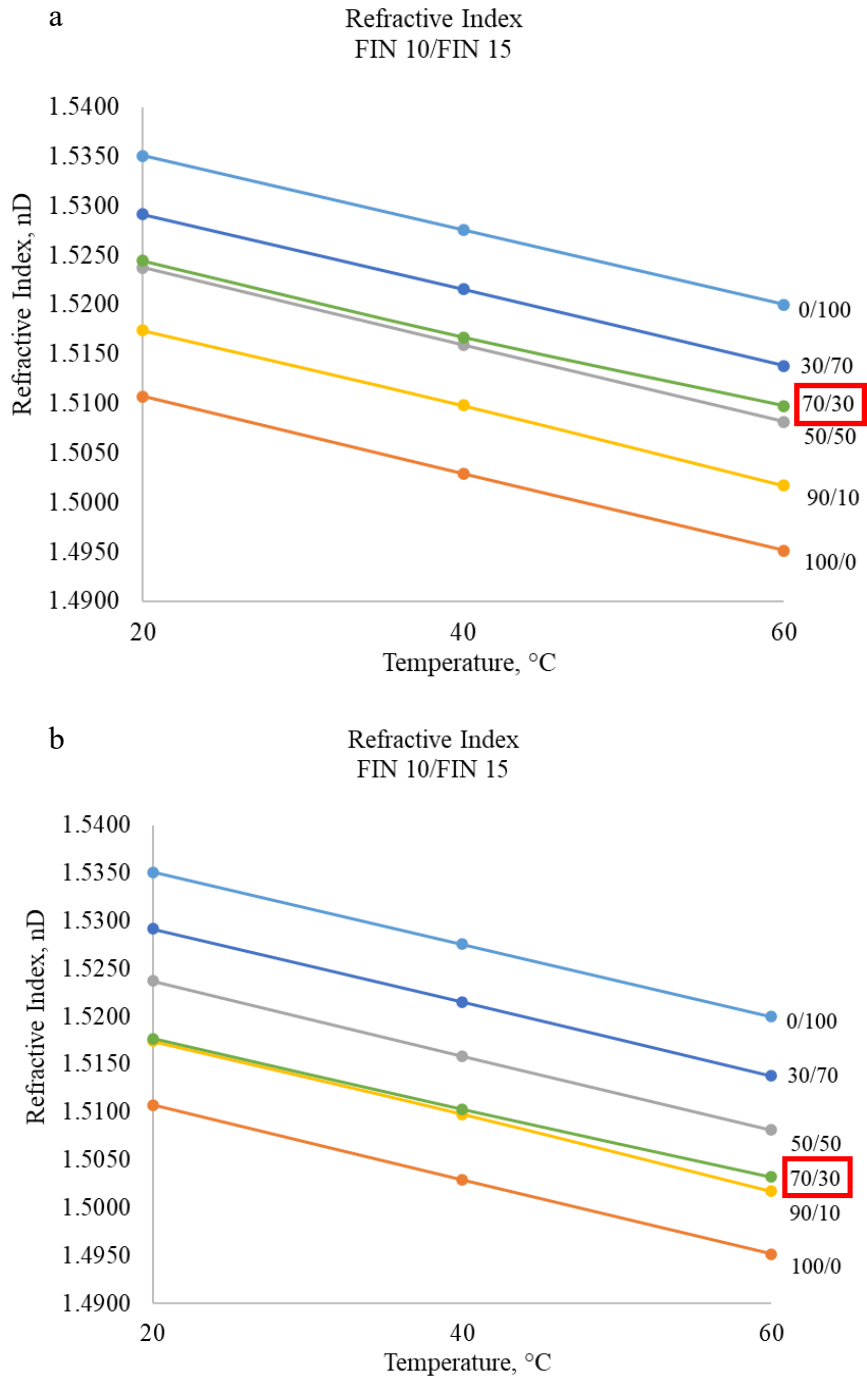


Figure 5.10 Refractive Index distribution for the FIN 10/FIN 15 blends.

5.4.5 Evaluating Density of Bitumen Distillation Blends

For density, fractions and blends distributions follow the same pattern (Figure 5.10, 5.11). All the plotted data is strictly based on the values found experimentally by the procedure in 5.2.2 Analyses.

Dependence like that can demonstrate that there are no chemical reactions taking place and the blending is a purely physical phenomenon in the given temperature range.

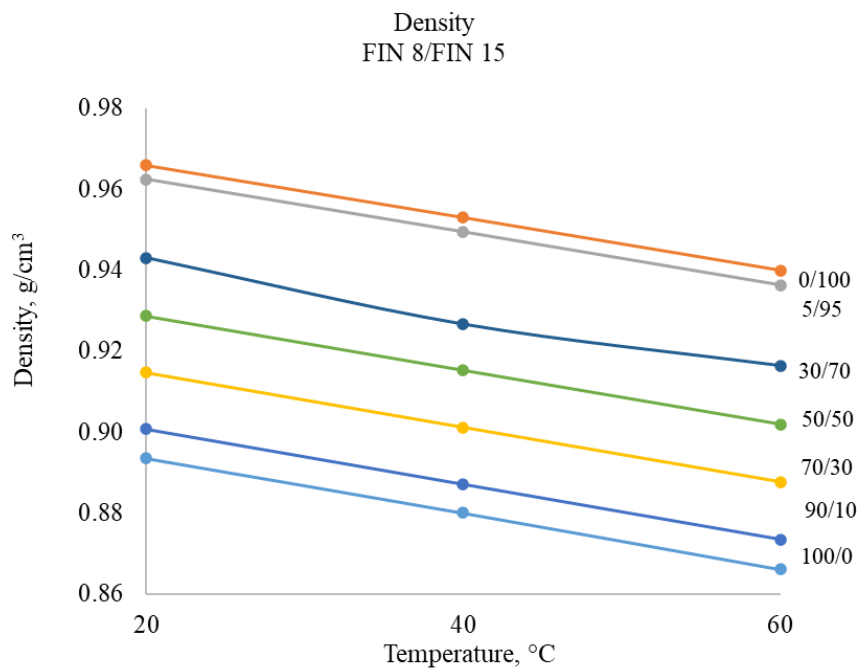


Figure 5.11 Density distribution for the FIN 8/FIN 15 blends.

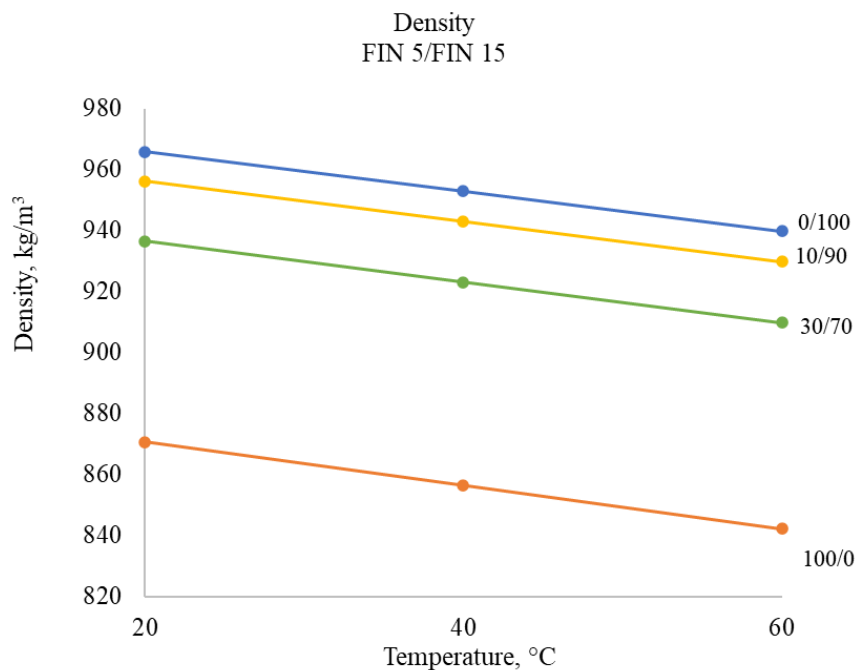


Figure 5.12 Density distribution for the FIN 5/FIN 15 blends.

5.4.6 Evaluating Viscosity of Bitumen Distillation Blends

When it comes to viscosity, it is very different.⁶ This was to be expected because the binary mixing rules for viscosity are non-linear. In Figure 5.11 the blue line represents the viscosity of pure FIN 15. Adding only 10 wt.% of FIN 5 decreases the viscosity dramatically.

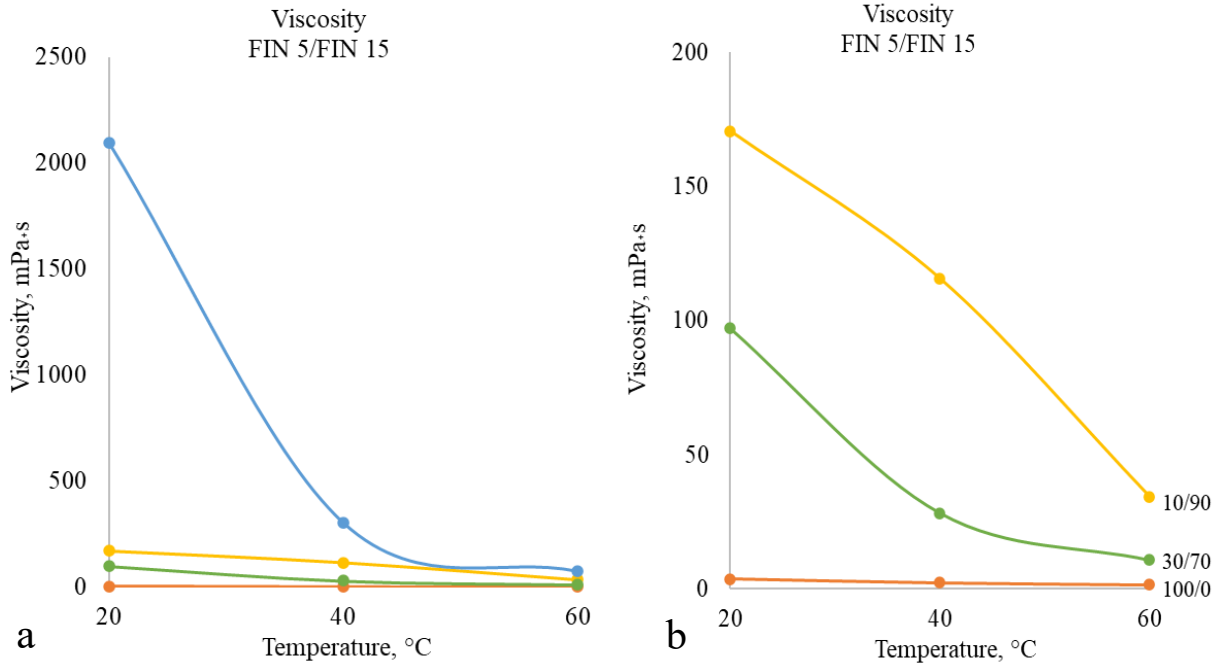


Figure 5.13 Viscosity distribution for the blends FIN 5/FIN 15 (a) with pure FIN 15 (blue line), (b) without pure FIN 15

Figure 5.14 illustrates the viscosity distribution for FIN 8/15. Since FIN 8 has a higher boiling range (270-290°C) compared to FIN 5 (210-230°C) its influence on FIN 15 viscosity is much lower. Still as low as 5 wt.% FIN 8 affects the viscosity of a heavy boiling fraction FIN 15 (410-430°C).

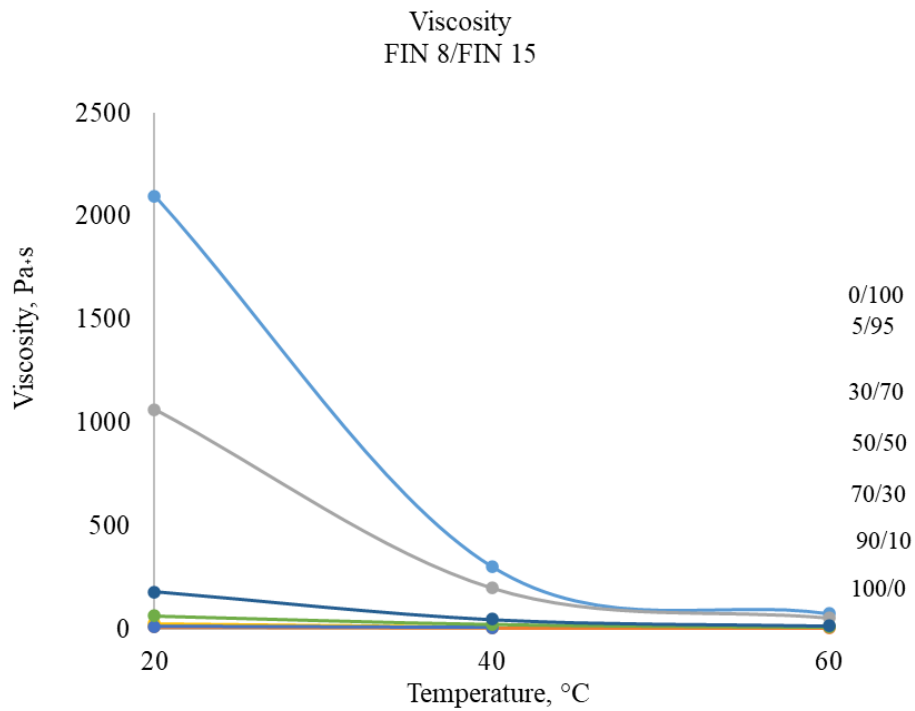


Figure 5.14 Viscosity distribution for the blends FIN 8/FIN 15

This study has not evaluated the binary mixing rules used to describe the change in viscosity on mixing. This would become the logical starting point for a follow-up study.

5.5 Conclusion

In this chapter, ASTM D341 – 20^{e1} standard was experimentally applied by comparing calculated and experimental data, with the result of being accurate for essentially every fraction with R^2 ranging from 0.9992 to 1.0000. The difference between experimentally found and calculated by ASTM D341 – 20^{e1} viscosity values for the 15 bitumen distillation reactions used in this study is expressed by an average error of 1.5%. However, the relationship is based on empirical data, and a deeper scientific explanation is required.

To give a physical meaning behind the viscosity of bitumen distillation fractions Hildebrand's molal volume change postulate was applied. Experimentally found viscosity values compared to the values calculated through the postulate demonstrated that this might be true for the lighter fractions, but as the viscosity of the fractions goes up a linear trend of temperature versus viscosity relationship turns exponential. This might be due to the fact that Hildebrand's proposal was based on viscosity dependencies in pure compounds, while bitumen distillation fractions are a very complex mix of hydrocarbons.

Another approach taken in this Chapter was to test how different bitumen distillation fractions compare to each other by forming a blend. 14 blends were created with known ratios from 15 distillation fractions that cover mostly higher boiling fractions since they are producing the most volume during bitumen distillation and do not fall under traditional viscosity interpretations. A follow-up study to evaluate how well this data is described by binary mixing rules is recommended.

Overall, it was found that the relationship between density and measurement temperature in a blend is linear over the range of 20-60°C, with density decreasing with an increase in temperature at the rate of - 0.0007 g/cm³/°C. The Refractive Index values also decreased with a temperature increase with a slope of the line equal to -0.0004 nD/°C.

The viscosity of the blends did not show a similar trend to refractive index and density relationships as was anticipated from the literature. This study did not evaluate the measured data for blends against predictions by binary mixing rules and it is recommended that this would be a good place to start for any follow-up work.

REFERENCES

- (1) Anton Paar GmbH. Limits of the Measuring Range: This Far and No Further <https://www.azom.com/article.aspx?ArticleID=18932> (accessed Jul 16, 2021).
- (2) Horovitz, K. L.; Johnson, V. A. *Solid State Physics, Part A*; ISSN; Elsevier Science, 1959.
- (3) Hildebrand, J. H. Motions of Molecules in Liquids: Viscosity and Diffusivity. *Science* **1971**, *174* (4008), 490–493.
- (4) Ewert, W Lewis, C. API Gravity and Viscosity of Residues from Conventional and Bitumen-Containing Crude Oils. In *Conference proceedings, 5th NCUT upgrading and refining conference 2009: bitumen, synthetic crude oil and heavy oil; by National Centre for Upgrading Technology*; Edmonton, 2009; pp 549–571.
- (5) Riazi, M. R. *Characterization and Properties of Petroleum Fractions*; ASTM manual series MNL 50; ASTM International, 2005.
- (6) Centeno, G.; Sánchez-Reyna, G.; Ancheyta, J.; Muñoz, J. A. D.; Cardona, N. Testing Various Mixing Rules for Calculation of Viscosity of Petroleum Blends. *Fuel* **2011**, *90* (12), 3561–3570.

CHAPTER 6 – CONCLUSION

6.1 Introduction

The objective of this thesis was to study the effect of solvents on free radical content in bitumen, perform fractional distillation of bitumen and analyse the physical properties of the obtained fractions. Those objectives share a common goal of finding potential use for bitumen upgrading or contributing to a general theoretical understanding behind the upgrading.

6.2 Solvent Effect on Bitumen Free Radical Content

Electron Spin Resonance (ESR) spectroscopy was used to generate data on how different solvents will affect the free radical content in bitumen by changing the dissociation equilibrium of radical pairs. The solubility of bitumen was checked in the 54 different solvents considered for the study prior to analysis to evaluate solubility. The g-factor and analyte spin content generated from the quantitative analysis of the ESR spectra were correlated with the solvents' properties like the dipole moment, dielectric constant, ionization potential, molecular weight, density, dynamic and kinematic viscosities.

6.2.1 Major conclusions

The main conclusion is that adding a solvent to bitumen at room temperature changes its free radical content. Using the same bitumen depending on added solvent analyte spin content ranges from 6×10^{17} to 1.5×10^{18} in the same bitumen sample. Solvent properties such as g-factor of dissociated radical pairs showed to be shifted depending on the dipole moment of the solvent. The higher the dipole moment, the more shifted is the g-factor. Surprisingly, the ionization potential of sulfur containing, monoaromatic and diaromatic solvents was linearly proportional to the free radical concentration observed. Free radical concentration was poorly correlated with the other solvent properties.

6.3 Bitumen Vacuum Distillation and Refractive Index Measurements

Another approach was to apply hands-on fractional distillation to receive liquid oil products from bitumen. While atmospheric distillation did not yield any liquid, vacuum distillation of bitumen was completed five times with an average liquid yield of 25 wt.%. It resulted in about 15 fractions for each of the five distillations with a temperature range of 20°C for each cut.

Atmospheric and vacuum fractional distillation of bitumen were carried out with the goal of receiving liquid products without causing a chemical reaction. Since the fractions were used for further study, the outcome of this work is listed in terms of achievements, rather than conclusions.

6.3.1 Major achievements

- Vacuum distillation of bitumen was completed five times with an average liquid yield of 25 wt.% which is very typical for bitumen when the final cut point was 430°C. It resulted in about 15 fractions for each of the five distillations with a temperature range of 20°C for each cut.
- In addition to the temperature range, the fractions were characterized by refractive index values. The intent behind this was to check that the same cut from different distillation runs was comparable. It showed a consistent result with an average difference of only 0.0025 nD.

6.4 Relationships in Physical Properties of Bitumen Fractions

Using the distillation fractions obtained, temperature dependent measurements of viscosity, Refractive Index and density were experimentally obtained and evaluated to find how relationships change in bitumen distillation fractions. Another approach taken in this Chapter was to test how the physical properties changed when blends of different bitumen distillation fractions were prepared. 14 blends were created with known ratios from 15 previously obtained bitumen distillation fractions. The blends were mostly made from higher boiling range fractions, for example, 270-290°C and 410-430°C, since they are producing the highest volume from distillation.

6.4.1 Major conclusions

The viscosity versus temperature relationship was evaluated through Hildebrand's change in molar volume postulate. The experimental results demonstrated that this might be true for the lighter fractions, but as the viscosity of the fractions goes up the linear trend turns to exponential. This might be due to the fact that Hildebrand's proposal was based on viscosity dependencies in pure compounds, while bitumen distillation fractions are a very complex mix of hydrocarbons.

Refractive Index and density data demonstrated that the relationship between blends is related by % by weight composition, i.e., knowing the density of two pure distillation fractions, refractive index and density can be accurately estimated by only knowing wt.% of each. An assumption can be made that no chemical reaction is taking place and the blending is a purely physical phenomenon in the temperature range of 20-60°C. However, one blend consisting of 70 wt.% of bitumen distillation fraction with a boiling range of 310-330°C and 30 wt.% of 410-430°C deviated from that relationship.

Overall, it was found that the relationship between density and measurement temperature in a blend is linear over the range of 20-60°C, with density decreasing with an increase in temperature at the rate of $-0.0007 \text{ g/cm}^3/\text{°C}$. The Refractive Index values also decreased with a temperature increase with a slope of the line equal to -0.0004 nD/°C .

The viscosity of the blends did not show a similar trend to refractive index and density relationships. As with the pure fractions, lighter blends had linear growth while heavier ones grow exponentially with respect to temperature. But it was found that adding a lighter boiling fraction with as little as 10 wt.% to a heavier fraction can dramatically decrease viscosity.

BIBLIOGRAPHY

- Abragam, A.; Bleaney, B. *Electron Paramagnetic Resonance of Transition Ions*; Dover Books on Physics and Chemistry; Dover Publications, 1986.
- Alberta Energy. Oil sands facts and statistics <https://www.alberta.ca/oil-sands-facts-and-statistics.aspx>.
- Alemán-Vázquez, L. O.; Cano-Domínguez, J. L.; García-Gutiérrez, J. L. Effect of Tetralin, Decalin and Naphthalene as Hydrogen Donors in the Upgrading of Heavy Oils. *Procedia Engineering* 2012, 42, 532–539. <https://doi.org/10.1016/j.proeng.2012.07.445>.
- Alili, A. *Persistent Free Radicals in Asphaltenes and Their Reactions*, University of Alberta, 2019.
- Alili, A. S.; Siddiquee, M. N.; de Klerk, A. Origin of Free Radical Persistence in Asphaltenes: Cage Effect and Steric Protection. *Energy & Fuels* 2020, 34 (1), 348–359. <https://doi.org/10.1021/acs.energyfuels.9b03836>.
- Anton Paar GmbH. Limits of the Measuring Range: This Far and No Further <https://www.azom.com/article.aspx?ArticleID=18932> (accessed Jul 16, 2021).
- ASTM D341. Standard Practice for Viscosity-Temperature Equations and Charts for Liquid Petroleum or Hydrocarbon Products. 2020, pp 1–6.
- Atherton, N. M.; Weissman, S. I. Association Between Sodium and Naphthalenide Ions. *Journal of the American Chemical Society* 1961, 83 (6), 1330–1334.
- Banerjee, D. K. *Oil Sands, Heavy Oil and Bitumen - From Recovery to Refinery*; PennWell Corporation: Tulsa, 2012.
- Barman, B. N.; Cebolla, V. L.; Membrado, L. Chromatographic Techniques for Petroleum and Related Products. *Crit. Rev. Anal. Chem.* 2000, 30 (2–3), 75–120.
- Bitzer, Z. T.; Goel, R.; Reilly, S. M.; Foulds, J.; Muscat, J.; Elias, R. J.; Richie, J. P. Effects of Solvent and Temperature on Free Radical Formation in Electronic Cigarette Aerosols. *Chem. Res. Toxicol.* 2018, 31, 4–12. <https://doi.org/10.1021/acs.chemrestox.7b00116>.
- Boduszynski, M. M. Composition of Heavy Petroleums. 1. Molecular Weight, Hydrogen Deficiency, and Heteroatom Concentration as a Function of Atmospheric Equivalent Boiling Point up to 1400°F (760°C). *Energy & Fuels* 1987, 1 (1), 2–11.

- Briner, E.; Ryffel, K.; Perrottet, E. Ozonation de l'allyl-, Du Propényl-et Du Méthovinylbenzène. Résultats de Déterminations Physico-chimiques (Spectres Raman, Spectres d'absorption Ultra-violette, Constantes Diélectriques et Moments Dipolaires). *Helvetica Chimica Acta* 1939, 22 (1), 927–934.
- Caminati, W. Low-Energy Vibrations of Indene. *Journal of the Chemical Society, Faraday Transaction* 1993, 89 (23), 4153–4155.
- Castellanos Díaz, O.; Sánchez-Lemus, M. C.; Schoeggl, F. F.; Satyro, M. A.; Taylor, S. D.; Yarranton, H. W. Deep-Vacuum Fractionation of Heavy Oil and Bitumen, Part I: Apparatus and Standardized Procedure. *Energy & Fuels* 2014, 28 (5), 2857–2865.
- Centeno, G.; Sánchez-Reyna, G.; Ancheyta, J.; Muñoz, J. A. D.; Cardona, N. Testing Various Mixing Rules for Calculation of Viscosity of Petroleum Blends. *Fuel* 2011, 90 (12), 3561–3570.
- Chen, H.; Wang, W.; Yang, Y.; Jiang, P.; Gao, W.; Cong, R.; Yang, T. Solvent Effect on the Formation of Active Free Radicals from H₂O₂ Catalyzed by Cr-Substituted PKU-1 Aluminoborate : Spectroscopic Investigation and Reaction Mechanism. *Applied Catalysis A, General* 2019, 588, 117283. <https://doi.org/10.1016/j.apcata.2019.117283>.
- Clarke, P. F.; Pruden, B. B. Asphaltene Precipitation from Cold Lake and Athabasca Bitumens. *Petroleum Science and Technology* 1998, 16 (3–4), 287–305. <https://doi.org/10.1080/10916469808949784>.
- Dalal, D. P.; Eaton, S. S.; Eaton, G. R. The Effects of Lossy Solvents on Quantitative EPR Studies. *Journal of Magnetic Resonance (1969)* 1981, 44 (3), 415–428. [https://doi.org/https://doi.org/10.1016/0022-2364\(81\)90276-6](https://doi.org/https://doi.org/10.1016/0022-2364(81)90276-6).
- de Klerk, A. Thermal Conversion in Upgrading Part I. University of Alberta: Edmonton 2020, p 32.
- de Klerk, A. Thermal Conversion in Upgrading Part II: Visbreaking. University of Alberta: Edmonton 2020, p 29.
- de Klerk, A. Thermal Conversion Modeling of Visbreaking at Temperatures below 400 °C. *Energy & Fuels* 2020, 34 (12), 15285–15298. <https://doi.org/10.1021/acs.energyfuels.0c02336>.
- de Klerk, A. Unconventional Oil: Oilsands. In *Future Energy*; Letcher, T., Ed.; Elsevier, 2020; pp 49–65.

- Dente, M.; Bozzano, G.; Bussani, G. A Comprehensive Program for Visbreaking Simulation: Product Amounts and Their Properties Prediction. *Computers & Chemical Engineering* 1997, 21 (10), 1125–1134. [https://doi.org/10.1016/S0098-1354\(96\)00323-7](https://doi.org/10.1016/S0098-1354(96)00323-7).
- Eaton, G. R.; Eaton, S. S.; Barr, D. P.; Weber, R. T. Basics of Continuous Wave EPR. In *Quantitative EPR*; Springer Wien New York, 2010; pp 1–3.
- Eaton, G. R.; Eaton, S. S.; Barr, D. P.; Weber, R. T. *Quantitative EPR*; Springer Vienna: Vienna, 2010.
- Ewert, W Lewis, C. API Gravity and Viscosity of Residues from Conventional and Bitumen-Containing Crude Oils. In *Conference proceedings, 5th NCUT upgrading and refining conference 2009: bitumen, synthetic crude oil and heavy oil*; by National Centre for Upgrading Technology; Edmonton, 2009; pp 549–571.
- Gendell, J.; Freed, J. H.; Fraenkel, G. K. Solvent Effects in Electron Spin Resonance Spectra. *The Journal of Chemical Physics* 1962, 37 (12), 2832–2841.
- Giese, B. Synthetic Applications of Radical C-C Bond Forming Reactions. *Research on Chemical Intermediates* 1986, 7 (1), 3–11.
- Gould, K. A.; Wiehe, I. A. Natural Hydrogen Donors in Petroleum Resids. *Energy and Fuels* 2007, 21 (3), 1199–1204. <https://doi.org/10.1021/ef060349t>.
- Government of Alberta. Oil Production <https://economicdashboard.alberta.ca/OilProduction> (accessed Jan 2, 2021).
- Gray, M. *Upgrading Oilsands Bitumen and Heavy Oil*; University of Alberta Press: Edmonton, 2015.
- Guo, A.; Wang, Z.; Feng, J.; Que, G. Mechanistic Analysis on Thermal Cracking of Petroleum Residue Using H-Donor as a Probe. *Preprints-American Chemical Society. Division of Petroleum Chemistry* 2001, 46 (4), 344–347.
- Guo, A.; Wang, Z.; Zhang, H.; Zhang, X.; Wang, Z. Hydrogen Transfer and Coking Propensity of Petroleum Residues under Thermal Processing. *Energy and Fuels* 2010, 24 (5), 3093–3100. <https://doi.org/10.1021/ef100172r>.
- Harmony, J. A. K. Molecule-Induced Radical Formation. In *Methods in free-radical chemistry vol. 5*; Huyser, E. S., Ed.; Marcel Dekker, Inc: New York, 1974; pp 101–176.
- Hassell, W. F.; Walker, S. Dielectric Studies. Part 4.—Relaxation Processes of Four Monoalkylbenzenes. *Transactions of the Faraday Society* 1966, 62, 861–873.

- Hayes, B. L. *Microwave Synthesis: Chemistry at the Speed of Light*; Cem Corporation, 2002.
- Hecht, E. *Optics*, 4th ed.; Pearson, 2002.
- Hendry, D. G.; Russell, G. A. Solvent Effects in the Reactions of Free Radicals and Atoms. IX. Effect of Solvent Polarity on the Reactions of Peroxy Radicals. *Journal of the American Chemical Society* 1964, 86 (12), 2368–2371.
- Herkes, F. E.; Friedman, J.; Bartlett, P. D. Peresters XIII. Solvent Effects in the Decomposition of t-Butylperoxy α -Phenylisobutyrate with Special Reference to the Cage Effect. *International Journal of Chemical Kinetics* 1969, 1 (2), 193–207.
- Hernández, M. S.; Coll, D. S.; Silva, P. J. Temperature Dependence of the Electron Paramagnetic Resonance Spectrum of Asphaltenes from Venezuelan Crude Oils and Their Vacuum Residues. *Energy and Fuels* 2019, 33, 990–997. <https://doi.org/10.1021/acs.energyfuels.8b03951>.
- Hildebrand, J. H. *Motions of Molecules in Liquids: Viscosity and Diffusivity*. *Science* 1971, 174 (4008), 490–493.
- Holtomo, O.; Nsangou, M.; Fifen, J. J.; Motapon, O. DFT Study of the Effect of Solvent on the H-Atom Transfer Involved in the Scavenging of the Free Radicals • HO₂ and •O₂- by Caffeic Acid Phenethyl Ester and Some of Its Derivatives. *Journal of molecular modeling* 2014, 20 (11), 2509. <https://doi.org/10.1007/s00894-014-2509-9>.
- Horovitz, K. L.; Johnson, V. A. *Solid State Physics, Part A*; ISSN; Elsevier Science, 1959.
- Ignasiak, T. M.; Strausz, O. P. Reaction of Athabasca Asphaltene with Tetralin. *Fuel* 1978, 57 (10), 617–621. [https://doi.org/10.1016/0016-2361\(78\)90191-6](https://doi.org/10.1016/0016-2361(78)90191-6).
- Isenberg, I.; Baird, S. L. Solvent Effects in Radical Ion Formation. *Journal of the American Chemical Society* 1962, 84 (20), 3803–3805.
- Jamaluddin, A. K. M.; Nazarko, T. W.; Sills, S.; Fuhr, B. J. Deasphalted Oil - A Natural Asphaltene Solvent. *SPE Production & Facilities* 2007, 11 (3), 161–165. <https://doi.org/10.2118/28994-pa>.
- Kappe, C. O. *Controlled Microwave Heating in Modern Organic Synthesis Angewandte*. 2004, 6250–6284. <https://doi.org/10.1002/anie.200400655>.

- Khulbe, K. C.; Mann, R. S.; Lu, B. C.-Y.; Lamarche, G.; Lamarche, A.-M. Effects of Solvents on Free Radicals of Bitumen and Asphaltenes. *Fuel Process. Technol.* 1992, 32 (3), 133–141.
- Kokorin, A. I.; Tran, V. A.; Rasmussen, K.; Grampp, G. Effect of Solvent Nature on Spin Exchange in Rigid Nitroxide Biradicals. *Applied Magnetic Resonance* 2006, 30 (1), 35–42.
- Langer, A. W.; Stewart, J.; Thompson, C. E.; White, H. T.; Hill, R. M. Hydrogen Donor Diluent Visbreaking of Residua. *Industrial and Engineering Chemistry Process Design and Development* 1962, 1 (4), 309–312. <https://doi.org/10.1021/i260004a014>.
- León, A. Y.; Guzman, A.; Laverde, D.; Chaudhari, R. V.; Subramaniam, B.; Bravo-Suárez, J. J. Thermal Cracking and Catalytic Hydrocracking of a Colombian Vacuum Residue and Its Maltenes and Asphaltenes Fractions in Toluene. *Energy and Fuels* 2017, 31 (4), 3868–3877. <https://doi.org/10.1021/acs.energyfuels.7b00078>.
- Lown, E.; Strausz, O. *The Chemistry of Alberta Oil Sands Bitumens and Heavy Oils*; Alberta Energy Research Institute publication: Calgary, 2003.
- Luckhurst, G. R.; Orgel, L. E. Solvent Effects in the Electron Spin Resonance Spectrum of Fluorenone Ketyl. *Molecular Physics* 1964, 8 (2), 117–124.
- Marquez, A.; Schoeggl, F. F.; Taylor, S. D.; Hay, G.; Yarranton, H. W. Viscosity of Characterized Visbroken Heavy Oils. *Fuel* 2020, 271. <https://doi.org/10.1016/j.fuel.2020.117606>.
- Mello, P. A.; Barin, J. S.; Guarnieri, R. A. Microwave Heating. In *Microwave-Assisted Sample Preparation for Trace Element Analysis*; Elsevier, 2014; pp 59–75.
- Neugebauer, J.; Louwse, M. J.; Belanzoni, P.; Wesolowski, T. A.; Baerends, E. J. Modeling Solvent Effects on Electron-Spin-Resonance Hyperfine Couplings by Frozen-Density Embedding. *The Journal of Chemical Physics* 2005, 123 (11), 114101.
- Nielsen, B. B.; Svrcek, W. Y.; Mehrotra, A. K. Effects of Temperature and Pressure on Asphaltene Particle Size Distributions in Crude Oils Diluted with N-Pentane. *Ind. Eng. Chem. Res.* 1994, 33, 1324–1330. <https://doi.org/10.1021/ie00029a031>.
- Oakes, J.; Symons, M. C. R. Solvation Spectra Part 24.-Effect of Solvent on the Electron Spin Resonance Spectra of 2,6-Dimethyl and Related p-Benzosemiquinones. *Transactions of the Faraday Society* 1968, 64, 2579–2585.

- Piette, L. H.; Ludwig, P.; Adams, R. N. Electron Paramagnetic Resonance of Aromatic and Aliphatic Nitro Anions in Aqueous Solution. *Journal of the American Chemical Society* 1962, 84 (22), 4212–4215.
- Pitt Quantum Repository pqr.pitt.edu.
- Plamondon, J. E.; Buenker, R. J.; Koopman, D. J.; Dolter, R. J. The Dipole Moment of Styrene. *Proceedings of the Iowa Academy of Science* 1963, 70 (1), 163–166.
- Poling, B. E.; Prausnitz, J. M.; O’Connell, J. P. *The Properties of Gases and Liquids*, 5th ed.; McGraw-Hill: New York, 2001.
- Rahimi, P. M.; Gentzis, T. Thermal Hydrocracking of Cold Lake Vacuum Bottoms Asphaltenes and Their Subcomponents. *Fuel Processing Technology* 2003, 80 (1), 69–79. [https://doi.org/10.1016/S0378-3820\(02\)00223-0](https://doi.org/10.1016/S0378-3820(02)00223-0).
- Rahimi, P.; Gentzis, T.; Fairbridge, C.; Khulbe, C. Chemistry of Petroleum Residues in the Presence of H-Donors. *Preprints-American Chemical Society. Division of Petroleum Chemistry* 1998, 43 (4), 634–636.
- Rahimi, P.; Gentzis, T.; Kubo, J.; Fairbridge, C.; Khulbe, C. Coking Propensity of Athabasca Bitumen Vacuum Bottoms in the Presence of H-Donors - Formation and Dissolution of Mesophase from a Hydrotreated Petroleum Stream (H-Donor). *Fuel processing technology* 1999, 60 (2), 157–170. [https://doi.org/10.1016/S0378-3820\(99\)00038-7](https://doi.org/10.1016/S0378-3820(99)00038-7).
- Rampolla, R. W.; Smyth, C. P. Microwave Absorption and Molecular Structure in Liquids. XXI. Relaxation Times, Viscosities and Molecular Shapes of Substituted Pyridines, Quinolines and Naphthalenes. *Journal of the American Chemical Society* 1958, 80 (5), 1057–1061.
- Raseev, S. *Thermal and Catalytic Processes in Petroleum Refining*; Marcel Dekker: New York, 2003.
- Riazi, M. R. *Characterization and Properties of Petroleum Fractions*; ASTM manual series MNL 50; ASTM International, 2005.
- Roberts, J. D.; Caserio, M. C. *Basic Principles of Organic Chemistry*, 2nd ed.; Addison-Wesley world student series; W. A. Benjamin, 1977.
- Rubinstein, M.; Colby, R. H. *Polymer Physics*; Oxford University Press: Oxford, 2003.

- Rueda-Velásquez, R. I.; Gray, M. R. A Viscosity-Conversion Model for Thermal Cracking of Heavy Oils. *Fuel* 2017, 197, 82–90. <https://doi.org/10.1016/j.fuel.2017.02.020>.
- Russell, G. A. Solvent Effects in the Reaction of Free Radicals and Atoms. V. Effects of Solvents on the Reactivity of t-Butoxy Radicals. *The Journal of Organic Chemistry* 1959, 24 (3), 300–302.
- Russell, G. A. Solvent Effects in the Reactions of Free Radicals and Atoms. II. Effects of Solvents on the Position of Attack of Chlorine Atoms upon 2,3-Dimethylbutane, Isobutane and 2-Deuterio-2-Methylpropane. *Journal of the American Chemical Society* 1958, 80 (18), 4987–4996.
- Russell, G. A. Solvent Effects in the Reactions of Free Radicals and Atoms. III. Effects of Solvents in the Competitive Photochlorination of Hydrocarbons and Their Derivatives. *Journal of the American Chemical Society* 1958, 80 (18), 4997–5001.
- Russell, G. A. Solvent Effects in the Reactions of Free Radicals and Atoms. IV. Solvents in Sulfuryl Chloride Chlorinations. *Journal of the American Chemical Society* 1958, 80 (18), 5002–5003.
- Russell, G. A. Solvent Effects in the Reactions of Free Radicals and Atoms. *Journal of the American Chemical Society* 1957, 79 (11), 2977–2978.
- Russell, G. A. Solvent Effects in the Reactions of Free Radicals and Atoms. VI. Separation of Polar and Resonance Effects in the Reactions of Chlorine Atoms. *Tetrahedron* 1960, 8 (1–2), 101–106.
- Russell, G. A.; Ito, A.; Hendry, D. G. Solvent Effects in the Reactions of Free Radicals and Atoms. VIII. The Photochlorination of Alkyl Hydrocarbons. *Journal of the American Chemical Society* 1963, 85 (19), 2976–2983.
- Sanderson, J. *Understanding Light Microscopy*; RMS - Royal Microscopical Society; Wiley, 2019.
- Seeton, C. Viscosity-Temperature Correlation for Liquids. *Tribol. Lett.* 2006, 22, 67–78.
- Senesi, N.; Senesi, G. S. *Electron-Spin Resonance Spectroscopy*; Elsevier: Oxford, 2005; pp 426–437.
- Sidgwick, N. V; Springall, H. D. 336. Dipole Moments and the Fixation of Aromatic Double Links: Bromohydrindenes and Bromotetralins. *Journal of the Chemical Society (Resumed)* 1936, 1532–1537.

- Sosnovsky, D. V; Morozova, O. B.; Yurkovskaya, A. V; Ivanov, K. L. Relation between CIDNP Formed upon Geminate and Bulk Recombination of Radical Pairs. *J. Chem. Phys.* 2017, 147, No. 024303.
- Speight, J. G. Chapter 10 - Fouling During Thermal Processes; Gulf Professional Publishing: Boston, 2015; pp 237–269. <https://doi.org/10.1016/B978-0-12-800777-8.00010-3>.
- Speight, J. G. *Heavy Oil Recovery and Upgrading*; Elsevier Science, 2019.
- Speight, J. G. Refining Heavy Oil and Extra-Heavy Oil. In *Heavy and Extra-heavy Oil Upgrading Technologies*; Gulf Professional Publishing: Boston, 2013; pp 1–13.
- Speight, J. G. Thermal Cracking. In *Heavy and Extra-heavy Oil Upgrading Technologies*; Elsevier: Boston, 2013; pp 15–38.
- Speight, J. G. Visbreaking: A Technology of the Past and the Future. *Scientia Iranica* 2012, 19 (3), 569–573. <https://doi.org/10.1016/j.scient.2011.12.014>.
- Sterck, B. De; Vaneerdeweg, R.; Prez, F. Du; Waroquier, M.; Speybroeck, V. Van. Solvent Effects on Free Radical Polymerization Reactions: The Influence of Water on the Propagation Rate of Acrylamide and Methacrylamide. *Macromolecules* 2010, 43, 827–836. <https://doi.org/10.1021/ma9018747>.
- Stone, E. W.; Maki, A. H. Electron Spin Resonance of Semiquinones in Aprotic Solvents. *The Journal of Chemical Physics* 1962, 36 (7), 1944–1945.
- Stone, E. W.; Maki, A. H. Solvent Effects on the Electron Spin Resonance Spectrum of P-Benzosemiquinone-1-C13. *Journal of the American Chemical Society* 1965, 87 (3), 454–458.
- Strausz, O. P.; Lown, E. M. Spectroscopic Probes Into the Molecular Structure of Asphaltene. In *The chemistry of Alberta Oil Sands, Bitumens and heavy oils*; Alberta Energy Research Institute: Calgary, Alberta, Canada, 2003; pp 592–604.
- Subramanian, H.; Landais, Y.; Sibi, M. P. Radical Addition Reactions. *Comprehensive Organic Synthesis: Second Edition* 2014, 4, 699–741. <https://doi.org/10.1016/B978-0-08-097742-3.00418-3>.
- Sueishi, Y.; Isozaki, T.; Yamamoto, S.; Nishimura, N. ESR Study of Solvent Effects on the Electronic Structure of 2-(4'-dialkylaminophenyl) Indan-1, 3-dionyl Radicals. *Journal of physical organic chemistry* 1992, 5 (4), 218–224.

- Tannous, J. H.; de Klerk, A. Quantification of the Free Radical Content of Oilsands Bitumen Fractions. *Energy & Fuels* 2019, 33 (8), 7083–7093. <https://doi.org/10.1021/acs.energyfuels.9b01115>.
- Thiyagarajan, P.; Hunt, J. E.; Winans, R. E.; Anderson, K. B.; Miller, J. T. Temperature-Dependent Structural Changes of Asphaltenes in 1-Methylnaphthalene. *Energy and Fuels* 1995, 9, 829–833. <https://doi.org/10.1021/ef00053a014>.
- Turuga, A. S. S. Effect of Solvent Deasphalting Process on the Properties of Deasphalted Oil and Asphaltenes From Bitumen, University of Alberta, 2017.
- Villamena, F. A. EPR Spin Trapping. In *Reactive Species Detection in Biology: From Fluorescence to Electron Paramagnetic Resonance Spectroscopy*; Elsevier: Boston, 2017; pp 163–202.
- Weather in Northeast Edmonton, July 13 world-weather.info/forecast/canada/northeast_edmonton/13-july/#2020 (accessed Oct 19, 2021).
- Wiehe, I. A. *Process Chemistry of Petroleum Macromolecules*; CRC Press: Boca Raton, 2008.
- Wiehe, I. A.; Yarranton, H. W.; Akbarzadeh, K.; Rahimi, P. M.; Tecler, A. The Paradox of Asphaltene Precipitation with Normal Paraffins. *Energy and Fuels* 2005, 19 (4), 1261–1267. <https://doi.org/10.1021/ef0496956>.
- Yan, Y.; C. Prado, G. H.; de Klerk, A. Storage Stability of Products from Visbreaking of Oilsands Bitumen. *Energy & Fuels* 2020, 34 (8), 9585–9598. <https://doi.org/10.1021/acs.energyfuels.0c01899>.
- Yokono, T.; Obara, T.; Sanada, Y.; Shimomura, S.; Imamura, T. Characterization of Carbonization Reaction of Petroleum Residues by Means of High-Temperature ESR and Transferable Hydrogen. *Carbon* 1986, 24 (1), 29–32.
- Zhang, L.; Zhang, L.; Xu, Z.; Guo, X.; Xu, C.; Zhao, S. Viscosity Mixing Rule and Viscosity–Temperature Relationship Estimation for Oil Sand Bitumen Vacuum Residue and Fractions. *Energy & Fuels* 2019, 33 (1), 206–214.
- Zhang, Y.; Siskin, M.; Gray, M. R.; Walters, C. C.; Rodgers, R. P. Mechanisms of Asphaltene Aggregation: Puzzles and a New Hypothesis. *Energy & Fuels* 2020, 34 (8), 9094–9107. <https://doi.org/10.1021/acs.energyfuels.0c01564>.

- Zhou, B.; Liu, Q.; Shi, L.; Liu, Z. Electron Spin Resonance Studies of Coals and Coal Conversion Processes: A Review. *Fuel Processing Technology* 2019, 188 (March), 212–227. <https://doi.org/10.1016/j.fuproc.2019.01.011>.

APPENDIX A

Distillation data extracted from B/R Instrument Corporation Crude Oil Distillation System Model 18 CODS

Distillation data was generated every day of running the Distillation System. Here, it will be represented in a way to indicate the day distillation started and the number of successful distillations. Table 4.3 Collected fractions for the Distillation 1 and consequent tables for the further distillation show that one complete distillation was done through three runs which equals three days. Extraction of the data was completed on software B/R Distillation Data View.

This data is valuable in a way to get an idea of real-life bitumen distillation behavior. The legends in the graph are best understood by looking at the distillation system elements illustrated in Figure 4.1. The basic meaning is that at one point in time the following temperatures are achievable during bitumen distillation before hitting theoretical cracking temperature that in this case is assumed to be 300°C (see Section 2.7.3 for details). All the information in this Appendix is very closely tied to the data from Chapter 4 such as feed bitumen mass and corresponding liquid products.

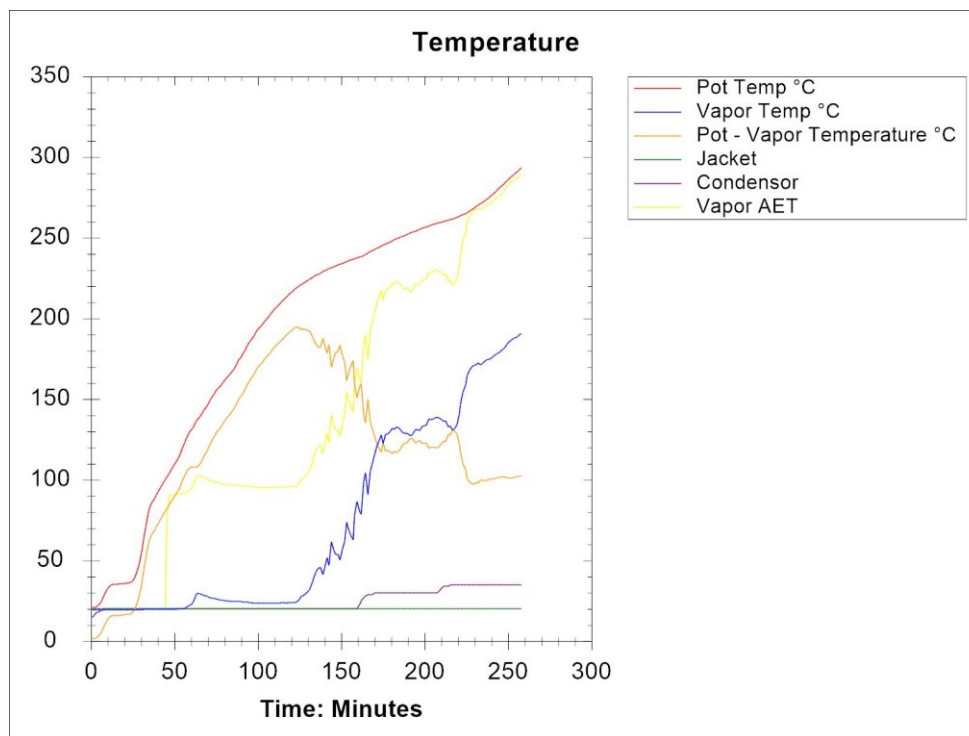


Figure A.1 Distillation data of the 1st day of Distillation 1 (Jul 14, 2020).

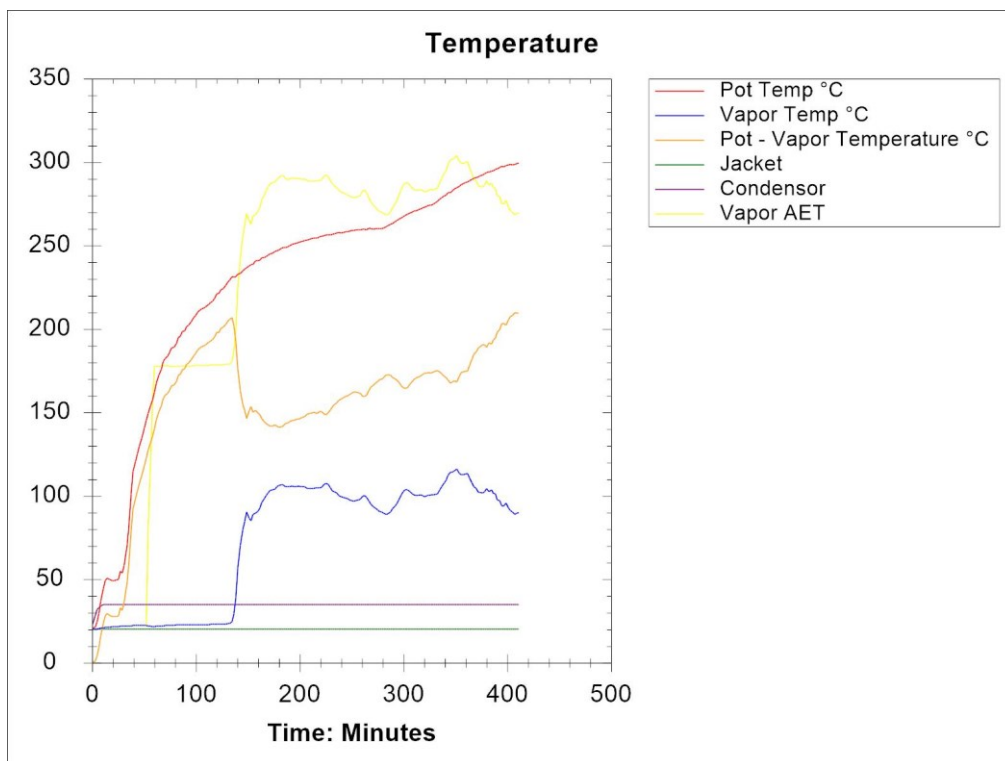


Figure A.2 Distillation data of the 2nd day of Distillation 1 (Jul 15, 2020).

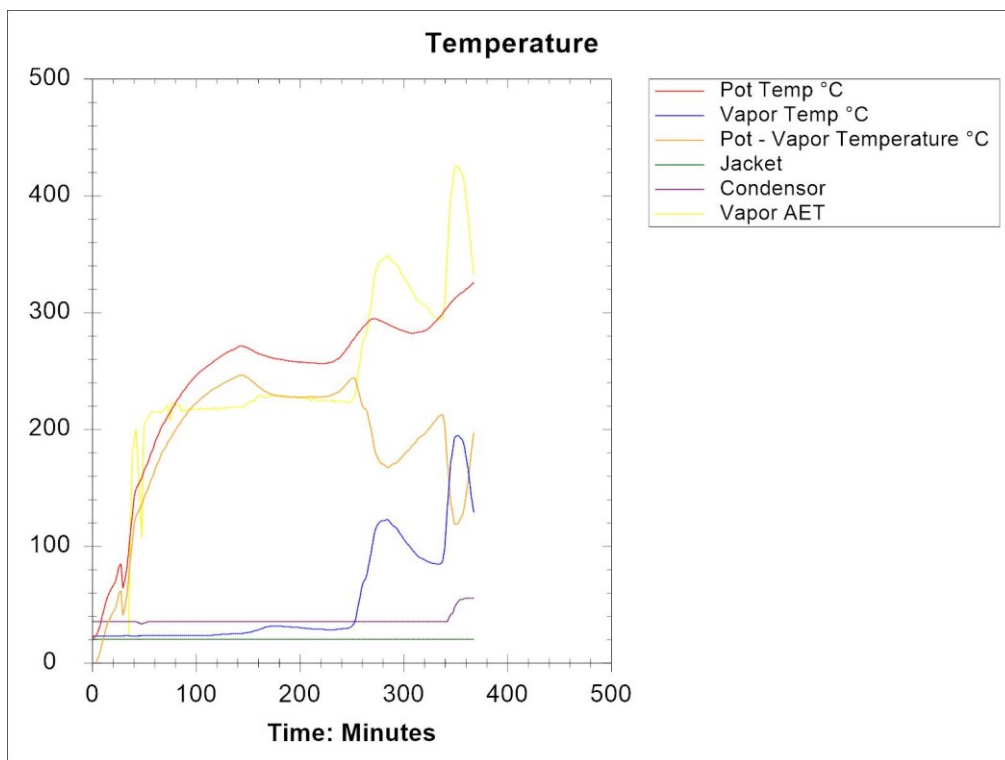


Figure A.3 Distillation data of the 3rd day of Distillation 1 (Jul 16, 2020).

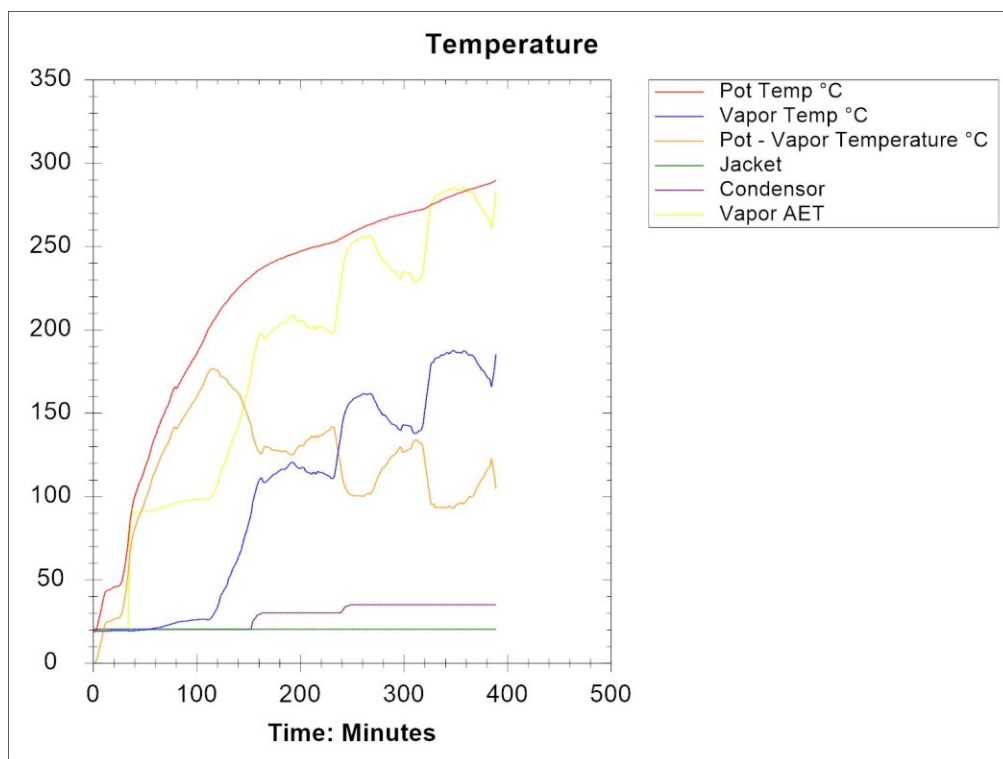


Figure A.4 Distillation data of the 1st day of Distillation 2 (Jul 21, 2020).

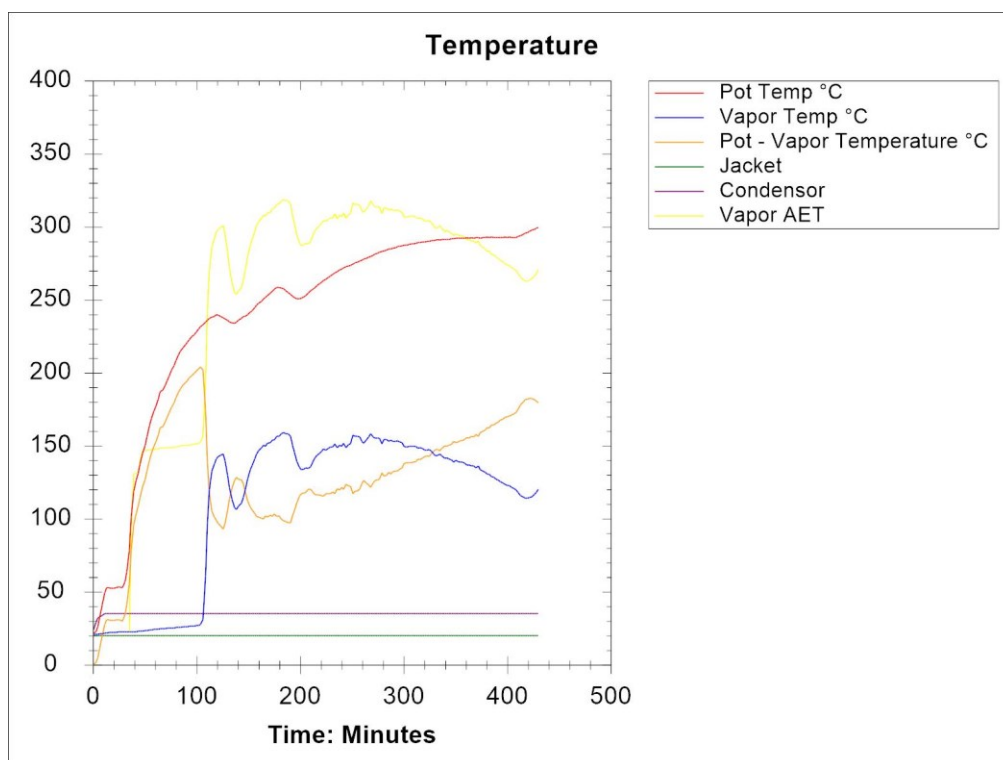


Figure A.5 Distillation data of the 2nd day of Distillation 2 (Jul 22, 2020).

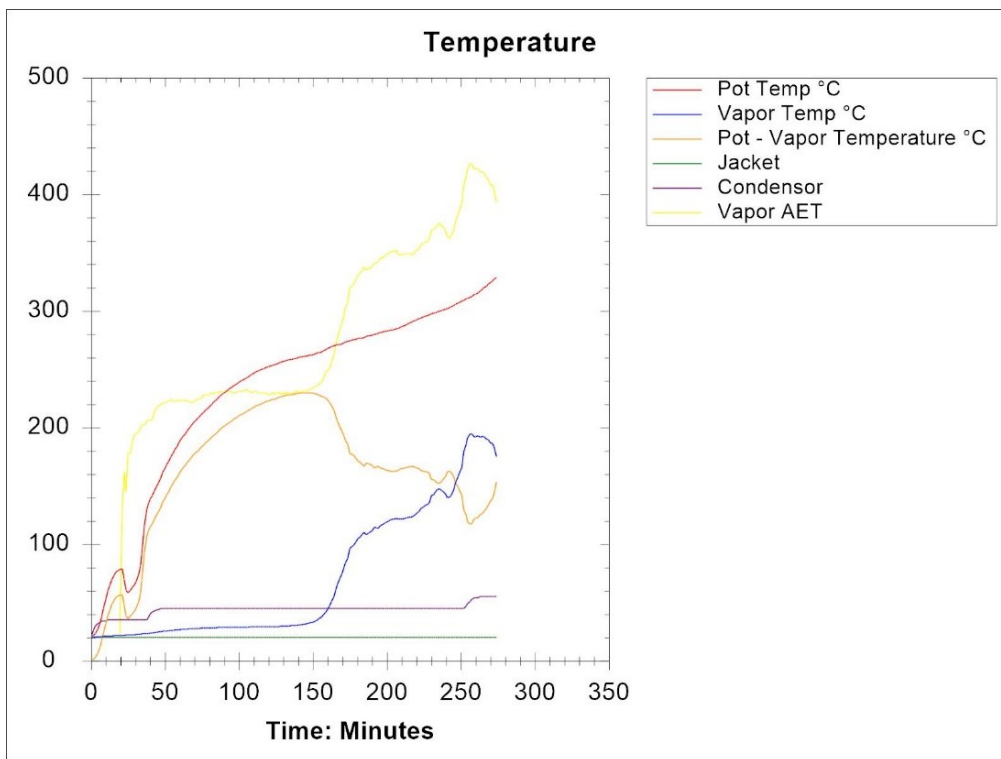


Figure A.6 Distillation data of the 3rd day of Distillation 2 (Jul 23, 2020).

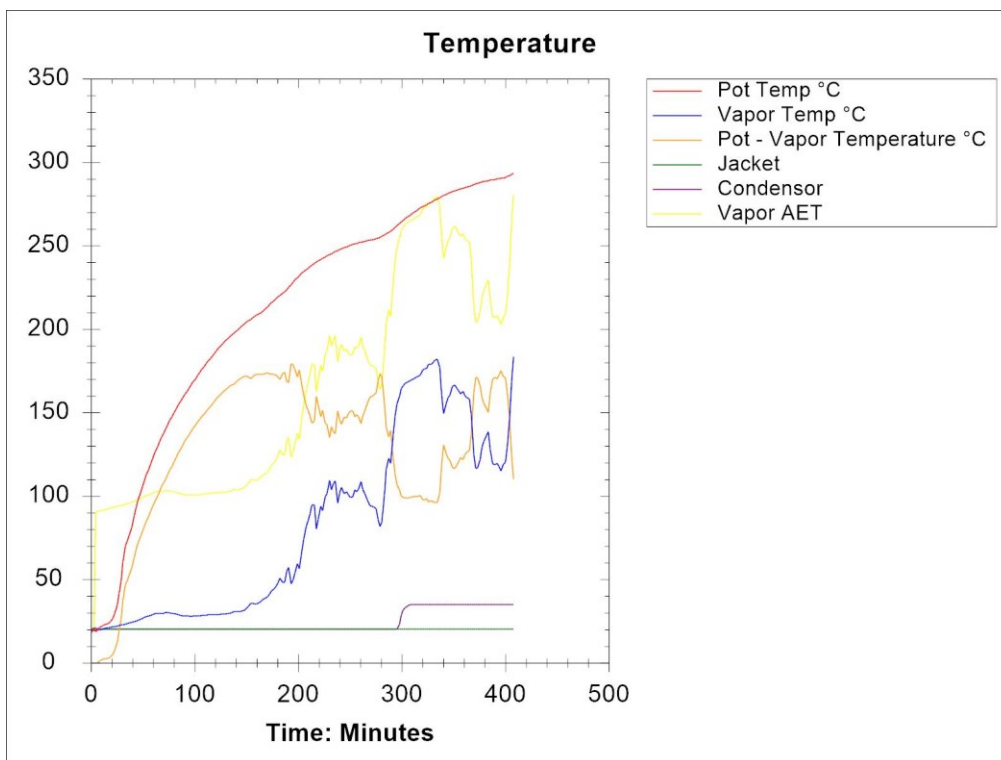


Figure A.7 Distillation data of the 1st day of Distillation 3 (Aug 11, 2020).

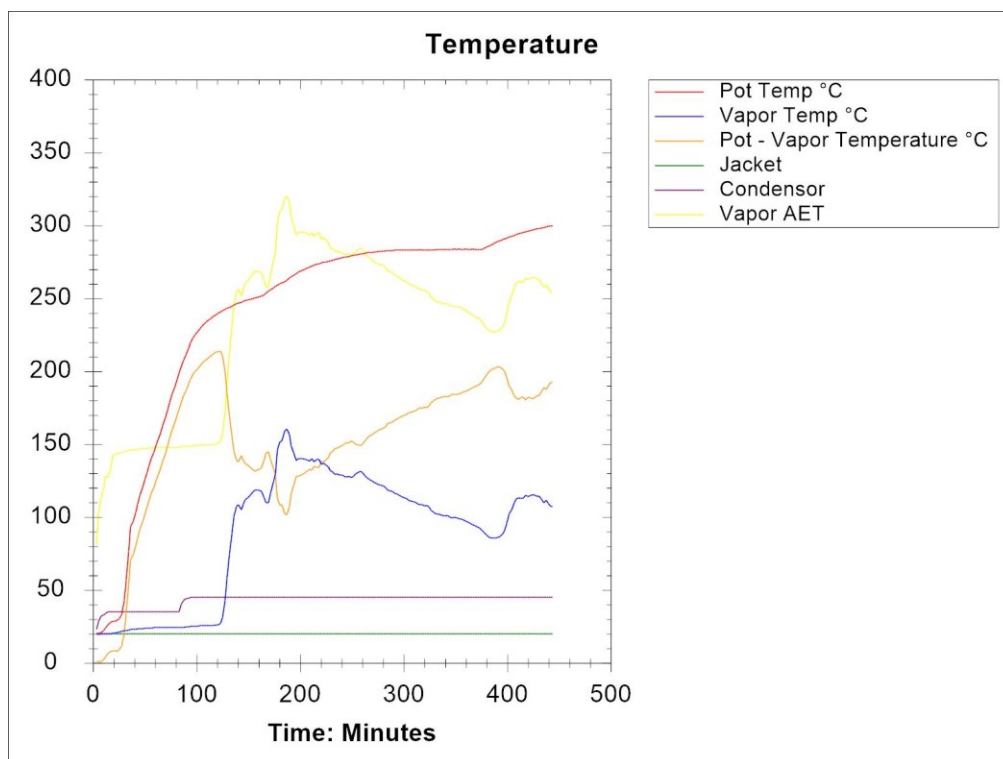


Figure A.8 Distillation data of the 2nd day of Distillation 3 (Aug 12, 2020).

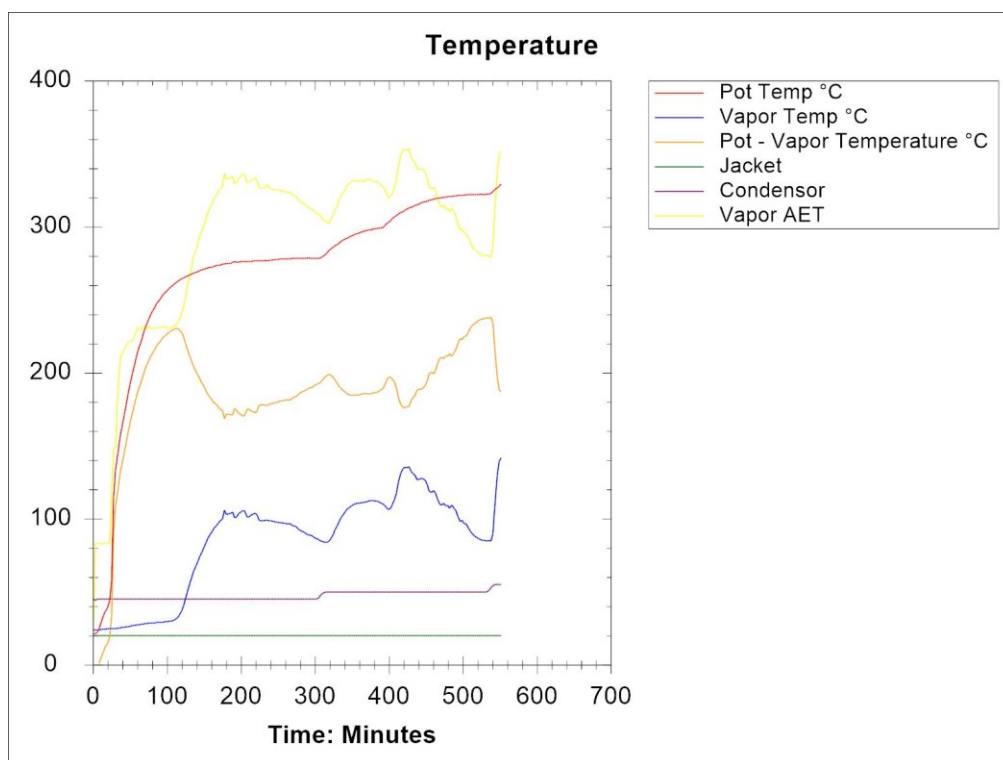


Figure A.9 Distillation data of the 3rd day of Distillation 3 (Aug 13, 2020).

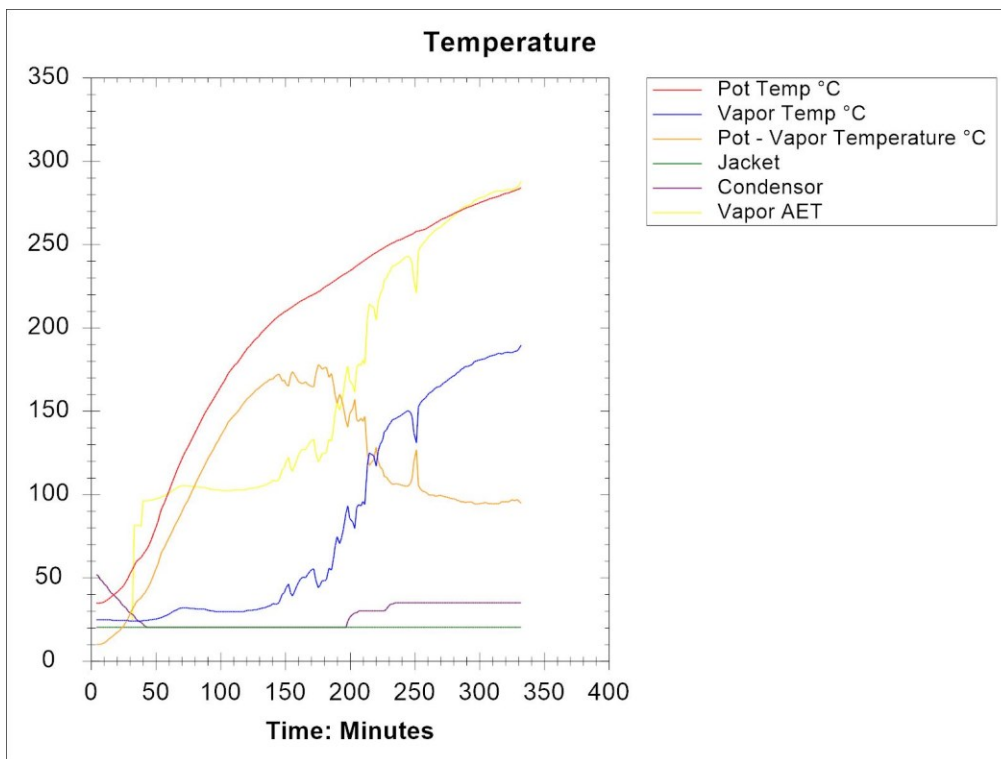


Figure A.10 Distillation data of the 1st day of Distillation 4 (Aug 17, 2020).

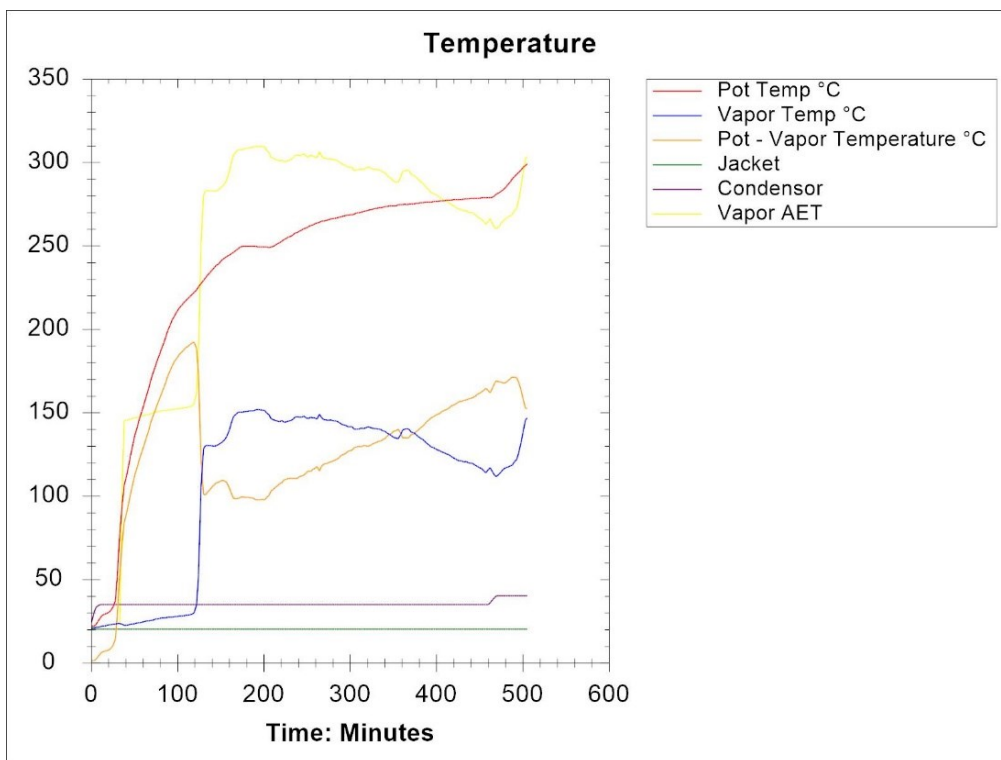


Figure A.11 Distillation data of the 2nd day of Distillation 4 (Aug 18, 2020).

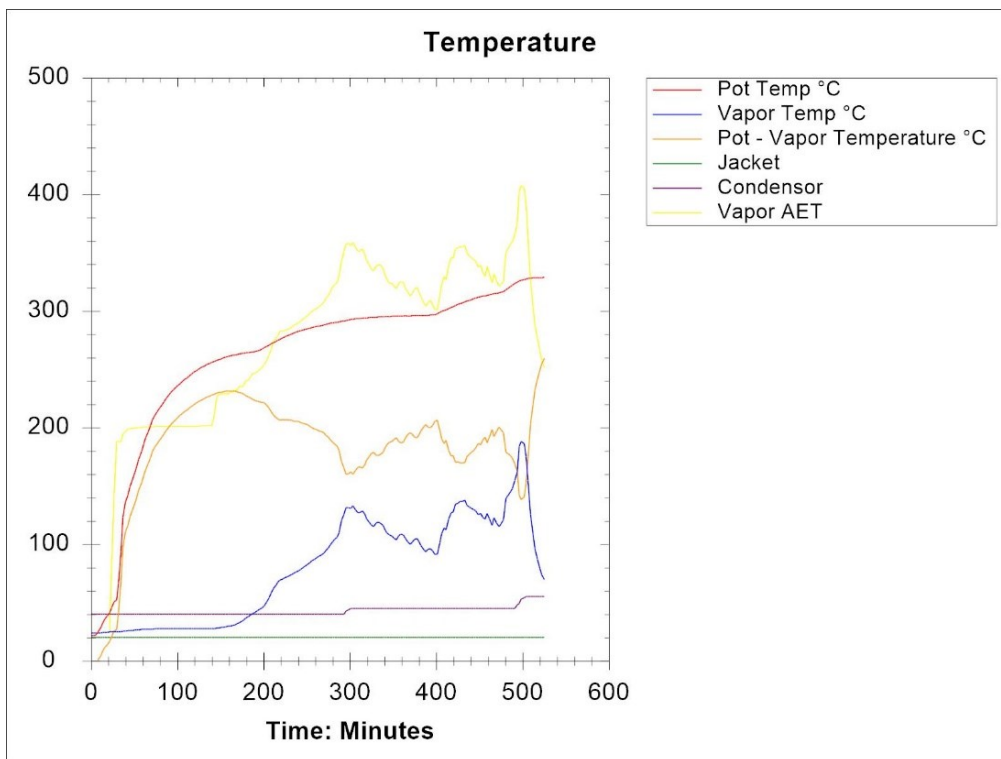


Figure A.12 Distillation data of the 3rd day of Distillation 4 (Aug 19, 2020).

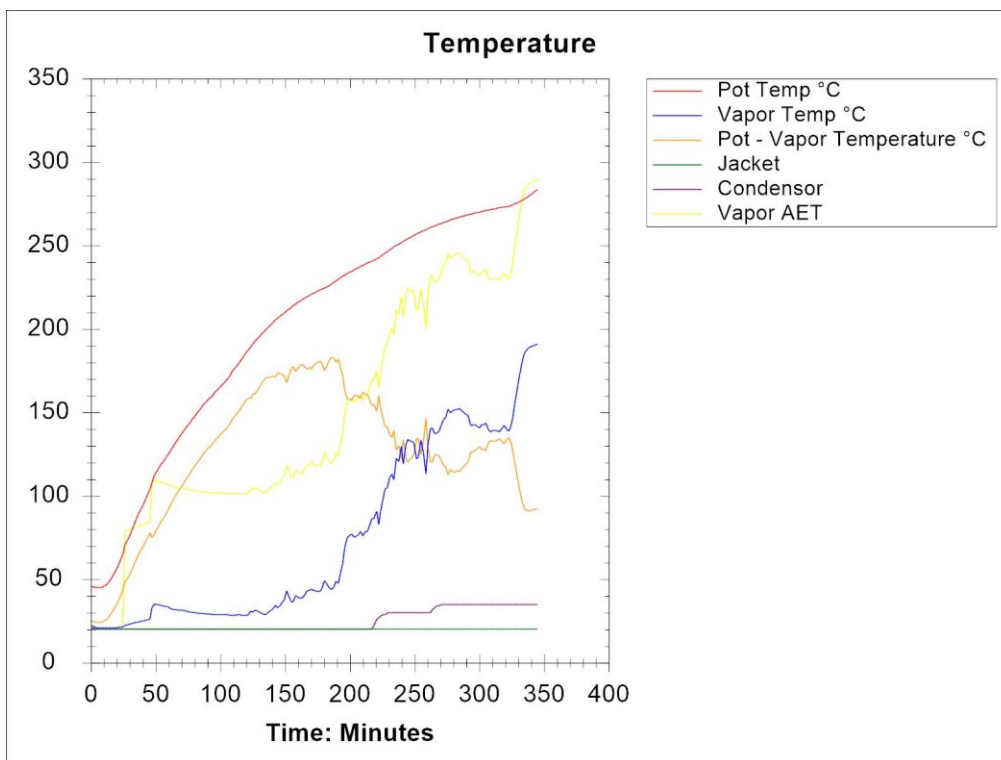


Figure A.13 Distillation data of the 1st day of Distillation 5 (Aug 20, 2020).

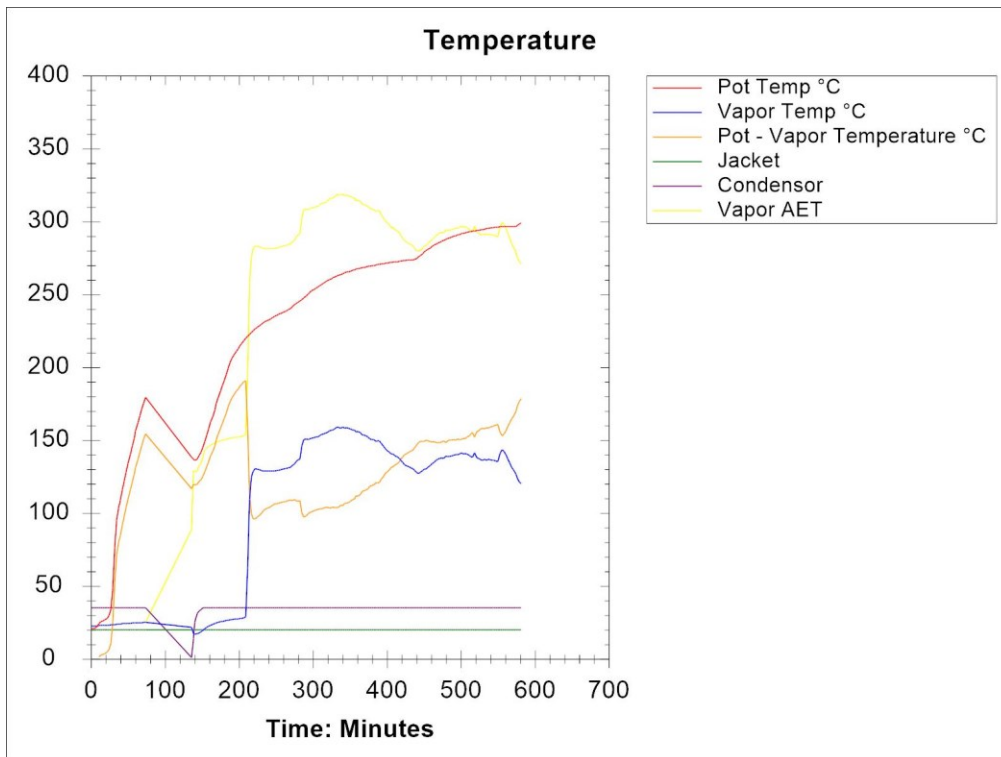


Figure A.14 Distillation data of the 2nd day of Distillation 5 (Aug 21, 2020).

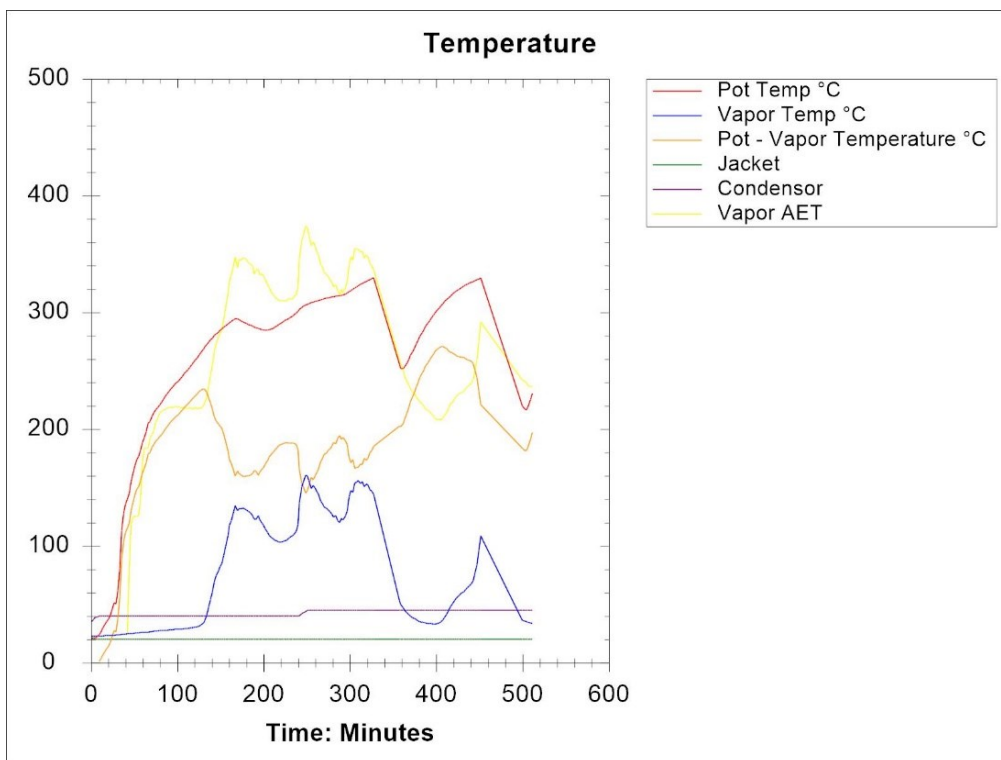


Figure A.15 Distillation data of the 3rd day of Distillation 5 (Aug 22, 2020).

Figure A.16 represents the progress of temperature rise for the attempted atmospheric distillation. As can be seen from the Vapor Temperature curve, no liquid product went to the collectors.

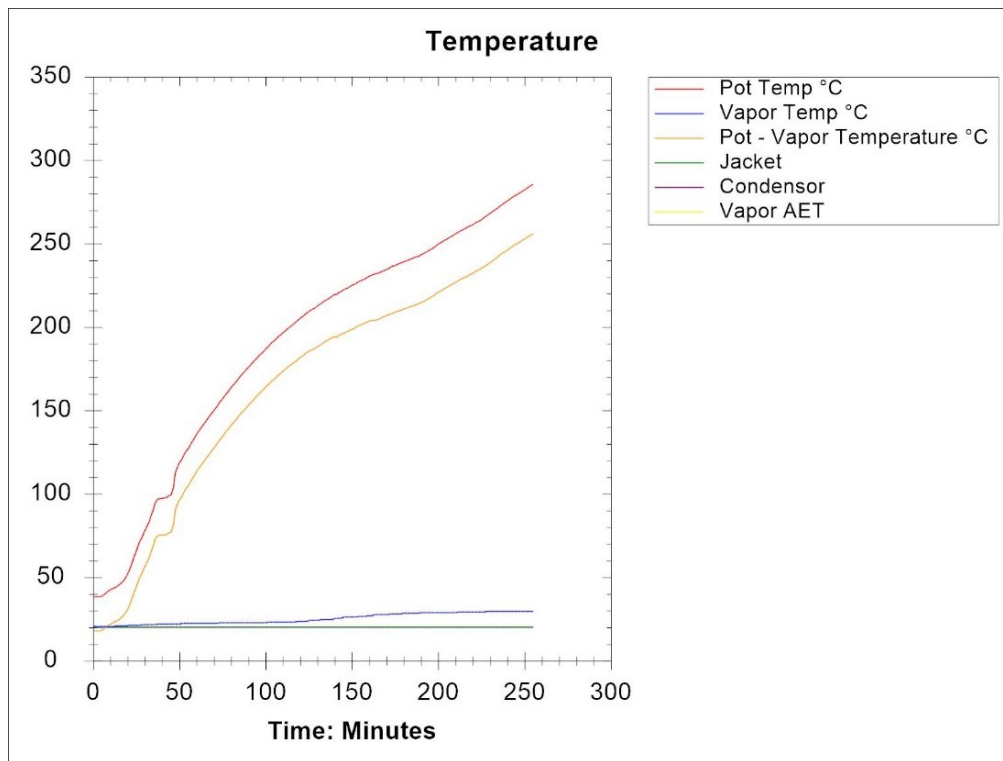


Figure A.16 Atmospheric distillation (Jul 20, 2020).

APPENDIX B

Complete Data Set of the Refractive Index

Refractive Index (RI) was measured on an Abbemat 200 Refractometer from Anton Paar. The range of the instrument is 1.30 to 1.72 nD and the accuracy is ± 0.0001 nD. The temperature probe accuracy of the instrument is $\pm 0.05^\circ\text{C}$.

Each measurement was conducted at the three temperatures: 20°C , 40°C , 60°C . To achieve an extra measure of certainty, each temperature was run twice in the order 20°C , 40°C , 60°C and 60°C , 40°C , 20°C .

The results are presented in the order the liquid products were received. For example, on the first day of Distillation 1, 8 samples from every fraction were received. For the second day of Distillation 1, only two samples were collected, since “1) 270-290” and “2) 290-310” come after “8) 270-290.”

Table B.1 Refractive Index values of liquid products from Distillation 1.

Distillation cut, $^\circ\text{C}$	Refractive Index, nD		
	20°C	40°C	60°C
1) 25-150	1.4411	1.4320	1.4236
	1.4415	1.4323	1.4236
2) 150-170	1.4572	1.4485	1.4399
	1.4572	1.4485	1.4399
3) 170-190	1.4602	1.4515	1.4431
	1.4604	1.4518	1.4433
4) 190-210	1.4636	1.4552	1.4469
	1.4637	1.4553	1.4469
5) 210-230	1.4706	1.4622	1.4541
	1.4706	1.4624	1.4542
6) 230-250	1.4761	1.4678	1.4598
	1.4761	1.4680	1.4600
7) 250-270	1.4796	1.4713	1.4633
	1.4796	1.4716	1.4636
8) 270-290	1.4868	1.4788	1.4709
	1.4869	1.4790	1.4711
1) 270-290	1.4917	1.4837	1.4758
	1.4917	1.4837	1.4759

Distillation cut, °C	Refractive Index, nD		
	20°C	40°C	60°C
2) 290-310	1.5102	1.5023	1.4946
	1.5101	1.5023	1.4946
1) 290-310	1.5169	1.5090	1.5011
	1.5168	1.5089	1.5011
2) 310-330	1.5066	1.4985	1.4906
	1.5065	1.4986	1.4908
3) 330-350	1.5267	1.5192	1.5112
	1.5272	1.5194	1.5117
4) 350-370	1.5252	1.5178	1.5106
	1.5257	1.5180	1.5104
5) 370-390	1.5281	1.5201	1.5125
	1.5278	1.5201	1.5124
6) 390-410	1.5282	1.5206	1.5131
	1.5293	1.5216	1.5138
7) 410-430	1.5353	1.5278	1.5204
	1.5354	1.5278	1.5203

Table B.2 Refractive Index values of liquid products from Distillation 2.

Distillation cut, °C	Refractive Index, nD		
	20°C	40°C	60°C
1) 25-150	1.4429	1.4335	1.4250
	1.4433	1.4338	1.4241
2) 150-170	1.4511	1.4421	1.4333
	1.4513	1.4422	1.4332
3) 170-190	1.4563	1.4474	1.4387
	1.4563	1.4475	1.4388
4) 190-210	1.4659	1.4574	1.4490
	1.4659	1.4575	1.4492
5) 210-230	1.4735	1.4654	1.4572
	1.4735	1.4654	1.4573
6) 230-250	1.4746	1.4665	1.4584
	1.4746	1.4665	1.4584
7) 250-270	1.4785	1.4705	1.4625
	1.4786	1.4705	1.4625
8) 270-290	1.4872	1.4792	1.4713

Distillation cut, °C	Refractive Index, nD		
	20°C	40°C	60°C
	1.4873	1.4793	1.4713
2) 290-310	1.4954	1.4875	1.4796
	1.4954	1.4875	1.4797
3) 310-330	1.5101	1.5023	1.4945
	1.5101	1.5023	1.4946
1) 410-430	1.5340	1.5265	1.5191
	1.5343	1.5267	1.5192

Table B.3 Refractive Index values of liquid products from Distillation 3.

Distillation cut, °C	Refractive Index, nD		
	20°C	40°C	60°C
1) 25-150	1.4556	1.4468	1.4389
	1.4564	1.4470	1.4379
2) 150-170	1.4592	1.4506	1.4420
	1.4593	1.4502	1.4419
3) 170-190	1.4637	1.4552	1.4468
	1.4638	1.4553	1.4470
4) 190-210	1.4702	1.4617	1.4536
	1.4702	1.4619	1.4538
5) 210-230	1.4768	1.4685	1.4605
	1.4767	1.4686	1.4606
6) 230-250	1.4776	1.4694	1.4614
	1.4776	1.4695	1.4615
7) 250-270	1.4800	1.4720	1.4640
	1.4800	1.4720	1.4640
8) 270-290	1.4872	1.4792	1.4713
	1.4873	1.4793	1.4713
1) 290-310	1.4975	1.4897	1.4818
	1.4975	1.4897	1.4818
2) 310-330	1.5091	1.5013	1.4935
	1.5092	1.5014	1.4936
1) 330-350	1.5289	1.5205	1.5127
	1.5280	1.5202	1.5124
2) 350-370	1.5317	1.5241	1.5167
	1.5320	1.5243	1.5169

Table B.4 Refractive Index values of liquid products from Distillation 4.

Distillation cut, °C	Refractive Index, nD		
	20°C	40°C	60°C
1) 25-150	1.4505	1.4416	1.4331
	1.4510	1.4420	1.4325
2) 150-170	1.4551	1.4463	1.4375
	1.4553	1.4465	1.4377
3) 170-190	1.4619	1.4533	1.4448
	1.4620	1.4534	1.4449
4) 190-210	1.4661	1.4576	1.4493
	1.4661	1.4577	1.4495
5) 210-230	1.4681	1.4598	1.4515
	1.4681	1.4598	1.4515
6) 230-250	1.4723	1.4641	1.4559
	1.4720	1.4639	1.4557
7) 250-270	1.4786	1.4703	1.4623
	1.4786	1.4705	1.4625
8) 270-290	1.4855	1.4775	1.4696
	1.4855	1.4775	1.4696
1) 290-310	1.4956	1.4877	1.4799
	1.4956	1.4877	1.4799
2) 310-330	1.5105	1.5026	1.4948
	1.5105	1.5026	1.4950
1) 330-350	1.5198	1.5119	1.5042
	1.5196	1.5118	1.5041
2) 350-370	1.5283	1.5206	1.5129
	1.5281	1.5204	1.5126
3) 370-390	1.5368	1.5293	1.5219
	1.5367	1.5292	1.5217
4) 350-370	1.5390	1.5317	1.5244
	1.5399	1.5323	1.5247

Table B.5 Refractive Index values of liquid products from Distillation 5.

Distillation cut, °C	Refractive Index, nD		
	20°C	40°C	60°C
1) 25-150	1.4419	1.4329	1.4244
	1.4422	1.4329	1.4236
2) 150-170	1.4606	1.4519	1.4434
	1.4607	1.4521	1.4436
3) 170-190	1.4661	1.4577	1.4494
	1.4661	1.4577	1.4494
4) 190-210	1.4694	1.4612	1.4530
	1.4695	1.4612	1.4530
5) 210-230	1.4739	1.4657	1.4576
	1.4738	1.4657	1.4576
6) 230-250	1.4807	1.4727	1.4647
	1.4807	1.4727	1.4647
7) 250-270	1.4849	1.4768	1.4689
	1.4849	1.4768	1.4689
8) 270-290	1.4867	1.4787	1.4708
	1.4867	1.4787	1.4708
1) 290-310	1.4960	1.4881	1.4802
	1.4960	1.4881	1.4803
2) 310-330	1.5096	1.5018	1.4941
	1.5097	1.5018	1.4942
1) 330-350	1.5272	1.5197	1.5123
	1.5276	1.5198	1.5121
2) 350-370	1.5269	1.5192	1.5117
	1.5271	1.5194	1.5118
3) 370-390	1.5302	1.5226	1.5151
	1.5305	1.5228	1.5153

Table B.6 shows Refractive Index values determined twice for the fractions that were mixed based on their boiling range. The order was from 20 to 60°C for the first run and from 60 to 20°C for the second run.

Table B.6 Complete Refractive Index data set

Distillation cut, °C	Refractive Index, nD		
	20°C	40°C	60°C
1) 25-150 °C	1.4466	1.4376	1.4292
	1.4474	1.4379	1.4283
2) 150-170	1.4589	1.4502	1.4415
	1.4590	1.4503	1.4416
3) 170-190	1.4629	1.4544	1.4460
	1.4630	1.4545	1.4460
4) 190-210	1.4674	1.4591	1.4508
	1.4675	1.4592	1.4509
5) 210-230	1.4714	1.4633	1.4551
	1.4715	1.4633	1.4551
6) 230-250	1.4764	1.4683	1.4602
	1.4764	1.4682	1.4602
7) 250-270	1.4789	1.4708	1.4628
	1.4789	1.4708	1.4628
8) 270-290	1.4866	1.4786	1.4708
	1.4866	1.4786	1.4706
9) 290-310	1.5038	1.4959	1.4881
	1.5038	1.4959	1.4881
10) 310-330	1.5107	1.5029	1.4951
	1.5108	1.5029	1.4952
11) 330-350	1.5276	1.5199	1.5121
	1.5276	1.5199	1.5121
12) 350-370	1.5303	1.5225	1.5144
	1.5304	1.5227	1.5150
13) 370-390	1.5319	1.5242	1.5166
	1.5318	1.5241	1.5165
14) 390-410	1.5337	1.5259	1.5182
	1.5339	1.5263	1.5188
15) 410-430	1.5350	1.5275	1.5200
	1.5352	1.5276	1.5200

Table B.7 shows refractive index values determined twice for the blended samples. The order was from 20 to 60°C for the first run and from 60 to 20°C for the second run.

Table B.7 Complete data set of Refractive Index for the 14 blends by BIN.

	RI of the Blends, nD							
T, °C	1		2		3		4	
20	1.5333	1.5332	1.5008	1.5007	1.4913	-	1.5241	1.5234
40	1.5257	1.5256	1.4929	1.4928	1.4833	-	1.5162	1.5156
60	1.5182	1.5181	1.4851	1.4851	1.4754	-	1.5082	1.5081
	RI of the Blends, nD							
T, °C	5		6		7		8	
20	1.5174	1.5174	1.5067	1.5067	1.4908	1.4911	1.5206	1.5204
40	1.51	1.5096	1.4988	1.4988	1.4827	1.483	1.5128	1.5126
60	1.5018	1.5016	1.4911	1.4911	1.4748	1.4748	1.5051	1.505
	RI of the Blends, nD							
T, °C	9		10		11		12 (first)	
20	1.5104	1.5104	1.5201	1.5201	1.5303	1.528	1.5243	1.5246
40	1.5026	1.5025	1.5123	1.5124	1.5218	1.5213	1.5165	1.5169
60	1.4948	1.4948	1.5049	1.5048	1.5138	1.5138	1.51	1.5095
	RI of the Blends, nD							
T, °C	12 (second)		13		14			
20	1.5177	1.5182	1.5305	1.5293	1.5158	1.5158		
40	1.5103	1.5104	1.5217	1.5216	1.508	1.508		
60	1.5032	1.5029	1.5141	1.5141	1.5003	1.5003		

-BIN 3 was measured only once.

APPENDIX C

Complete Data Set of the Elemental Analysis

Complete data set for the Elemental Analysis as received from the Analytical Laboratory.

Sample	Distillation cut	Wt. (mg.)	%N	%C	%H	%S	<i>Sum</i>
FIN 1	25-150°C	1.16	<0.2	74.61	11.57	0.75	<i>86.94</i>
FIN 1	25-150°C	1.36	<0.2	76.97	12.11	0.75	<i>89.84</i>
FIN 2	150-170°C	1.31	0.00	81.14	12.65	0.39	<i>94.18</i>
FIN 2	150-170°C	1.32	0.00	82.89	12.96	0.40	<i>96.25</i>
FIN 2	150-170°C	1.48	0.00	81.57	12.61	0.94	<i>95.12</i>
FIN 3	170-190°C	1.50	0.00	83.23	12.89	0.78	<i>96.91</i>
FIN 3	170-190°C	1.34	0.00	83.07	12.95	0.48	<i>96.50</i>
FIN 4	190-210°C	1.48	0.00	83.64	13.00	0.58	<i>97.22</i>
FIN 4	190-210°C	1.41	0.00	83.97	13.05	0.60	<i>97.62</i>
FIN 5	210-230°C	1.35	0.00	85.00	13.02	0.77	<i>98.79</i>
FIN 5	210-230°C	1.35	0.00	84.66	13.09	0.72	<i>98.48</i>
FIN 6	230-250°C	1.53	<0.2	85.05	13.01	1.06	<i>99.12</i>
FIN 6	230-250°C	1.22	<0.2	85.12	12.96	0.98	<i>99.06</i>
FIN 7	250-270°C	1.49	<0.2	85.32	12.89	1.34	<i>99.55</i>
FIN 7	250-270°C	1.34	<0.2	85.36	12.97	1.10	<i>99.43</i>
FIN 8	270-290°C	1.48	<0.2	85.72	12.70	1.47	<i>99.89</i>
FIN 8	270-290°C	1.36	<0.2	85.52	12.67	1.32	<i>99.50</i>
FIN 9	290-310°C	1.57	0.15	85.35	12.10	2.02	<i>99.61</i>
FIN 9	290-310°C	1.38	0.15	85.46	12.08	2.08	<i>99.78</i>
FIN 10	310-330°C	1.33	0.15	85.13	11.76	2.33	<i>99.38</i>
FIN 10	310-330°C	1.34	0.15	85.26	11.81	2.30	<i>99.52</i>
FIN 11	330-350°C	1.44	<0.2	85.23	11.26	3.24	<i>99.73</i>
FIN 11	330-350°C	1.38	<0.2	85.04	11.29	2.97	<i>99.30</i>
FIN 12	350-370°C	1.60	<0.2	85.05	11.33	3.10	<i>99.48</i>
FIN 12	350-370°C	1.41	<0.2	85.14	11.31	3.06	<i>99.51</i>
FIN 13	370-390°C	1.37	<0.2	85.09	11.27	3.07	<i>99.43</i>
FIN 13	370-390°C	1.58	<0.2	84.96	11.31	3.14	<i>99.41</i>
FIN 14	390-410°C	1.41	<0.2	85.03	11.16	3.08	<i>99.28</i>
FIN 14	390-410°C	1.33	<0.2	85.13	11.17	3.15	<i>99.45</i>
FIN 15	410-430°C	1.84	0.23	84.94	11.21	3.20	<i>99.58</i>
FIN 15	410-430°C	1.46	0.25	84.97	11.21	3.17	<i>99.59</i>